0-315-09157-6

National Library of Canada | Bibliothèque nationale du Canada | CANADIAN THESES ON MICROFICHE | *THÈSES CANADIENNES SUR MICROFICHE*

99

57074

NAME OF AUTHOR/*NOM DE L'AUTEUR* Brian D. Dickie

TITLE OF THESIS/*TITRE DE LA THÈSE* "Thermal and Photochemical Cis/Trans Isomerizations of Some α,B Unsaturated Iminium Salts"

UNIVERSITY/*UNIVERSITÉ* McMaster

DEGREE FOR WHICH THESIS WAS PRESENTED/*GRADE POUR LEQUEL CETTE THÈSE FUT PRÉSENTÉE* Ph.D.

YEAR THIS DEGREE CONFERRED/*ANNÉE D'OBTENTION DE CE DEGRÉ* 1982

NAME OF SUPERVISOR/*NOM DU DIRECTEUR DE THÈSE* Dr. R.F. Childs

Permission is hereby granted to the NATIONAL LIBRARY OF CANADA to microfilm this thesis and to lend or sell copies of the film.

The author reserves other publication rights, and neither the thesis nor extensive extracts from it may be printed or otherwise reproduced without the author's written permission.

*L'autorisation est, par la présente, accordée à la BIBLIOTHÈQUE NATIONALE DU CANADA de microfilmer cette thèse et de prêter ou de vendre des exemplaires du film.*

*L'auteur se réserve les autres droits de publication; ni la thèse ni de longs extraits de celle-ci ne doivent être imprimés ou autrement reproduits sans l'autorisation écrite de l'auteur.*

DATED/*DATÉ* October 22, 1982 SIGNED/*SIGNÉ* Brian Dickie

PERMANENT ADDRESS/*RÉSIDENCE FIXÉ* 219 Rodgers Rd

HAMILTON, ONT

L8K 3C3

# THERMAL AND PHOTOCHEMICAL CIS/TRANS ISOMERIZATIONS OF SOME α,β-UNSATURATED IMINIUM SALTS

By

© BRIAN DAVID DICKIE, B.Sc.

A Thesis

Submitted to the School of Graduate Studies

in Partial Fulfilment of the Requirements

for the Degree

Doctor of Philosophy

McMaster University

(October 1982)

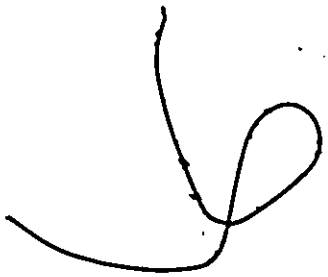

# CIS/TRANS ISOMERIZATIONS

# OF

# IMINIUM SALTS

DOCTOR OF PHILOSOPHY (1982)

McMASTER UNIVERSITY
Hamilton, Ontario

TITLE: Thermal and Photochemical Cis/Trans Isomerizations of Some α,β-Unsaturated Iminium Salts.

AUTHOR: Brian David Dickie, B.Sc. (McMaster University)

SUPERVISOR: Professor R.F. Childs

NUMBER OF PAGES: xv, 175

## ABSTRACT

This thesis presents some investigations of the ground and excited state properties and reactions of some α,β-unsaturated iminium salts. These studies were instigated primarily by the vast number of reports on the photoreceptor pigments, rhodopsin and bacteriorhodopsin. Both of these natural systems are believed to contain iminium salt chromophores which undergo efficient cis/trans isomerizations in their ground and/or excited states.

A series of aliphatic and aromatic substituted α,β-unsaturated iminium salts were prepared and characterized by $^{1}H$ nmr spectroscopy. The ground state structure and charge distribution were investigated by MINDO/3 calculations, an analysis of solution and solid state $^{13}C$ nmr chemical shift data and x-ray crystal structure determinations. It was concluded that the positive charge of these systems resides principally in the iminium moiety and that the s-trans conformation is predominant in solution.

The photochemical reactions of the iminium salts in strong acid media ($FSO_3H$, $H_2SO_4$ and TFA) were examined. All of the systems formed a photostationary state mixture among some or all of the possible geometric isomers. The unambiguous identification of a photon-induced cis/trans isomerization about the $C=N^+$ bond was particularly significant as this was the first report of such an occurrence.

The quantum yields for some of these isomerization processes

were determined in the above solvents. The substituent and viscosity dependence of these yields were used in an attempt to elucidate the mechanism of isomerization and the charge distribution of the excited state. It was concluded that on going from the ground to the excited state there was a shift of the positive charge from the iminium moiety onto the carbon framework. This was completely in accord with the sudden polarization effect proposed by Salem and Bruckmann. A mechanism involving the rotation about one of the multiple bonds per quantum absorbed was consistent with these data.

A quantitative investigation of the ground state cis to trans isomerizations about the C=C bonds in a series of para-substituted aromatic iminium salts was undertaken. The results were indicative of a change in mechanism with a variation in the electron demand of the substituent. Salts with electron-withdrawing substituents were concluded to isomerize by the Michael addition of a nucleophile whereas, a pathway involving protonation at the iminium nitrogen was proposed for the salts with electron-donating substituents.

ACKNOWLEDGEMENTS

First and foremost I wish to acknowledge Ron Childs. His guidance and, in particular, his enthusiasm throughout the course of this work cannot be over-emphasized. The financial support from Ontario Graduate and Natural Sciences and Engineering Research Council scholarships was appreciated.

A special thank you goes to Aravamuthan Varadarajan ("John") for the many helpful discussions of chemistry and other assorted topics during our sojourn together. I thank also, my committee members, Drs. J. Warkentin and A.J. Yarwood.

My work at McMaster was made so much easier by the superlative technical support staff. For this reason I gratefully acknowledge B. Sayer, I. Thompson and C. Schonfeld. As well, I wish to thank B. MacDonald at the Southwestern Regional NMR Centre at the University of Guelph for his efforts in obtaining the 400 MHz $^{1}H$ nmr spectra.

The superb typing skills of Miss K. Stockman were a major asset and a thank you is extended to Mrs. M. Pankratz for critiquing and proof reading many parts of this manuscript.

Finally, I am grateful for the support, encouragement and sympathetic understanding of my parents and family.

"With a little help from my friends..."[†]

[†] The Beatles.

TABLE OF CONTENTS


| | | Page |
|---|---|---|
| DESCRIPTIVE NOTE | | ii |
| ABSTRACT | | iii |
| ACKNOWLEDGEMENTS | | v |
| INTRODUCTION | | |
| CHAPTER I | THE VISION PROCESS | 1 |
| | A. Schiff Bases of Retinals: Model Visual Pigments | 4 |
| | *Ground State Properties* | 4 |
| | *Absorption Spectra and Photophysical Properties* | 7 |
| | *Photoisomerism* | 12 |
| | B. Rhodopsin: A Visual Pigment | 13 |
| | *The Protein* | 13 |
| | *Chromophore Conformation* | 15 |
| | *State of Protonation* | 15 |
| | *Bathochromic Shift* | 18 |
| | *Primary Photochemical Event* | 19 |
| | *Light-Induced Reactions* | 21 |
| | *Visual Transduction* | 22 |

| | | Page |
|---|---|---|
| CHAPTER 2 | SOME CHEMISTRY OF IMINIUM SALTS | 24 |
| | A. Photochemistry | 25 |
| | *Electron Transfer* | 25 |
| | *Photocyclization* | 28 |
| | *Photoisomerism* | 28 |
| | B. Thermal Isomerism | 30 |
| | *Intramolecular Mechanisms* | 30 |
| | *Intermolecular Mechanisms* | 33 |
| RESULTS AND DISCUSSION | | |
| CHAPTER 3 | THE STRUCTURE OF IMINIUM SALTS | 38 |
| | A. Preparation of Imines and Iminium Salts | 40 |
| | B. Double Bond Configurations | 42 |
| | C. Charge Distribution | 45 |
| | *Theoretical Calculations* | 45 |
| | *Analysis of $^{13}C$ Chemical Shifts* | 50 |
| | *Crystallographic Structure Determination* | 58 |
| | D. Conclusions | 65 |
| CHAPTER 4 | PHOTOCHEMISTRY | 67 |
| | A. Qualitative Observations | 67 |
| | B. Identification of Photoproducts | 73 |
| | C. Quantitative Measurements | 86 |
| | *Multiplicity of Excited State* | 93 |
| | *Substituent Effects* | 95 |
| | *Possible Isomerization Mechanisms* | 97 |
| | *Viscosity Dependence* | 103 |

| | | Page |
|---|---|---|
| | D. Conclusions | 105 |
| CHAPTER 5 | THERMAL CHEMISTRY | 107 |
| | A. Qualitative Observations | 107 |
| | B. Quantitative Measurements | 109 |
| | *Substituted Effects* | 109 |
| | *Possible Isomerization Mechanisms* | 114 |
| | *Effect of Solvent Acidity* | 122 |
| | *Deuterium Exchange* | 129 |
| | C. Conclusions | 134 |
| EXPERIMENTAL | | |
| CHAPTER 6 | EXPERIMENTAL METHODS | 136 |
| | A. Materials | 136 |
| | B. Instrumental Techniques | 136 |
| | *$^{1}H$ nmr Spectra* | 136 |
| | *Solution $^{13}C$ nmr Spectra* | 137 |
| | *Solid State $^{13}C$ nmr Spectra* | 138 |
| | *Electronic Absorption Spectra* | 138 |
| | *Infrared Spectra* | 138 |
| | *Gas Chromatography* | 139 |
| | C. Synthesis | 139 |
| | *trans,trans-N-t-butyl-2-butenylidenimine, 32* | 141 |
| | *trans,trans-N-n-butyl-2-methyl-2-butenylidenimine, 33 and trans-N-n-butyl-2-methyl-2-propenylidenimine, 34* | 141 |

Page

*trans,trans-N-n-butyl-3-phenyl-2-propenylidenimine, 35* 142

*trans,trans-N-n-butyl-3-(p-nitrophenyl)-2-propenylidenimine, 36* 142

*Protonation Methods* 142

*trans-N,N-dimethyl-3-(p-x-phenyl)-2-propenylideniminium perchlorates, 42* 42 (X=H), 43 (X=$OCH_3$), 44 (X=$CH_3$), 45 (X=Cl), 46 (X=$NO_2$) 143

D. MINDO/3 Calculations 143

E. Crystal Structure Determinations 144

*Collection of the Data* 144

*Solution of the Structures* 144

F. Fluorescence Measurements 151

G. Quantum Yield Measurements 152

*Aliphatic Iminium Salts* 152

*Aromatic Iminium Salts* 156

H. Kinetic Measurements 159

*$H_o$ Measurements* 159

*Isomerization Rate Constants* 160

*Rate Constants for Deuterium Exchange at C2* 161

REFERENCES 164

## LIST OF TABLES


| | | Page |
|---|---|---|
| Table 1-1 | Absorption band maxima and quantum yields of photophysical processes for retinal Schiff base 9 and retinal protonated Schiff base 10 | 8 |
| Table 1-2 | $^{13}C$ nmr data for retinal Schiff bases 9 and 11 and protonated Schiff base 12 | 10 |
| Table 2-1 | Iminium salt isomerization data | 31 |
| Table 3-1 | $^{1}H$ nmr data for aliphatic imines and iminium salts | 43 |
| Table 3-2 | $^{1}H$ nmr data for aromatic imines and iminium salts | 44 |
| Table 3-3 | MINDO/3 energies, Mulliken populations and bond lengths | 47 |
| Table 3-4 | STO-3G energies and Mulliken populations | 48 |
| Table 3-5 | $^{13}C$ nmr data for aliphatic imines and iminium salts | 51 |
| Table 3-6 | $^{13}C$ nmr data for aromatic imines and iminium salts | 52 |
| Table 3-7 | Solid State $^{13}C$ nmr data of iminium salts | 56 |
| Table 3-8 | Selected interatomic distances (Å) and angles (deg):.. | 62 |
| Table 4-1 | Electronic absorption data for iminium salts | 68 |
| Table 4-2 | $^{1}H$ nmr data for the aliphatic iminium salts and their principal photoproducts | 70 |
| Table 4-3 | $^{1}H$ nmr data for the aromatic N-n-butyliminium salts and their principal photoproducts | 71 |
| Table 4-4 | $^{1}H$ nmr data for the aromatic N,N-dimethyliminium salts and their principal photoproducts | 72 |

| | | Page |
|---|---|---|
| Table 4-5 | Quantum yields of isomerization for the aliphatic salts in $H_2SO_4$, $FSO_3H$ and TFA solution | 87 |
| Table 4-6 | Quantum yields of isomerization for the aromatic salts in TFA solution | 90 |
| Table 5-1 | Isomerization rate constants at 100 ± 0.5°C for the para-substituted iminium salts in TFA | 110 |
| Table 5-2 | MINDO/3 activation energies and Mulliken populations for the bond rotation and azetinium mechanisms | 117 |
| Table 5-3 | Isomerization rate constants at 100 ± 0.5°C for the para-substituted iminium salts in TFA and 0.015M $H_2SO_4$/TFA. | 126 |
| Table 5-4 | Rate constants of deuterium exchange at 100 ± 0.5°C for the C2 proton in TFA-d and $D_2SO_4$/TFA-d | 133 |
| Table 6-1 | Some physical data and elemental analyses for the imines and iminium salts | 140 |
| Table 6-2 | Crystal data for $(C_{11}H_{14}N^+)(ClO_4^-)$, 42 and $(C_{12}H_{16}NO^+)(ClO_4^-)$, 43 | 145 |
| Table 6-3 | Atomic positional parameters for trans-N,N-dimethyl-3-phenyl-2-propenylideniminium perchlorate, 42 | 146 |
| Table 6-4 | Atomic positional parameters for trans-N,N-dimethyl-3-(p-methoxyphenyl)-2-propenylideniminium perchlorate, 43 | 147 |
| Table 6-5 | Temperature factors ($Å^2$) for non-hydrogen atoms (x$10^3$) for $(C_{11}H_{14}N^+)(ClO_4^-)$, 42 | 148 |
| Table 6-6 | Temperature factors ($Å^2$) for non-hydrogen atoms (x$10^3$) for $(C_{12}H_{16}NO^+)(ClO_4^-)$, 43 | 149 |
| Table 6-7 | Best planes and torsional angles for ..., 43 | 150 |
| Table 6-8 | Raw quantum yield data for the aliphatic iminium salts | 155 |

| | | Page |
|---|---|---|
| Table 6-9 | Raw quantum yield data for the aromatic iminium salts | 158 |
| Table 6-10 | Raw rate constant data for the isomerization of the unsubstituted aromatic iminium salt, 66 → 42 | 162 |

LIST OF FIGURES


| | | Page |
|---|---|---|
| Figure 1-1 | Schematic of rod photoreceptor cell | 14 |
| Figure 1-2 | External point charge model for (a) bovine rhodopsin and (b) bacteriorhodopsin | 17 |
| Figure 3-1 | Stereo- and conformational isomers of an $\alpha,\beta$-unsaturated iminium salt | 39 |
| Figure 3-2 | $^{13}C$ nmr spectra of trans-N,N-dimethyl-3-(p-methoxyphenyl)-2-propenyliden-iminium perchlorate, 43 (a) solution, (b) solid state, (c) suppressed | 57 |
| Figure 3-3 | ORTEP diagram for the trans-N,N-dimethyl-3-phenyl-2-propenylideniminium cation, 42 | 60 |
| Figure 3-4 | ORTEP diagram for the trans-N,N-dimethyl-3-(p-methoxyphenyl)-2-propenylideniminium cation, 43 | 61 |
| Figure 3-5 | Crystal packings for (a) ..., 42 and (b) ..., 43 | 64 |
| Figure 4-1 | Vinyl region of the 400 MHz $^1H$ nmr spectrum of the trans-N-n-butyl-2-methyl-2-propenylideniminium cation 39, in TFA | 74 |
| Figure 4-2 | Vinyl region of the 400 MHz $^1H$ nmr spectrum of the photostationary state mixture formed by the irradiation of ... 39, in TFA | 75 |
| Figure 4-3 | Vinyl region of the 400 MHz $^1H$ nmr spectrum of the trans,trans-N-t-butyl-2-butenylideniminium cation 37, in TFA | 77 |
| Figure 4-4 | Vinyl region of the 400 MHz $^1H$ nmr spectrum of the photostationary state mixture formed by the irradiation of ... 37, in TFA | 78 |
| Figure 4-5 | Double resonance experiments used to identify the trans,cis-N-t-butyl-2-butenylideniminium cation 54 | 81 |

| | | Page |
|---|---|---|
| Figure 4-6 | Double resonance experiments used to identify the cis,trans- and cis,cis-N-t-butyl-2-butenylideniminium cations, 53 and 55 respectively | 83 |
| Figure 5-1 | Hammett $\sigma^+$ plot for the rate constants determined in TFA | 113 |
| Figure 5-2 | MINDO/3 activation barrier for C=C bond rotation of the parent α,β-unsaturated iminium cation, 48a | 118 |
| Figure 5-3 | MINDO/3 energy surface for the conrotatory ring opening of the parent azetinium ion, 72 | 120 |
| Figure 5-4 | Hammett $\sigma^+$ plot for the rate constants determined in TFA and $H_2SO_4$/TFA | 128 |

# INTRODUCTION

# CHAPTER 1

## THE VISION PROCESS

The vertebrate visual pigment rhodopsin, 1, consists of a chromophore, 11-cis retinal (1), bound via a Schiff base linkage to a lysine residue (2,3) of an apoprotein called opsin.

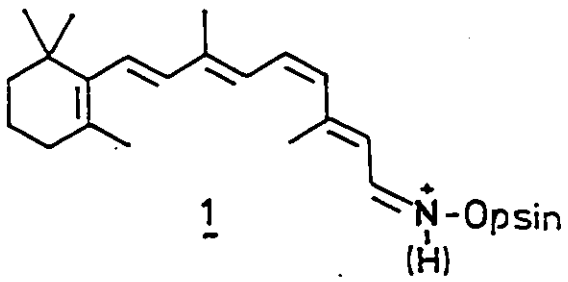


1

The word rhodopsin is derived from the two Greek words meaning "rose" and "vision" reflecting simultaneously its pink colour and its function. Vision has been the subject of extensive study in the last forty years and yet many aspects of the process are poorly understood and their interpretation is controversial.

The absorption of light by the chromophore causes a cis/trans isomerization producing the pigment containing the all-trans chromophore. This pigment dissociates to give all-trans retinal and opsin, equation 1. An understanding of the chromophore photoisomerization is

essential to the discernment of the vision process.

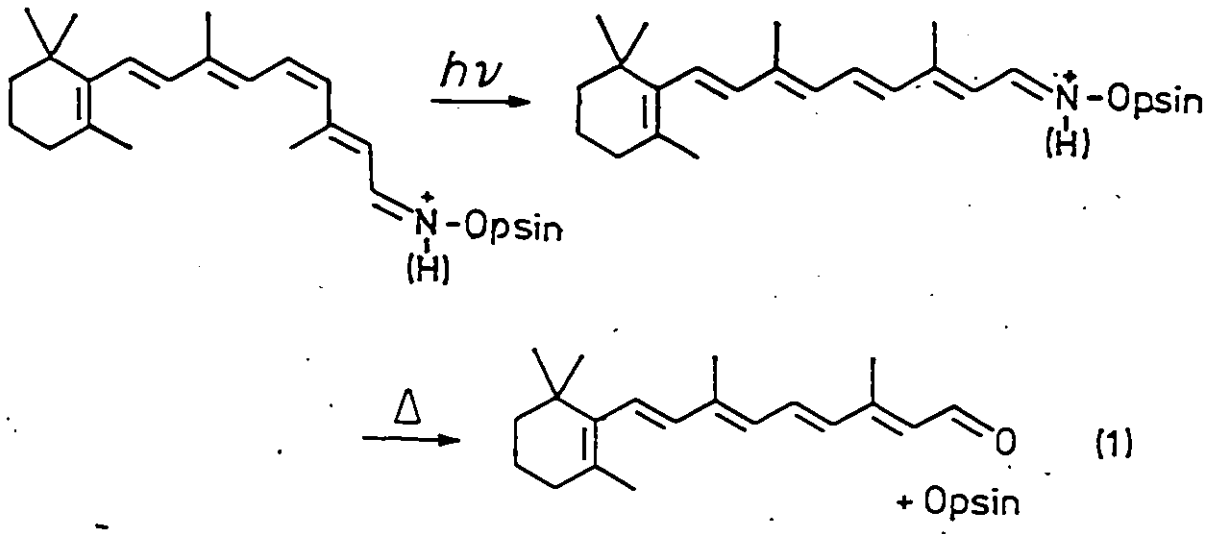


(1)

Bacteriorhodopsin is a light harvesting protein of the purple membrane of the microorganism Halobacterium halobium and its function is to pump protons across the cell membrane under anaerobic conditions (4,5). The bacterium uses the resulting hydrogen ion gradient to drive chemiosmotically the synthesis of ATP.

In 1971, Oesterhelt and Stockenius (6) discovered that bacteriorhodopsin contains a retinal chromophore. The dark-adapted pigment, in fact, contains two isomeric retinal chromophores (all-trans and 13-cis), in thermal equilibrium, which are bound to the protein by a Schiff base linkage, equation 2 (4,5). Light-adapted bacteriorhodopsin contains predominantly the all-trans isomer and it is this form of the pigment which undergoes a photon-induced cyclical reaction sequence in the proton pumping process. Unlike rhodopsin, the absorption of a photon does not cause the dissociation of the pigment chromophore.

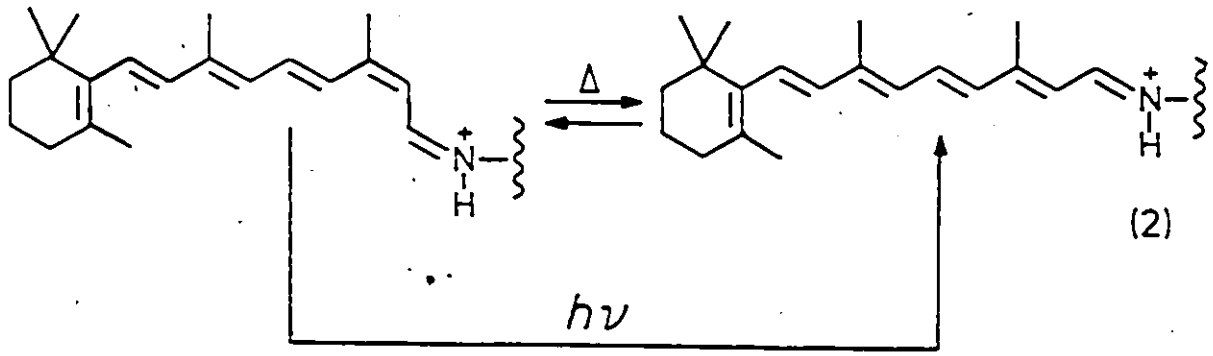


(2)

Rhodpsin and bacteriorhodopsin have strong absorptions in the green and yellow regions of the visible spectrum respectively, while retinals and simple retinal Schiff bases formed in vitro absorb in the ultra violet region. The origin of this large spectral shift in the natural pigments is controversial. To account partially for the shift it is generally accepted that the chromophore/protein Schiff base linkage is either protonated (4,5,7,8,9-13) or strongly hydrogen bonded (5,9,14-18).

The solution chemistry of neutral and protonated Schiff bases of retinals has been investigated to obtain a better understanding of the above processes since it is believed that the protonated alkyl Schiff base of 11-cis retinal is the best solution model for rhodopsin (4,5,7,8). The following discussion will focus mainly on the chemistry pertaining to rhodopsin and the vision process, although on a number of occasions reference will be made to bacteriorhodopsin. First, the ground and excited state chemistry of neutral and protonated Schiff

bases will be reviewed. This is followed by a discussion of the natural pigment.

A. Schiff Bases of Retinals: Model Visual Pigments

Retinal, the chromophore in rhodopsin and bacteriorhodopsin, can exist in a number of isomeric configurations, 2-8, but only certain ones form stable pigments. The protein opsin forms a stable pigment with the 11-cis and 9-cis isomers, 4 and 5 respectively, but only 4 is found in natural pigments (1). Bacteriorhodopsin, on the other hand, contains both all-trans, 2, and 13-cis, 3, isomers (4,5). In both photoreceptor pigments, however, the chromophore is bound to the protein by a Schiff base linkage (2-5).

*Ground State Properties*

A Schiff base is formed by the condensation of a carbonyl group with a primary amine, equation 3. The alkyl amine most commonly used in model pigment studies is n-butylamine since the lysine residue in opsin consists of a four carbon chain with an amino group at the terminal end.

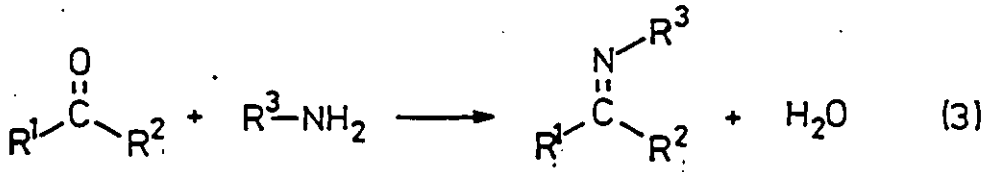


(3)

Alkyl Schiff bases of all retinal isomers have a distorted 6-s-cis geometry. Apart from the 11-cis isomer, 9, the s-trans conformation about the other formal single bonds is preferred with all the isomers studied. The 11-cis isomer, 9, is reputed to exist as an

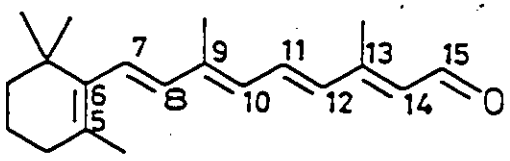


2 (all-trans)

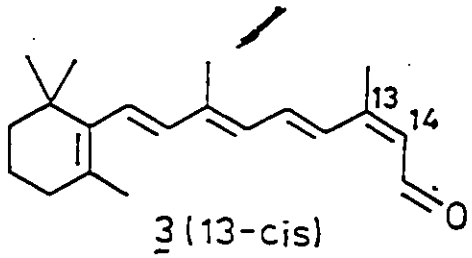


3 (13-cis)

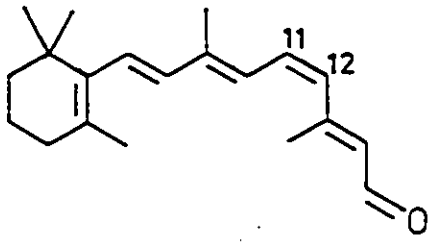


4 (11-cis)

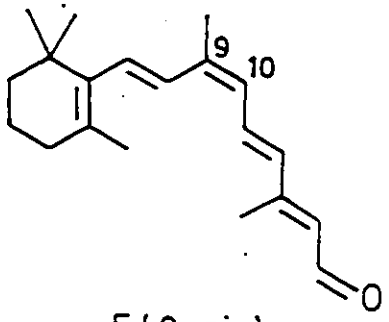


5 (9-cis)

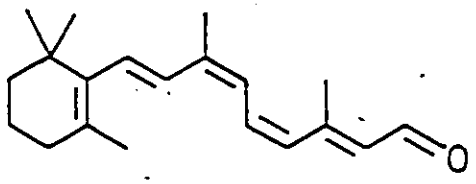


6 (9,11-dicis)

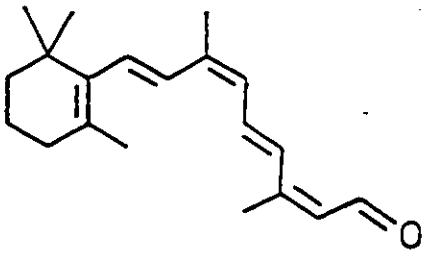


7 (9,13-dicis)

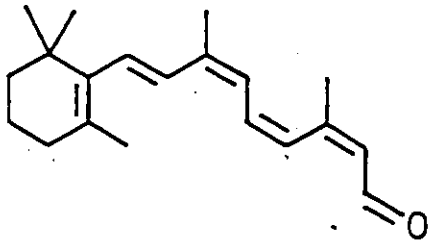


8 (9,11,13-tricis)

equilibrium mixture of the 12-s-cis, 9a, and 12-s-trans, 9b, conformers, equation 4 (4,5,7,8). Both $^{1}H$ and $^{13}C$ nmr data indicate that in solution 9a is favoured (9).

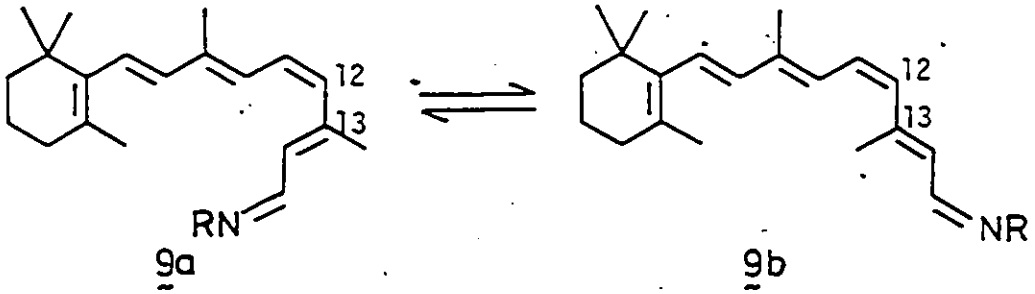


9a 9b (4)

Uhl and Abrahamson (9) claim that this conformational equilibrium, equation 5, is still maintained when the Schiff base is protonated and that 10a is the favoured conformer.

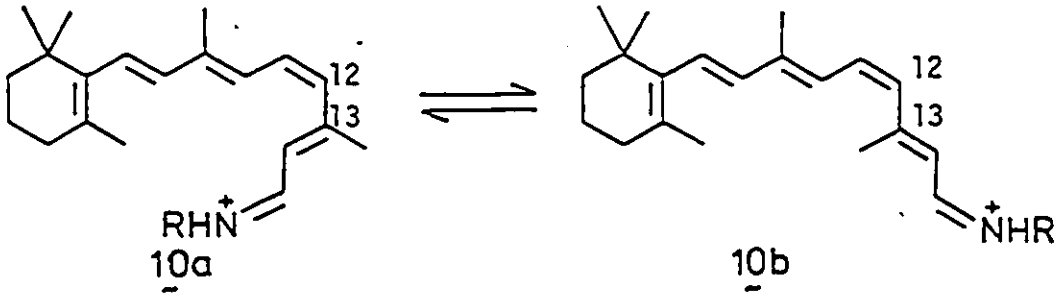


10a 10b (5)

Resonance Raman data is also consistent with an equilibrium mixture of 10a and 10b in solution (10). Both conformers have a trans arrangement about the carbon, nitrogen double bond (9,19).

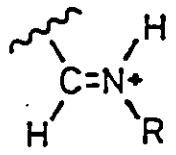

The state of protonation of the chromophore/protein Schiff base linkage is important to the understanding of the vision process so that some idea of the basicity of 9 is necessary. A pKa in the range of 7 - 8 has been estimated for 10 (23,24). This value increases to about 17 in the first excited state which means that the excited state is much more basic than the ground state (23). It has been suggested that a pKa of 7 may not be high enough to ensure that the Schiff base linkage in rhodopsin is fully protonated (14,24), but evidence indicates that the ground state pKa is much higher in the protein environment (17,18). Further discussion on the problem of Schiff base protonation will be left until the next section.

*Absorption Spectra and Photophysical Properties*

Electronic absorption spectral properties for 9 and 10 are summarized in Table 1-1. The spectrum of 9 exhibits a maximum at 350 nm for the lowest energy absorption band (26). Upon protonation the maximum of this band shifts dramatically to longer wavelengths such that the maximum of 10 occurs at about 440 nm (27).

Absorption maxima for 9 and 10 are both temperature and solvent dependent and, in addition, the molar absorptivity is temperature dependent. An increase in the extinction coefficient of about 20% is observed for 9 and 10 at low temperature, Table 1-1. It has been suggested that a shift in the conformational equilibrium towards the 12-s-trans conformer (9b and 10b) as the temperature is lowered is the cause of this increase in molar absorptivity (26,27). This argument, which has generally been accepted in the literature, contains an inconsistency.

Table 1-1

Absorption Band Maxima and Quantum Yields of Photophysical Processes For Retinal Schiff base 9 and Retinal protonated Schiff base 10

| Compound | Temp. | $\lambda_{max}$(nm)[a] | Oscillator Strength[a] | Quantum Yields[f] | | | |
|---|---|---|---|---|---|---|---|
| | | | | $\Phi_f$ | $\Phi_{ISC}$ | $\Phi_{PI}$ | $\Phi_{PI}^T$ |
| 9 | 77K | 368 | 1.01 | obsd. | - | - | - |
| | 295K | 350 | 0.81 | <0.001[b] | <0.01[c] | 0.004[c] | 0.45[e] |
| 10 | 77K | 442 | 0.83 | obsd. | - | - | - |
| | 295K | 438 | 0.72 | <0.001[b] | <0.01[b] | 0.05[d] | 1[e] |

[a]Reference 26 and/or 27.

[b]Reference 31 and/or 32.

[c]Reference 31 and 33.

[d]Reference 31 and 35, value is strongly wavelength dependent.

[e]Reference 31 and 36.

[f]Quantum yields of fluorescence ($\Phi_f$), intersystem crossing ($\Phi_{ISC}$), isomerization upon direct irradiation ($\Phi_{PI}$) and isomerization by sensitization to the triplet state ($\Phi_{PI}^T$).

Based on the expectation that the conformational entropy differences are small (151), the 12-s-cis conformer (9a and 10a), which is favoured at room temperature, should become even more favoured as the temperature is lowered.

A study of environmental effects (solvent, acid strength and presence of amino acid analogues) demonstrates that the absorption maximum of 10 is readily shifted to about 500 nm, the absorption maximum of rhosopsin (28).

The large bathochromic shift observed upon protonation has been suggested to result from the collapse of bond alternation and an accompanying charge delocalization (29).

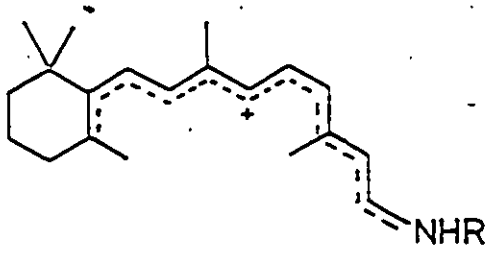


Charge delocalization is supported by $^{13}C$ nmr data, Table 1-2 (20-22,29). The resonances due to the odd numbered carbons move downfield while those for the even numbered carbons move upfield. This phenomenon is consistent with the possible resonance forms for a protonated Schiff base and is in qualitative agreement with theoretical calculations of $\pi$ electron densities and $\pi$ bond orders (29).

Direct excitation of Schiff base, 9, or protonated Schiff base 10 leads to the formation of their lowest excited singlet state, $S_1$. These excited states can return to the ground state by a number of different pathways, Scheme 1-1. Relaxation can be achieved by the emission of light (fluorescence), a radiationless process such as

Table 1-2

$^{13}C$ nmr Data for Retinal Schiff Bases, 9 and 11, and Protonated Schiff Base, 12

| Carbon Atom | Chemical Shift (ppm) 9[a] | 11[b] | 12[b] |
|---|---|---|---|
| 5 | 130.8 | 129.73 | 131.77 |
| 6 | 139.9 | 137.82 | 137.42 |
| 7 | 129.0 | 127.79 | 132.09 |
| 8 | 140.3 | 137.52 | 136.89 |
| 9 | 140.0 | 139.94 | 145.33 |
| 10 | 129.3 | 130.05 | 129.55 |
| 11 | 128.8 | 127.79 | 137.42 |
| 12 | 134.4 | 136.09 | 133.64 |
| 13 | 145.0 | 143.91 | 162.33 |
| 14 | 132.8 | 129.55 | 120.14 |
| 15 | 160.7 | 159.37 | 163.65 |

[a] Reference 30.

[b] Reference 20.

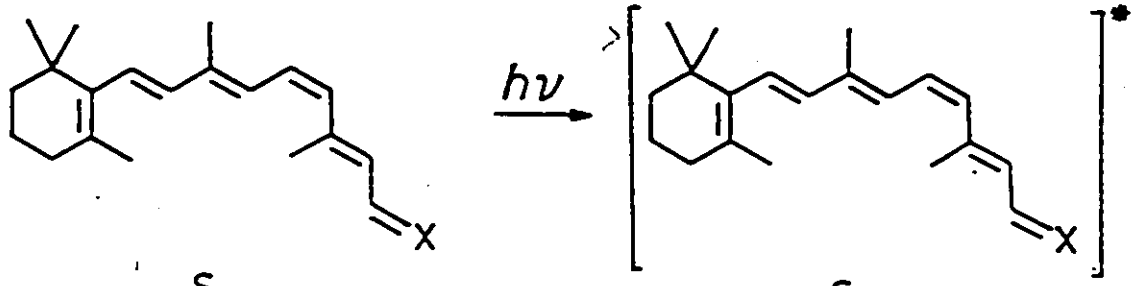


$S_o$

9 X=NR

10 X=$\overset{+}{N}$HR

$S_1$

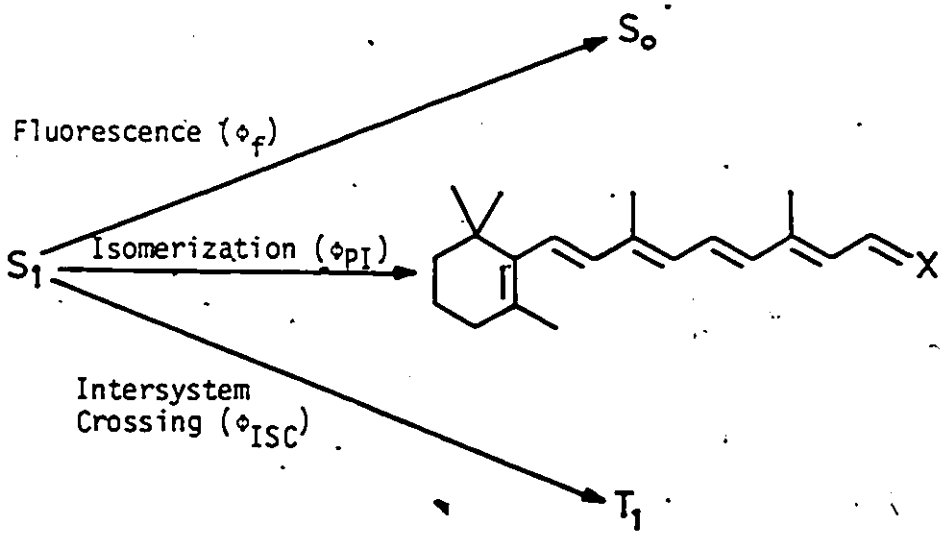


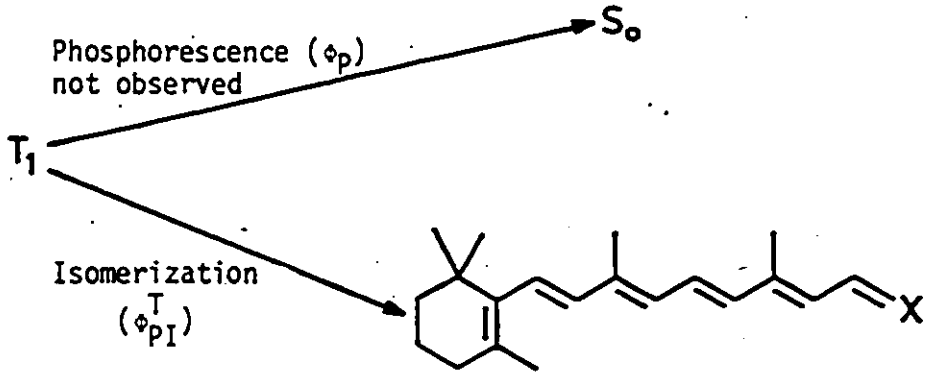


Scheme 1-1

isomerization, or the singlet state can intersystem cross to the lowest excited triplet state. The triplet state can also lose its energy by the emission of light (phosphorescence) or by a radiationless process such as isomerization. The efficiencies of these processes are given in Table 1-1.

Neither 9 nor 10 fluoresce at room temperature, but both fluoresce weakly at low temperature (31,32). Phosphorescence has not been observed for either compound, consistent with low quantum yields for intersystem crossing (31,33,91). These results are compatible with a first excited state of $\pi$-$\pi^*$ character for both 9 and 10 (31,32). Schiff base formation causes a large enough blue shift of the n-$\pi^*$ transition to make a $\pi$-$\pi^*$ state lowest in energy and protonation transforms the nitrogen non-bonding orbital into a bonding orbital eliminating the n-$\pi^*$ transition (5). Theoretical calculations of energy level ordering support these conclusions (5,34).

*Photoisomerism*

The irradiation of 9 and 10 leads to the formation of the all-trans isomers 11 and 12, respectively (31,33,35). Photoisomerization efficiencies are low (see Table 1-1) and the value for 10 is strongly wavelength dependent. Rhodopsin, on the other hand, undergoes an efficient wavelength independent cis/trans isomerization (73,77).

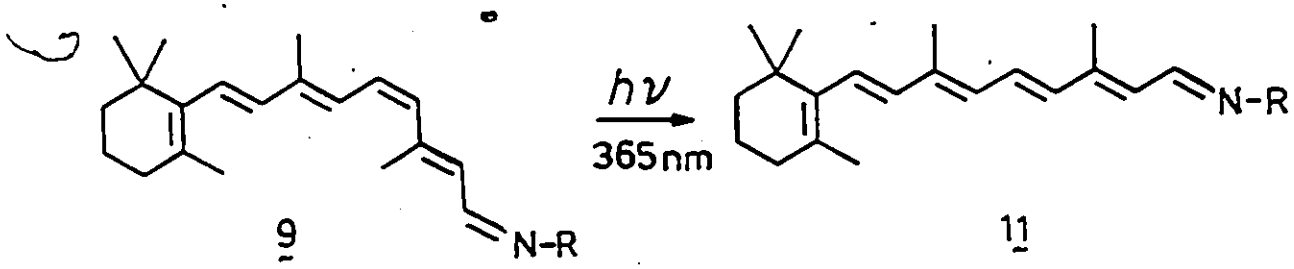


9 11

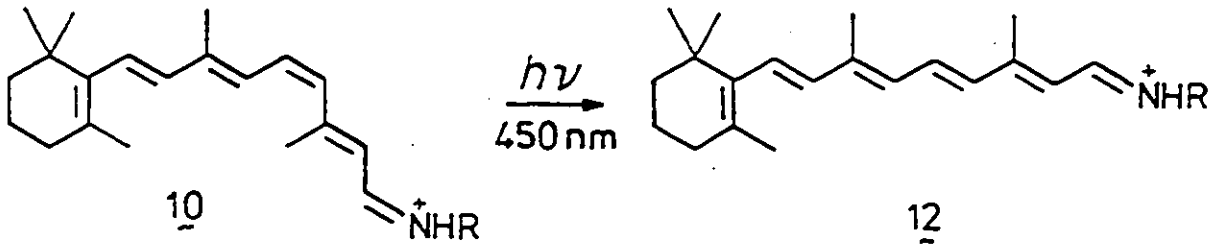


10 12

Upon sensitization to the triplet state efficient isomerization is observed for both 9 and 10 (31,33,36). Due to their low quantum yields for intersystem crossing, however, isomerization from the triplet state is probably not important in the direct irradiation of retinal Schiff bases (31,33).

B. Rhodopsin: A Visual Pigment

Rhodopsin has a complex chemistry which can only be discussed briefly in this review. A number of recent reviews are available for more details (4,5,7-9). In this discussion emphasis will be placed on the origin of the pigment absorption spectrum and the elucidation of the primary photochemical event.

*The Protein*

Opsin is a single polypeptide chain of approximate molecular weight 36,000 and consists of about 300 amino acids, the sequence of which is not completely known (5,8,9). Rhodopsin is found in the rod photoreceptor, Figure 1-1, and constitutes about 90% of the protein in the disk membrane. The pigment is a highly asymmetric molecule which is long enough to transcend the thickness of the disk membrane (5,8,9).

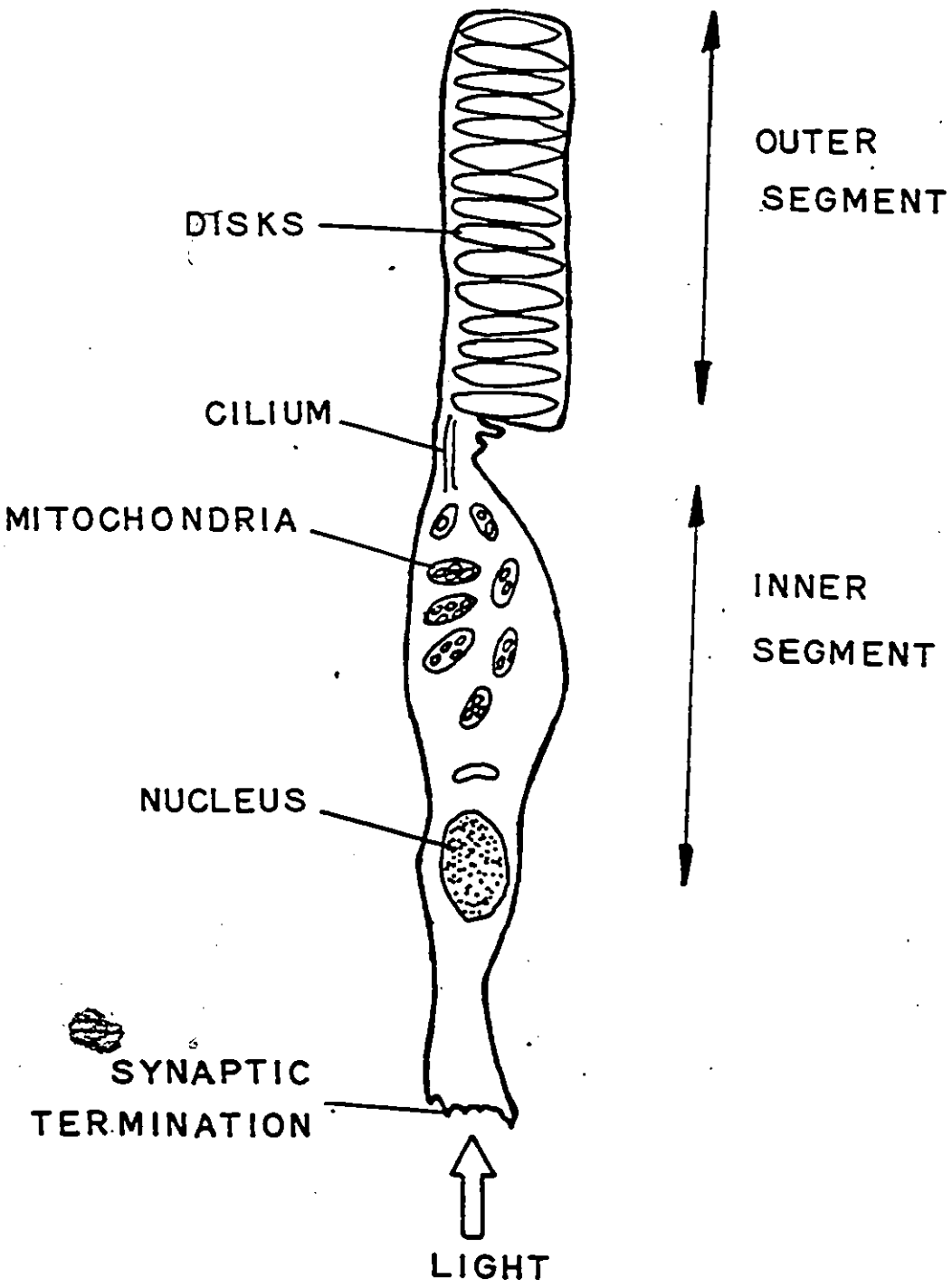


Figure 1-1: Schematic of rod photoreceptor cell.

*Chromophore Conformation*

The specific geometry of the 11-cis retinal chromophore is not known (4,5,8,9). There is, however, indirect evidence suggesting that the 12-s-trans conformer is favoured in the protein environment. A protein bound 12-s-cis conformer, as in solution, should have a weaker absorption band than is observed for rhodopsin (4). The 14-methyl derivative of retinal, which has an unstable 12-s-cis conformer, forms an artificial pigment with properties very similar to those of rhodopsin (37). Finally the resonance Raman spectrum of rhodopsin has a similar pattern in the methyl stretching region as solutions of 11-cis retinal containing the 12-s-trans conformer (10,38).

*State of Protonation*

Rhodopsin has an absorption maximum at 498 nm (4,5,7,8), while 11-cis retinal has a maximum at 369 nm (5,7,8). To account partially for this large red shift in the spectrum of the pigment it was proposed that the protein/chromophore Schiff base linkage is protonated (7,39,40).

There was no direct evidence for Schiff base protonation until the application of resonance Raman spectroscopy to the study of the visual pigment. The $\nu_{C=N}$ in rhodopsin is found to be close to that observed in model protonated Schiff bases of retinal (25,54). On this basis it was suggested that the Schiff base linkage in rhodopsin is protonated (54). In deuterated media $\nu_{C=N}$ of rhodopsin is shifted from 1655 $cm^{-1}$ to 1630 $cm^{-1}$, a shift which is also in agreement with that of model compounds (25). A normal mode analysis demonstrated that the above shift in vibrational frequency can be accounted for by the replacement of a proton by a deuteron on the Schiff base linkage (10,55).

Favrot et al (14,15,24) claim, however, that $\nu_{C=N}$ is not a good indication of whether or not the nitrogen atom is protonated, since its assignment is difficult. They conclude, from an infra red and Raman spectroscopic study of simple unsaturated Schiff bases and their picrate salts, that the Schiff base linkage is hydrogen bonded. Additional support for the hydrogen bond hypothesis comes from a study of the proton/deuterium exchange rate in bacteriorhodopsin (17,18).

The state of protonation has also been examined using $^{13}C$ nmr spectroscopy. In model compounds, the resonance due to C14 occurs at about 130 ppm in the neutral Schiff base and this shifts to about 120 ppm upon protonation, Table 1-2. Shriver et al (56), using retinal enriched at the C14 position, found that the protein bound chromophore has a $^{13}C$ resonance at 130.8 ppm. They concluded that the Schiff base linkage is unprotonated.

Experimental results (42,52,53) indicate that in rhodopsin there is a counterion in the vicinity of C14 (see Figure 1-2) and it has been calculated that such a counterion could cause a downfield shift of the C14 resonance (42). Thus the above result can be explained with a protonated Schiff base linkage. A similar $^{13}C$ nmr study of bacteriorhodopsin exhibited a C14 resonance at 118 ppm consistent with a protonated Schiff base (57). Bacteriorhodopsin has a counterion in the proximity of the β-Ionone ring (43), Figure 1-2, which should not effect the resonance frequency of C14 as is postulated to occur in rhodopsin (42).

Although the state of protonation for the protein/chromophore Schiff base linkage is still somewhat controversial, it is generally believed that the linkage is protonated rather than hydrogen bonded

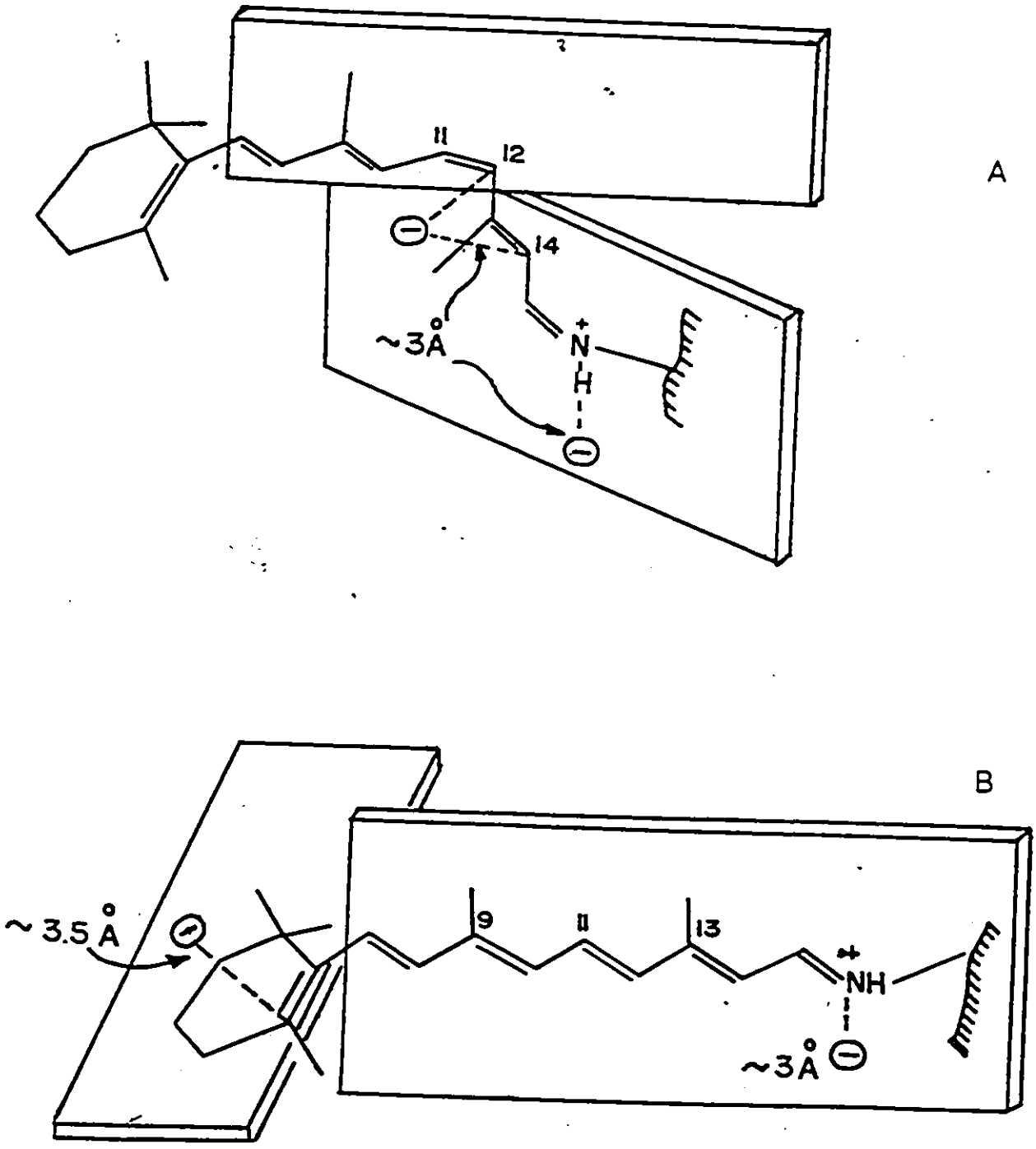


Figure 1-2: External point charge model for (a) bovine rhodopsin and (b) bacteriorhodopsin.

(4,5,7,8).

*Bathochromic Shift*

As discussed previously, 10 in solution absorbs at about 440 nm (27) so that a number of models (14,16,28,41-53) involving a secondary protein/chromophore interaction have been proposed to account for the additional red shift. All of these models assume that either a protonated (28,41-53) or a strongly hydrogen bonded (14,16) Schiff base linkage is present in rhodopsin.

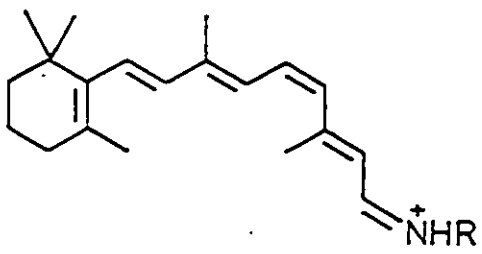


10

Twisting about carbon, carbon double bonds induced by the protein environment could account for a further red shift of the pigment spectrum (44,58). Although this mechanism is possible, one must question why the molecule would twist about double bonds when torsional deformations about single bonds are facile (47).

The solution absorption maximum of 10 can be shifted to about 500 nm by the addition of amino acid analogues suggesting that the polarity or polarizability of the protein environment can significantly alter the absorption maximum (28). The use of such an electrostatic model to explain the bathochromic shift was first proposed by Kropf and Hubbard (51). This model involves the protonation or hydrogen bonding of the Schiff base, a counterion in the vicinity of the nitrogen

atom and a second negatively charged group placed somewhere along the polyene chain (14,16,42,43,46,47). Recent elegant experiments, involving artificial pigments containing various dihydroretinals, indicate that the second charged group is in the region of C12 - C14, Figure 1-2 (42,52,53).

*Primary Photochemical Event*

Upon illumination, rhodopsin reacts to yield eventually all-trans retinal and opsin. This process is termed bleaching because the pink colour of the pigment is lost. The absorption of a photon by the chromophore triggers the sequence of events illustrated in Scheme 1-2.

At physiological temperatures, the primary photoproduct of rhodopsin and isorhodopsin (the pigment formed from 9-cis retinal and opsin) is bathorhodopsin. The observation, in 1963 (59), that there was a photostationary state formed among rhodopsin, bathorhodopsin and isorhodopsin (equation 6) provided the first experimental evidence that the bathorhodopsin chromophore has an all-trans or transoid configuration. This meant that the primary event involved the cis/trans isomerization of the rhodopsin chromophore.

$$\underset{\text{(11-cis)}}{\text{Rhodopsin}} \underset{}{\overset{h\nu}{\rightleftharpoons}} \text{Bathorhodopsin} \overset{h\nu}{\rightleftharpoons} \underset{\text{(9-cis)}}{\text{Isorhodopsin}} \qquad (6)$$

The all-trans configuration for bathorhodopsin was generally accepted until Busch et al (60) showed that bathorhodopsin is formed in less than 6 psec. It was believed by many people that this was not sufficient time for a one bond cis/trans isomerization to occur and a number of models involving proton translocation were proposed

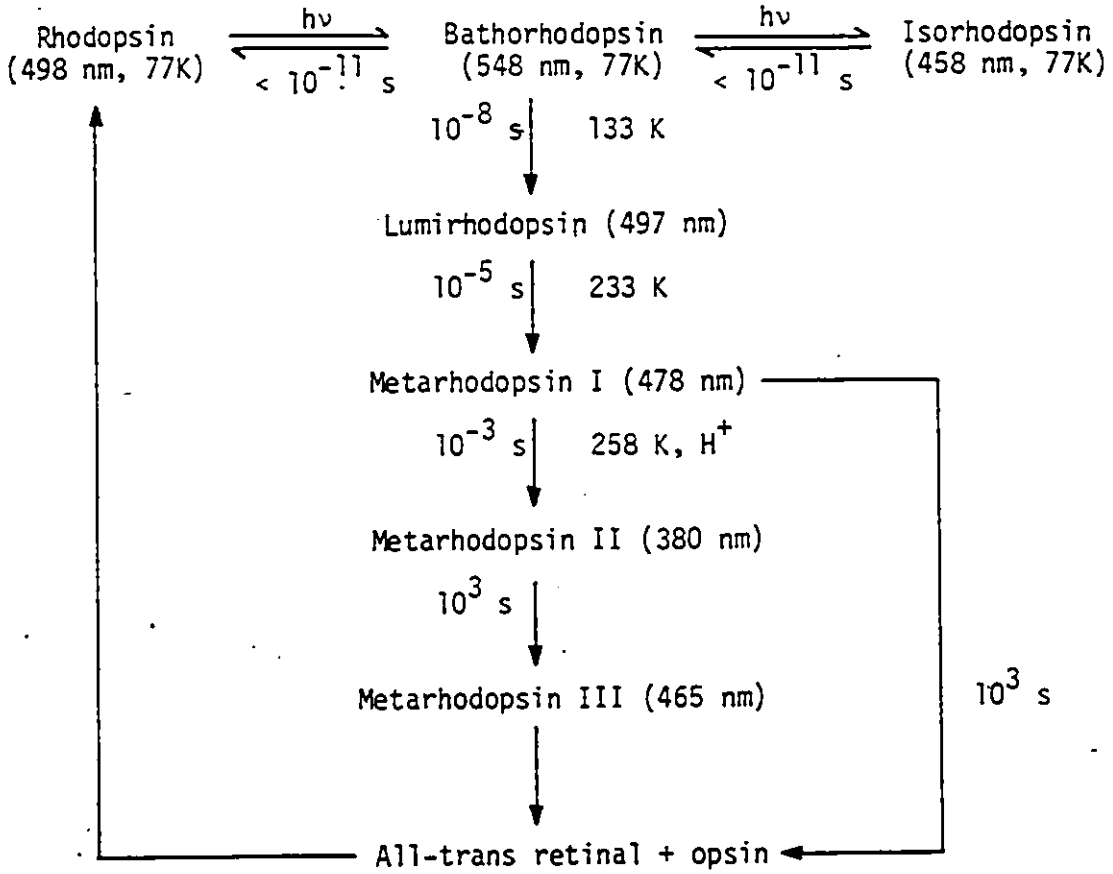


Scheme 1-2: Wavelengths given are absorption maxima and times are the approximate rate of conversion at room temperature.

(14,16,60-66). The observation of a deuterium isotope effect on the rate of formation of bathorhodopsin added weight to these models (61). None of the proton translocation models, however, can adequately account for the photostationary state data (59,67). Recent calculations indicate that photoisomerization could be much faster than originally thought (34,68). A one bond isomerization has been calculated to occur with a high quantum efficiency ($\phi_{calc}$ = 0.61) in about 2 psec (34).

Resonance Raman results have been interpreted to show that bathorhodopsin has a distorted all-trans configuration (69-71) and that this structure is present 30 psec after irradiation (72). These results, coupled with studies of non-bleachable retinal analogues (73,74) and the photostationary state data (59,67), provide substantial evidence that the primary event involves a cis/trans photoisomerization. The deuterium isotope effect remains to be fully explained but a reasonable hypothesis has been presented (75,76).

*Light-Induced Reactions*

Bathorhodopsin is stable up to 133 K and its formation is both wavelength and temperature (down to 77 K) independent. In dark-adapted rhodopsin, bathorhodopsin is formed with a quantum yield of 0.67 while the analogous quantum yield from isorhodopsin is 0.33 (73,77). At temperatures above 133 K, bathorhodopsin is converted to lumirhodopsin (76). Little is known about lumirhodopsin but its rapid formation implies that only minor changes in chromophore and protein configuration have taken place (5,9). The intermediate metarhodopsin I is formed at 233 K (78) and is in thermal equilibrium with metarhodopsin II at temperatures above 258 K (79,80). The metarhodopsin I to meta-

rhodopsin II transition involves, among other things, the deprotonation of the Schiff base linkage and it is believed that this step in the bleaching sequence triggers the transduction mechanism (5,9). At this point the pathway divides (39,80,81), one fraction goes to all-trans retinal while the other goes first through the intermediate metarhodopsin III. The above intermediates, which were first studied in aqueous-glycerol glasses, have all been identified as genuine parts of the rhodopsin photolytic cycle at room temperature (60,61,82-84). All-trans retinal is thermally isomerized back to the 11-cis isomer (9), rhodopsin is reformed, and the process repeats itself. A more detailed discussion of these processes can be found in a number of excellent reviews (4,5,9,85,86).

*Visual Transduction*

The absorption of light ultimately causes a change in potential across the plasma membrane that in some manner blocks the passage of sodium ions ($Na^+$) into the rod outer segment. Salem and Bruckmann (87,88) have suggested that this change in potential is induced by a sudden polarization of the charge distribution in the chromophore upon excitation. The most widely accepted theories, however, assume that some internal transmitter substance is involved (5,9). This transmitter blocks $Na^+$ transmission either by its presence or by its absence. Therefore within the transmitter model of transduction, light either induces an increase or a decrease in transmitter concentration.

It has been shown that both an increase in the concentration of calcium ions ($Ca^{2+}$) (89) and a decrease in the concentration of cyclic nucleotides (90), such as cyclic guanosine monophosphate (cGMP),

mimic the action of light. There is evidence, however, against both of these hypotheses of visual transduction and in fact the validity of the transmitter model itself has been questioned (9).

## CHAPTER 2

## SOME CHEMISTRY OF IMINIUM SALTS[†]

In the previous chapter, the chemistry pertaining to the vision process was reviewed. An iminium salt of 11-cis retinal is believed to be the chromophore for this process, which upon irradiation undergoes an efficient cis/trans isomerization. This photoinduced isomerization is the key step in vision.

In rhodopsin, the corresponding thermal isomerization is a high energy process, whereas bacteriorhodopsin contains two retinal isomers in rapid thermal equilibrium (4,5,92). The probability of thermal isomerization, and hence a nerve impulse, should be negligible in vision to ensure the necessary visual sensitivity (5). Bacteriorhodopsin, on the other hand, is used as a proton pump, so that any thermally induced isomerization will just increase its efficiency in this capacity (5).

Studies of the photochemical and thermal isomerizations in simpler systems could aid in the understanding of the chemistry of the two photoreceptor pigments. Although iminium salts have been used widely in organic synthesis and many of their chemical and physical

---

[†]The IUPAC name for Schiff base is imine and a protonated Schiff base is an iminium salt. In rhodopsin and visual pigment studies the term Schiff base is generally used so that in the discussion of these compounds the non-systematic nomenclature was kept. The systematic names will be used throughout the remainder of this thesis.

properties are known (93), there is comparatively little information about the ground and exicted state chemistry of simple acyclic conjugated systems.

The purpose of this chapter will be to give a brief review of the photochemical reactions and thermal isomerizations of iminium salts. Emphasis will be placed on acyclic systems since the chemistry of such compounds is more pertinent to vision and to the work to be presented in this thesis.

A. Photochemistry

Photochemical studies of iminium salts are scarce. The large majority of the reported work has dealt with the vision process, which has already been discussed (31-33,35,73,77). Some studies of simpler systems have been reported and examples of reactions involving electron transfer processes (94-99), photocyclization (100-102) and cis/trans isomerization (103-105) are known.

*Electron Transfer*

Recent results of Mariano et al (94,95,97-99) show that aryl substituted iminium salts react with electron rich olefins in methanol via an electron transfer process. Reactions of this type are illustrated in equations 7-10.

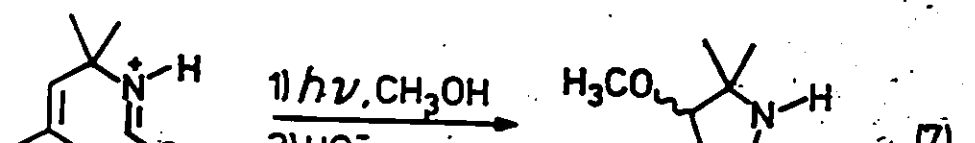


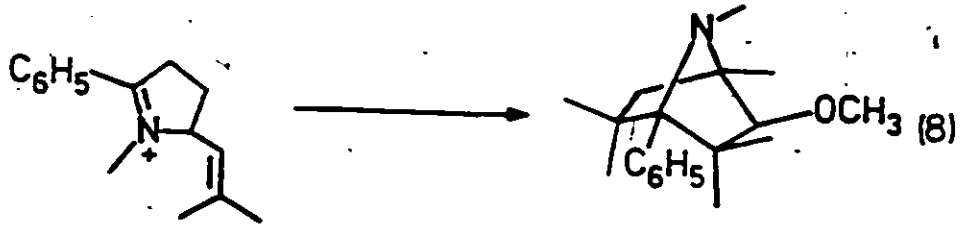

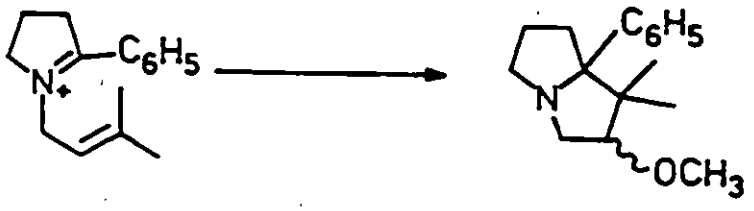

(9)

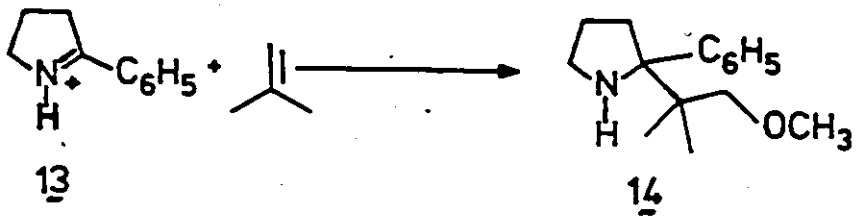

13 14

(10)

All the reactions are thought to proceed by electron transfer from the ground state olefin to the excited state iminium salt and can be rationalized by the mechanism given in Scheme 2-1.

For 13, electron transfer is predicted to occur when the olefin has a π-oxidation potential lower than about 2.6 eV (97). This point is illustrated by the reaction of 13 with electron deficient olefins to give spiro amines such as 15. Reaction is believed to proceed via a 2 + 2 arene-olefin cycloaddition followed by ring expansion rather than electron transfer (95-98).

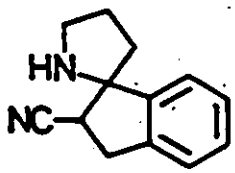

15

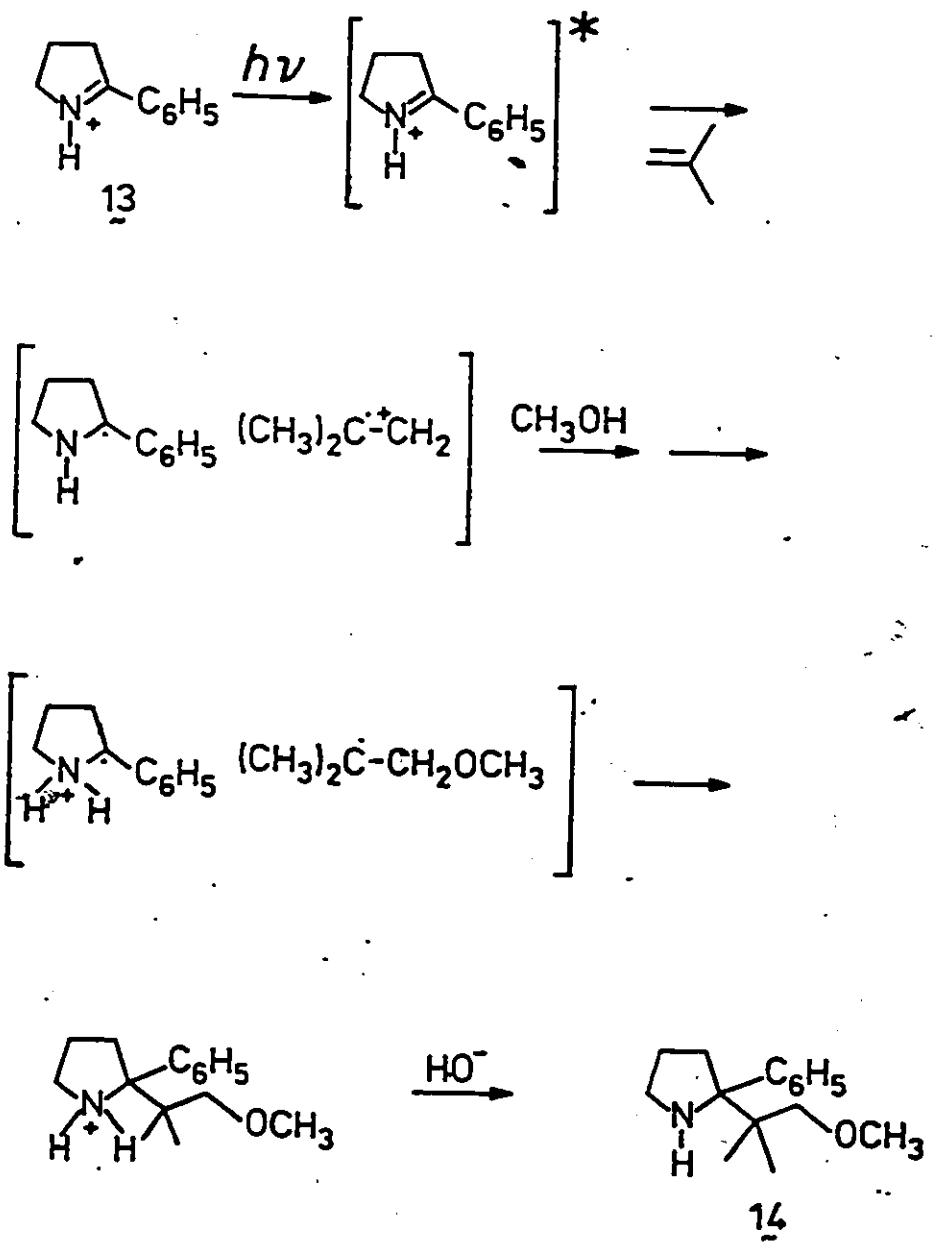

Scheme 2-1

*Photocyclization*

An oxidative photocyclization of benzalaniline, 16, to phenanthridine, 17, occurs in concentrated sulphuric acid (100). The ring closure reaction presumably takes place from the cis configuration and the low yield is consistent with an efficient cis/trans isomerization about the $C=N^+$ bond (100-102). Photoisomerization about a $C=N^+$ bond, however, has not been shown unequivocally.

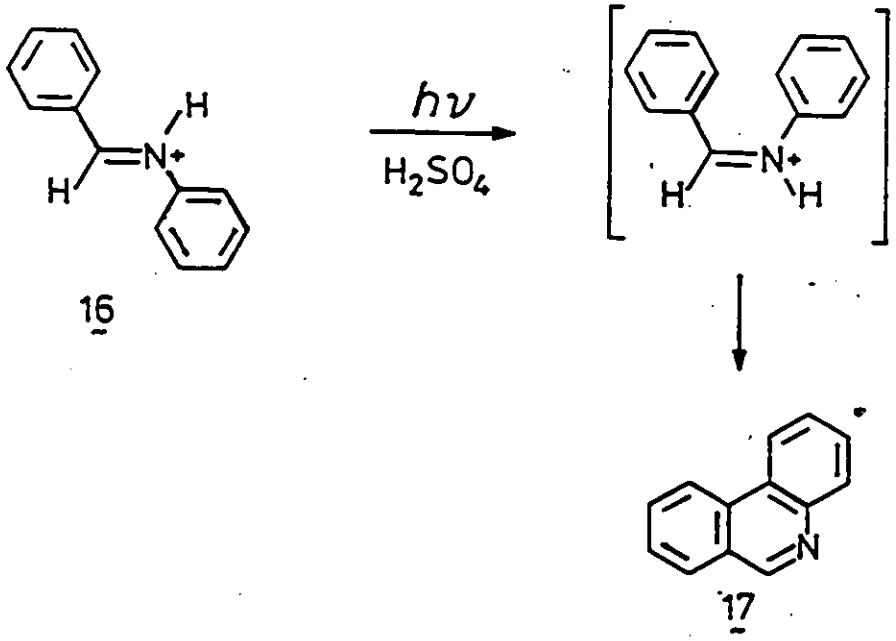


16 17

*Photoisomerism*

The previous example of cyclization implied that a photochemical cis/trans isomerization about the $C=N^+$ bond was possible. Isomerization has been shown to occur about C=C bonds conjugated to an iminium function. Iminium salts of retinals (31,33,35) and rhodopsin itself (73,77) are

the best examples of C=C bond photoisomerization, although stereomutation in simpler systems has been reported.

The 4-substituted quinolinium salt, 18, forms a photostationary state with its geometric isomer, 19, upon irradiation in methanol (105). Photoisomerization is efficient while the rate of thermal equilibration is slow (106,107).

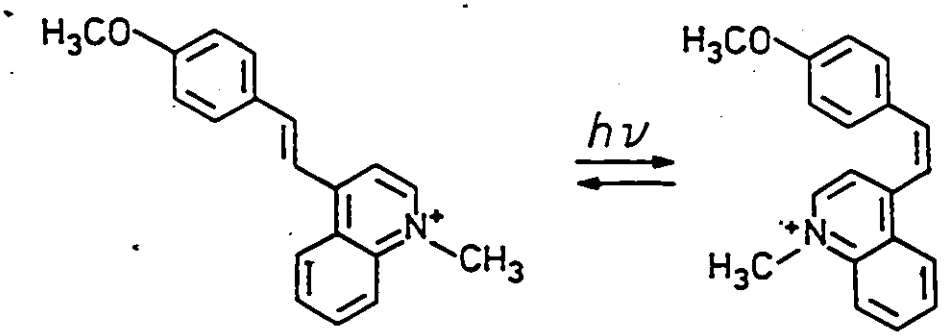


18 19

Efficient cis/trans isomerization of the isomeric cyanine dyes, 20 and 21, has also been observed (103,104). In this case irradiation at low temperature prevents thermal equilibration (104,108).

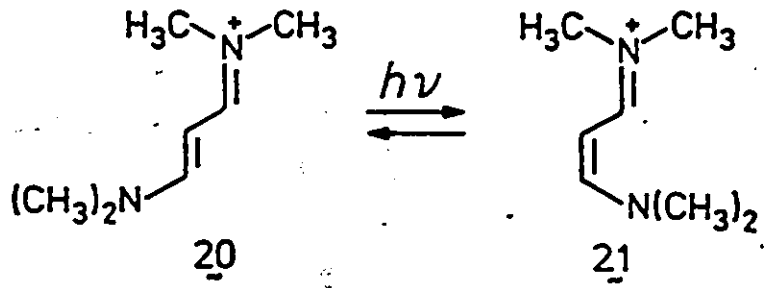


20 21

B. Thermal Isomerism

Thermally-induced cis/trans isomerizations in iminium salts have been reported for a variety of compounds (106-115). Although the majority of accounts have dealt with $C=N^+$ bond isomerization (108-114), there are also a few reports of the isomerization about a C=C bond (106,107,110,115) conjugated to an iminium function.

The salts 20 and 22 to 25 are typical examples of compounds which exhibit stereomutation about a $C=N^+$ bond (see Table 2-1) (108-114). Bacteriorhodopsin, which contains two isomeric retinal chromophores in thermal equilibrium (4,5), is the best example of an iminium system which undergoes isomerization about a conjugated double bond although the salts 19 (106,107,115) and 22 (110) have been examined, Table 2-1.

Isomerization about a $C=N^+$ and a C=C bond can be accomplished by a range of intra and intermolecular pathways. These mechanisms are discussed with reference to the iminium salts 26 and 27.

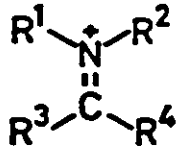

26

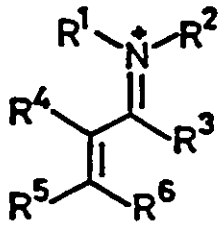

27

*Intramolecular Mechanisms*

Rotation and electrocyclic ring closure and re-opening are possible intramolecular pathways for both $C=N^+$ and C=C bond stereo-

Table 2-1

Iminium Salt Isomerization Data

| Compound | $\Delta G^{\ddagger}$(kcal/mol) | Compound | $\Delta G^{\ddagger}$(kcal/mol) |
|---|---|---|---|
| 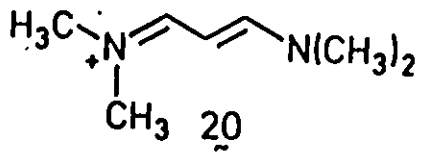 20 | 21.5[a] | 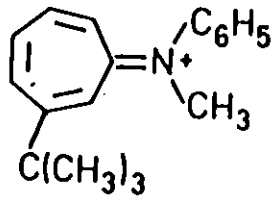 24 | 16.0[d] |
| 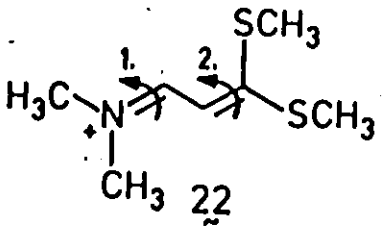 22 | (1) 22.5[b]<br>(2) 18.7[b] | 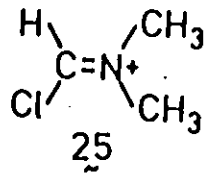 25 | 21.1[e] |
| 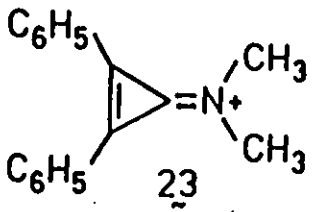 23 | 24.0[c] | 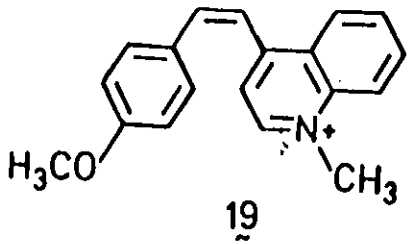 19 | 24.1[f] |

[a]Reference 108; [b]Reference 110; [c]Reference 112; [d]Reference 113; [e]Reference 114; [f]Reference 106 and 107

mutation. A lateral shift mechanism, which is a favourable process for C=N bond isomerization in many imines (116-120), is not possible in iminium salts since the nitrogen lone pair is employed in bonding.

Isomerization about the $C=N^+$ bond in salts 20 and 22 to 24 and C=C bond isomerization in 19 and 22 is believed to occur by the rotation mechanism. What changes in charge distribution might be expected in these reactions? The transition state involved in each case could be one of two possible extremes - 28 or 29, and 30 or 31 are conceivable for $C=N^+$ and C=C bond stereomutation respectively.

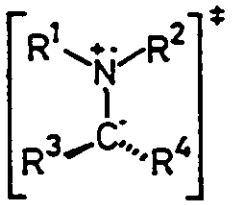

28

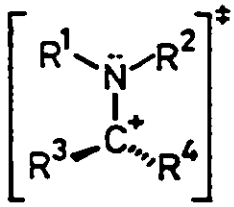

29

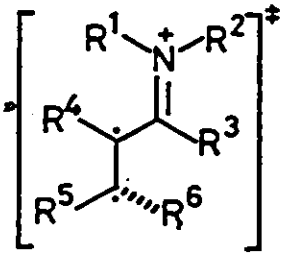

30

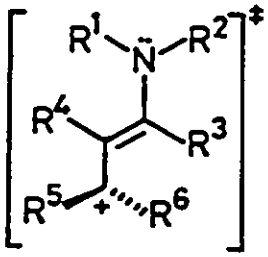

31

The low free energies of activation (see Table 2-1) for stereomutation about either type of double bond in the salts 19, 20 and 22 to 24 are significant. All of these systems contain good positive charge stabilizing substituents which appears to support the charge distrib-

utions illustrated in 29 and 31.

A pathway involving electrocyclic ring closure and re-opening (equation 11) requires the presence of conjugated carbon, carbon double bonds and involves simultaneous $C=N^+$ and C=C bond isomerization. The process can only occur from an s-cis conformation of the conjugated iminium salt. Although this mechanism, to my knowledge, has not been considered for iminium salts it was suggested to occur in the thermal isomerization of the related protonated enones (124).

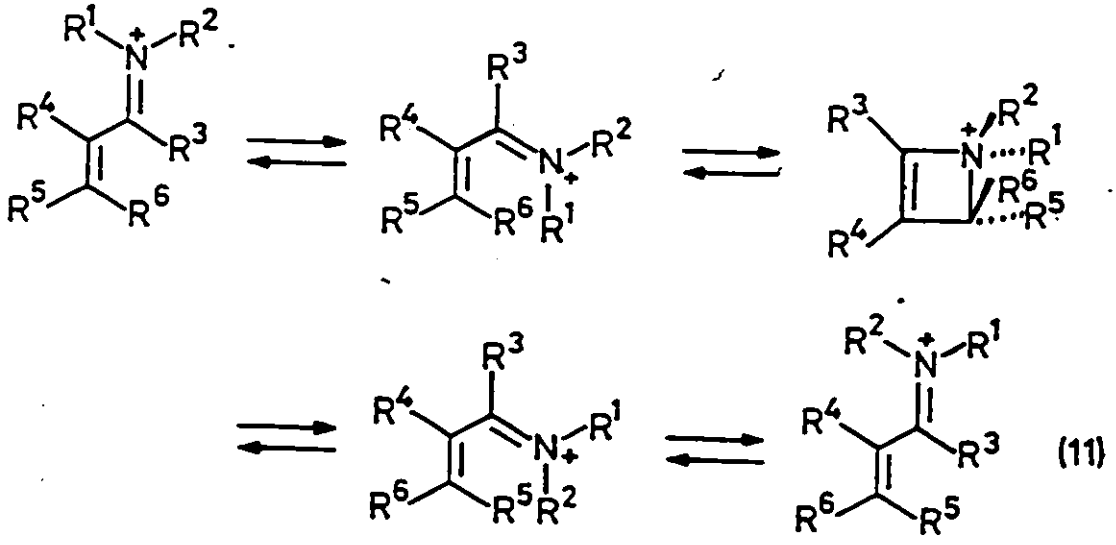

(11)

*Intermolecular Mechanisms*

There are two conceivable intermolecular processes by which double bond stereomutation could be achieved. First, addition of a nucleophile at C1 or C3 (Michael addition) could result in $C=N^+$ or C=C bond isomerization respectively. A second more poorly defined mechanism involves deprotonation followed by isomerization of the resulting imine or enamine.

Stereomutation about a $C=N^+$ bond via addition of a nucleophile (equation 12) has been observed for chloro-iminium salt 25, Table 2-1

(114) and Michael addition (equation 13) has been proposed as a possible mechanism for an enzyme-catalysed C=C bond isomerization of a retinal iminium salt (125). It has also been reported that, in solution, an iminium salt of 13-cis retinal undergoes Michael addition (126).

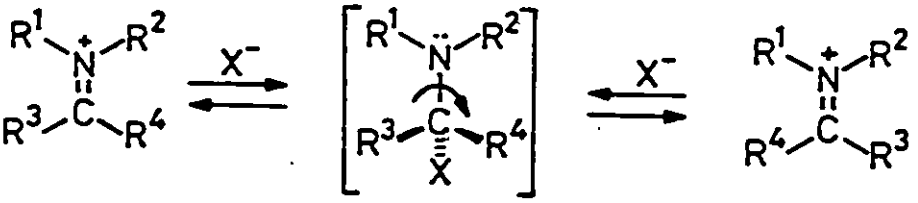

(12)

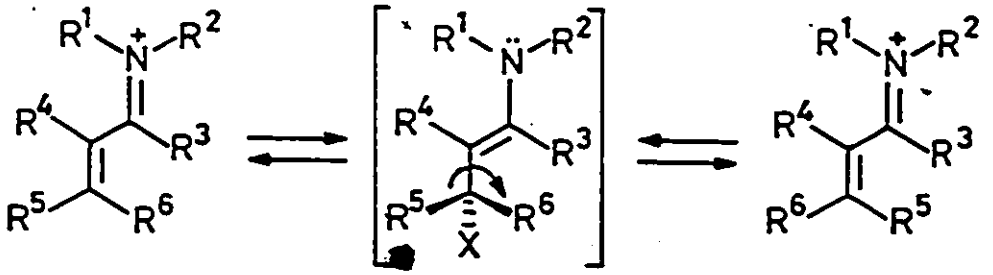

(13)

The deprotonation mechanism (equations 14 and 15) can occur if $R^1$ and/or $R^2$ = H or if there is an appropriately situated alkyl group. Isomerization of the imine can proceed by a variety of pathways (117, 121-123,126). This process has not been unambiguously established for $C=N^+$ bond isomerization (111) but it has been suggested as a possible mechanism for the thermal equilibration of the retinal isomers in bacteriorhodopsin (127).

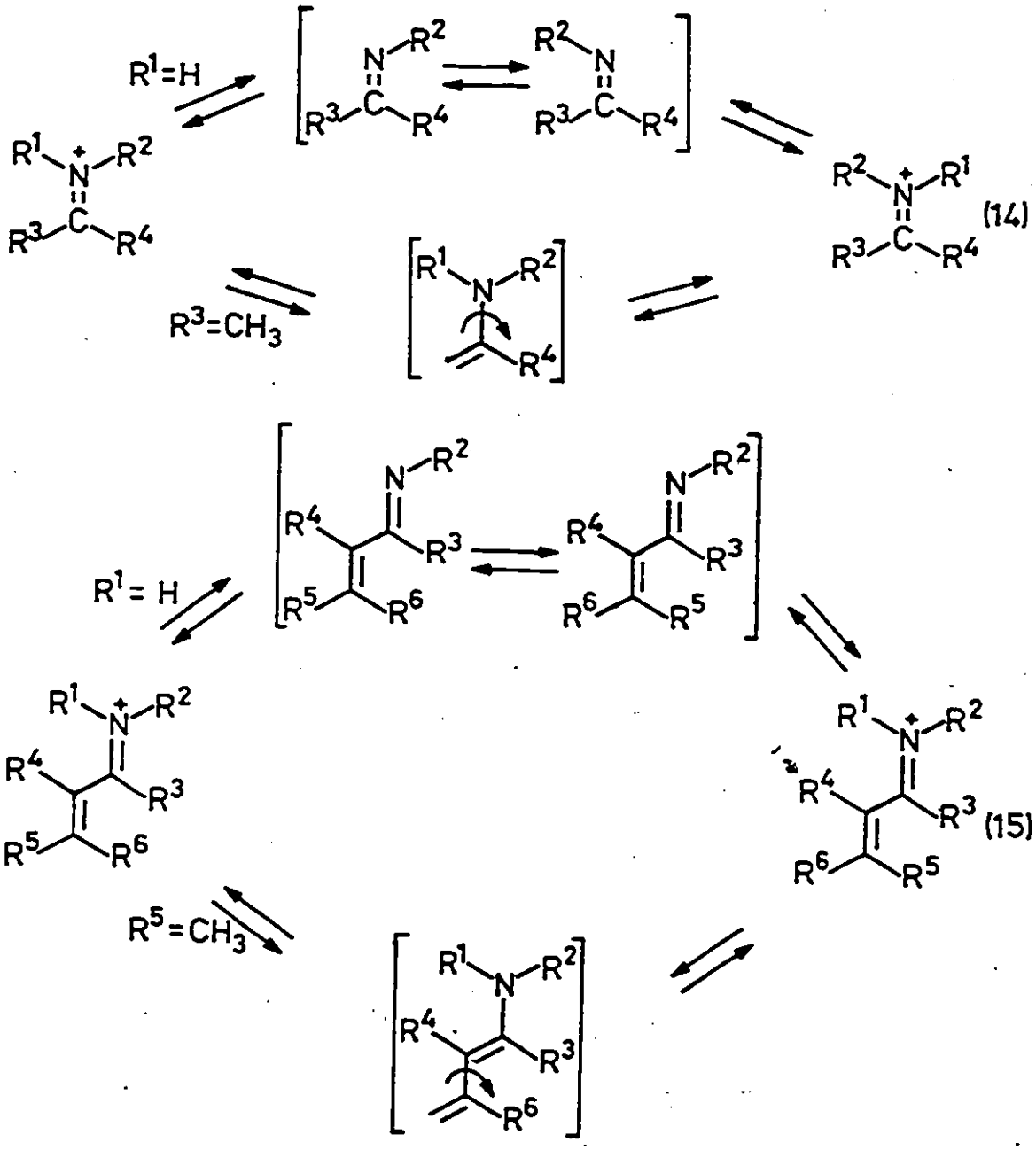


(14)

(15)

Although this review is brief, it gives some idea of the lack of chemical information about the ground and excited state properties of simple aliphatic conjugated iminium salts. This seems surprising considering the great interest in the two photoreceptor pigments, rhodopsin and bacteriorhodopsin.

In order to alleviate this problem I undertook the study of a

series of α,β-unsaturated iminium salts. The topics to be addressed in this thesis are briefly outlined below.

The conformation and charge distribution in the rhodopsin chromophore have been examined by experimental ($^{1}H$ and $^{13}C$ nmr spectroscopy) and theoretical techniques. Chromophore conformation, however, remains unknown and the charge delocalization suggested by nmr data and theoretical calculations has yet to be substantiated by structural information. To gain further insight into these factors the same techniques were used to examine the above properties in a series of simpler α,β-unsaturated iminium salts where electronic factors could easily be altered by substituent changes. Moreover, single crystal x-ray structure determination was employed to confirm chain conformation and to inspect the extent of charge delocalization.

Other than the work on rhodopsin, bacteriorhodopsin and some iminium salts of retinals there are few reports of photoisomerizations in conjugated iminium salts. Due to their complexity, the natural and in vitro retinal iminium salts are difficult to examine. The large number of bonds about which isomerizations can occur, particularly in solution, complicates the analysis of experimental results. An examination of C=C bond photoisomerization in simpler conjugated systems, in which solvent and substituent effects can be more easily monitored, could reveal some of the excited state properties of this process. There is also the possibility of observing $C=N^{+}$ bond photoisomerization which, as far as I am aware, has not been unambiguously reported.

Another area in which accounts are lacking is the thermal isomerization of iminium salts. This is particularly true for the

isomerization about conjugated C=C bonds. Bacteriorhodopsin, which contains two retinal chromophores in thermal equilibrium, has been examined superficially. Again, due to the complexity, a solution study of thermal stereomutations in retinal iminium salts would be arduous. Inspection of an α,β-unsaturated system, in which experimental variables are more easily defined, could give some insight into the likely isomerization pathways of conjugated iminium salts.

# RESULTS AND DISCUSSION

# CHAPTER 3

## THE STRUCTURE OF IMINIUM SALTS

Despite the importance of iminium salts, there is comparatively little definitive evidence about their structures and extent of charge delocalization. Nmr studies (9,19,20,22,29,30) and theoretical calculations (29,128,137) have been reported but very few crystal structure determinations (141,142). A retinal iminium salt structure reported by Hamanaka et al at the 12th Annual Meeting of the Biophysical Society in Japan in 1973 has been referenced (128), but to my knowledge, has not appeared in the open literature. In this chapter the question of the structures and charge distributions of some α,β-unsaturated iminium salts is addressed (129).

Before presenting the results of work carried out it is important to define the possible stereo- and conformational isomers which can exist for an α,β-unsaturated iminium salt. In these iminium salts there are three partial double bonds and while the magnitudes of the rotational barriers might be expected to differ there are eight different isomers possible. These isomers are illustrated in Figure 3-1.

The naming of these various isomers is important so as to prevent confusion in the discussion which is to follow. The older method was to define each formal double bond as being either cis or trans and to

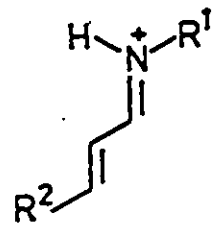

s-trans, trans, trans

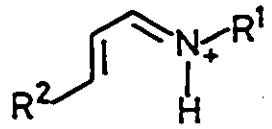

s-cis, trans, trans

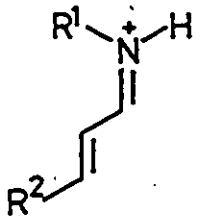

s-trans, cis, trans

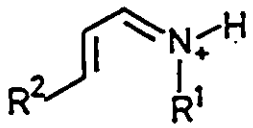

s-cis, cis, trans

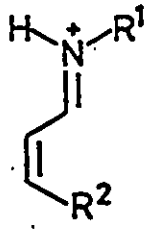

s-trans, trans, cis

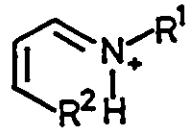

s-cis, trans, cis

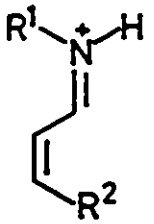

s-trans, cis, cis

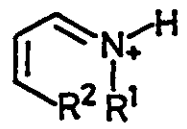

s-cis, cis, cis

Figure 3-1: Stereo- and conformational isomers of an α,β-unsaturated iminium salt.

use the term s-cis or s-trans to define the conformation about the C1,C2 bond. This type of nomenclature is still widely used in the literature, especially by workers in the area of the visual pigments. For this reason this nomenclature was used in the introduction of this thesis. Although it has been recommended that the E,Z notation be employed to distinguish between the various isomers (145) I have decided, for the sake of continuity, to maintain the use of the older system.

A. Preparation of Imines and Iminium Salts

The imines 32 to 36 were prepared by condensation of the appropriate amine and trans aldehyde, equation 16 (148). The corresponding iminium salts, 37 to 41 were formed by dissolving the imines in fluorosulphonic ($FSO_3H$), 96% sulphuric ($H_2SO_4$) or trifluoroacetic (TFA) acids, equation 17. The dimethyliminium perchlorate salts, 42 to 46, were synthesized by the reaction of dimethylammonium perchlorate with the appropriate trans aldehyde, equation 18 (149,150).

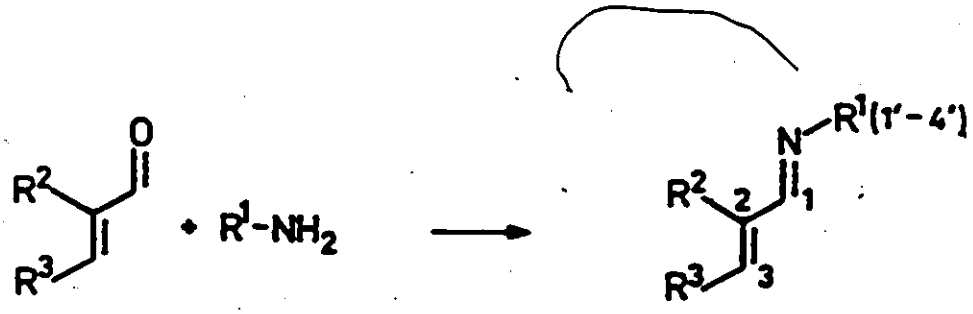


(16)

32 $R^1$=t-Bu, $R^2$=H, $R^3$=$CH_3$
33 $R^1$=n-Bu, $R^2$=$R^3$=$CH_3$
34 $R^1$=n-Bu, $R^2$=$CH_3$, $R^3$=H
35 $R^1$=n-Bu, $R^2$=H, $R^3$=$C_6H_5$
36 $R^1$=n-Bu, $R^2$=H, $R^3$=p-$NO_2C_4H_4$

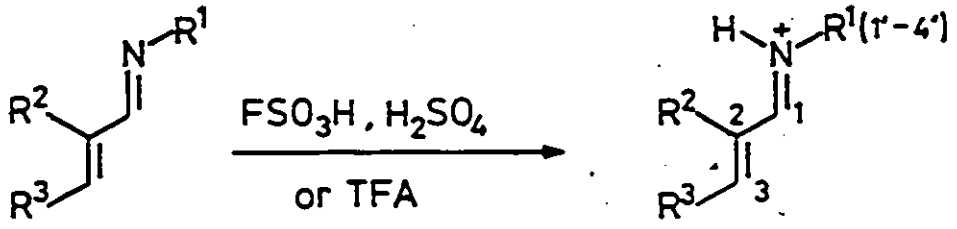


(17)

32–36

37 $R^1$=t-Bu, $R^2$=H, $R^3$=$CH_3$
38 $R^1$=n-Bu, $R^2$=$R^3$=$CH_3$
39 $R^1$=n-Bu, $R^2$=$CH_3$, $R^3$=H
40 $R^1$=n-Bu, $R^2$=H, $R^3$=$C_6H_5$
41 $R^1$=n-Bu, $R^2$=H, $R^3$=p-$NO_2C_4H_4$

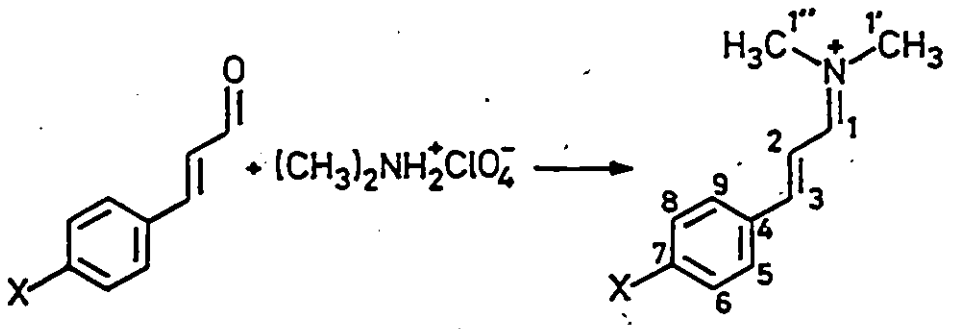


(18)

42 X=H
43 X=$OCH_3$
44 X=$CH_3$
45 X=Cl
46 X=$NO_2$

Except for the iminium salts 37, 38 and 40, which contain minor isomeric impurities, all the cations were formed in a unique isomeric form. The configurations of the cation structures illustrated in equations 17 and 18 are consistent with the $^1$H nmr data summarized in Tables 3-1 and 3-2. A detailed discussion of their assignment follows. The proton chemical shifts were not dependent on the acid

medium used and all compounds had satisfactory elemental analyses.

B. Double Bond Configurations

The configuration about the $C=N^+$ and C=C bonds was defined by examination of the proton,proton coupling constants across these bonds. For the $C=N^+$ bond a coupling constant ($J_{N,1}$) of 16 - 18 Hz is indicative of a trans configuration (19,133,134), whereas a value of about 12 Hz would be consistent with a cis configuration (134). Typical values for the corresponding coupling constant across a C=C bond ($J_{2,3}$) are 14 - 17 Hz and 10 - 14 Hz for the trans and cis configurations respectively (135).

As the data in Tables 3-1 and 3-2 show, cations 37 to 41 have a coupling constant across the $C=N^+$ bond of about 17 Hz indicative of a trans configuration. Cations 42 to 46 are symmetrically substituted about this bond so that its configuration cannot be defined. Except for 38 and 39, the coupling constant across the C=C bond ($J_{2,3} \sim 15$ Hz) for each salt is indicative of a trans configuration. Cation 38 has a methyl substituent at C2 so that this coupling is eliminated. The starting aldehyde, however, had a trans configuration and by analogy to the other cations this is not expected to change upon salt formation. Configuration about the C=C bond in 39 cannot be defined due to symmetric substitution at C3.

The isomeric impurities in 37 and 38 were identified as the trans,cis-isomers whereas the impurity in 40 was found to be the cis,trans-isomer. Confirmation for these structures was provided by the analysis of $^1H$ nmr chemical shift data and proton, proton coupling constants. A detailed discussion is given in Chapter 4.

Table 3-1

$^1H$ nmr data for Aliphatic Imines and Iminium Salts

| Compound | Chemical Shift[a] (ppm) | | | | | | | | | Coupling Constant (Hz) | | | |
|---|---|---|---|---|---|---|---|---|---|---|---|---|---|
| | H1 | $R^2$ | H3 | $R^3$ | N-H | H1' | H2' | H3' | H4' | $J_{N,1}$ | $J_{1,2}$ | $J_{2,3}$ | $J_{3,CH_3}$ |
| 32[b] | 7.85d | 6.23m | 6.23m | 1.88d | - | - | 1.19s | - | - | - | 7.5 | - | 5.0 |
| 33[b] | 7.77s | 1.84s | 5.90q | 1.81d | - | 3.40t | 1.66m | 1.38m | 0.94t | - | - | - | 6.0 |
| 34[b] | 7.80s | 1.83d | 5.44s[d] | 5.23s[d] | - | 3.40t | 1.66m | 1.38m | 0.94t | - | - | - | - |
| 37[c] | 8.14dd | 6.48dd | 7.29dq | 2.03d | 9.2bd | - | 1.38s | - | - | 17.4 | 10.1 | 14.8 | 6.9 |
| 38[c] | 8.08d | 1.85s | 7.09q | 2.01d | 9.2bd | 3.69q | 1.66m | 1.28m | 0.83t | 17.1 | - | - | 7.3 |
| 39[c] | 8.26d | 2.07s | 6.56s[d] | 6.47s[d] | 9.2bd | 3.85q | 1.68m | 1.32m | 0.85t | 17.6 | - | - | - |

a bd = broad doublet, d = doublet, dd = doublet of doublets, m = multiplet, q = quartet, dq=doublet of quartets, s = singlet, t = triplet.

b in ppm from TMS in $CDCl_3$.

c in ppm from $(CH_3)_4N^+BF_4^-$ (3.10 ppm) in TFA.

d assignment could be reversed.

Table 3-2

$^1H$ nmr data for Aromatic Imines and Iminium Salts

| | Chemical Shift[a,b] (ppm) | | | | | | | | | | | | Coupling Constant (Hz) | | |
|---|---|---|---|---|---|---|---|---|---|---|---|---|---|---|---|
| Compound | H1 | H2 | H3 | Aryl | H | | N-H | H1'/H1" | H2' | H3' | H4' | Other | $J_{N,1}$ | $J_{1,2}$ | $J_{2,3}$ |
| 35[c] | 8.01d | 6.91d | 6.89s | 7.28m | 7.45d | | - | 3.51t | 1.66m | 1.38m | 0.94t | | - | 7.6 | - |
| 36[c] | 8.07m | 7.00m | 6.95s | 7.58d | 8.23d | | - | 3.51t | 1.60m | 1.31m | 0.90t | | - | - | - |
| 40 | 8.25dd | 7.06dd | 7.75d | 7.32dd | 7.42d | 7.52d | 9.2bd | 3.70q | 1.68m | 1.32m | 0.85t | | 17.2 | 10.3 | 15.5 |
| 41 | 8.43dd | 7.23dd | 7.83d | 7.73d | 8.20 | | 9.2bd | 3.77q | 1.71m | 1.33m | 0.85t | | 16.5 | 9.8 | 15.9 |
| 42 | 8.20d | 7.08dd | 7.79d | 7.34dd | 7.43d | 7.60d | - | 3.50s/3.59s[d] | | | | | - | 10.6 | 15.3 |
| 43 | 8.09d | 6.92dd | 7.71d | 7.61d | 6.92d | | - | 3.45s/3.54s[d] | | | | 3.82s | - | 10.8 | 14.8 |
| 44 | 8.13d | 7.01dd | 7.74d | 7.44d | 7.16d | | - | 3.47s/3.56s[d] | | | | 2.26s | - | 10.8 | 14.8 |
| 45 | 8.20d | 7.05dd | 7.73d | 7.52d | 7.30d | | - | 3.50s/3.59s[d] | | | | | - | 10.8 | 15.5 |
| 46 | 8.36d | 7.29dd | 7.86d | 8.20d | 7.81d | | - | 3.60s/3.67s[d] | | | | | - | 10.3 | 15.5 |

a bd = broad doublet, d = doublet, dd=doublet of doublets, m = multiplet, q = quartet, s = singlet, t = triplet.

b in ppm from $(CH_3)_4N^+BF_4^-$ (3.10 ppm) in TFA.

c in ppm from TMS in $CDCl_3$.

d assignment could be reversed.

The $^1H$ nmr spectral data for salts 42 to 46 (see Table 3-2) show two separate resonances for the protons of the methyl groups bonded to nitrogen and cation 39 has two signals for the C3 protons (see Table 3-1). These results indicate that rotation about the $C=N^+$ and C=C bonds is slow on the nmr time scale. In salts 42 to 46 there is only one signal each for the pairs of ortho and meta ring protons indicating that rotation about the C3,C4 bond is rapid. Conformation about the C1,C2 bond cannot be unequivocally established from these data. The presence of a single resonance for each type of proton is consistent with the existence of one conformation (s-trans or s-cis) or a rapid equilibration of the two conformers.

C. Charge Distribution

Three approaches have been used to probe the ground state charge distribution of iminium salts - theoretical calculations, an analysis of the chemical shifts of their $^{13}C$ nmr spectra and x-ray crystallography (129,130). The latter technique has the advantage of providing conformational information.

*Theoretical Calculations*

Previous theoretical studies on imine and iminium systems have revealed that upon protonation alterations in the bond lengths and $\pi$ and atom electron densities take place (29,128,137). Iminium salt formation causes the formal double bonds to lengthen and the formal single bonds to shorten. Mulliken populations show a similar alternation. The electron densities of the odd numbered carbons decrease upon protonation while those of the even numbered carbons increase.

The MINDO/3 method was used for the calculations in this work. This method was chosen primarily to probe ground state energy surfaces in the thermal isomerizations of α,β-unsaturated iminium salts which are discussed in Chapter 5. The inexpensive operating costs and known reliability were the principal determining factors in the selection of the MINDO/3 method.

MINDO/3 energies, Mulliken populations and bond lengths for the parent enimine 47, and its protonated conformers 48a and 48b, are summarized in Table 3-3. Kollman (137) has determined the relative energies and Mulliken populations of 48a and 48b using a STO-3G basis set. These data are given in Table 3-4. Although these properties are expected to be substituent dependent, the parent system should give a good indication of the gross changes which occur upon protonation.

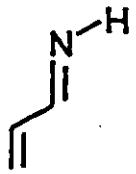

47

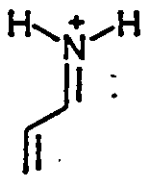

48a

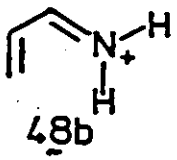

48b

The relative energy difference between 47 and 48 (∿ 140 kcal/mol) given in Table 3-3 appears large. However, it must be remembered that these energies correspond to gas phase species. Thus the cations, which do not have the stabilizing influences of counterion and solvent interactions, are expected to have a calculated energy much higher than the neutral imine.

MINDO/3 results show that conformer 48b is favoured over 48a by

Table 3-3

MINDO/3 Energies, Mulliken Populations and Bond Lengths[a]

| Compound | Relative Energy (kcal/mol) | Mulliken Populations | | | | | | | | Bond Lengths (Å) | | |
|---|---|---|---|---|---|---|---|---|---|---|---|---|
| | | N(total) | (π) | C1(total) | (π) | C2(total) | (π) | C3(total) | (π) | C1,N | C1,C2 | C2,C3 |
| 47 | 0 | 7.19 | 1.16 | 5.77 | 0.85 | 6.01 | 1.02 | 6.00 | 0.97 | 1.26 | 1.47 | 1.33 |
| 48a | 143.2 | 6.91 | 1.46 | 5.68 | 0.66 | 6.12 | 1.14 | 5.81 | 0.74 | 1.28 | 1.45 | 1.34 |
| 48b | 140.2 | 6.93 | 1.45 | 5.68 | 0.67 | 6.11 | 1.13 | 5.83 | 0.75 | 1.28 | 1.45 | 1.34 |

a This work.

Table 3-4

STO-3G Energies and Mulliken Populations[a]

| Compound | Relative Energy (kcal/mol) | Mulliken Populations | | | | | | | |
|---|---|---|---|---|---|---|---|---|---|
| | | N(total) | (π) | C1(total) | (π) | C2(total) | (π) | C3(total) | (π) |
| 48a | 0 | 7.31 | 1.52 | 5.76 | 0.63 | 6.08 | 1.12 | 6.01 | 0.74 |
| 48b | 6.2 | 7.31 | 1.52 | 5.76 | 0.62 | 6.07 | 1.09 | 6.02 | 0.78 |

a from reference 137.

2.8 kcal/mol although the STO-3G results of Kollman (137) show that 48a is favoured by 6.2 kcal/mol. The MINDO/3 method is known to give poor results for the energy difference between the butadiene conformers (138). However, these differences are small pointing out the similarity in energy of the two conformers. The starting aldehydes are thought to exist in an s-trans conformation (136) and the iminium moiety, which has a higher steric requirement than the aldehyde oxygen, is not expected to alter this equilibrium significantly. It must be admitted at this point, however, that the evidence for the preference for one conformer is weak.

It can be seen from the MINDO/3 results that iminium salt formation causes an increase in the $\pi$ electron density at N (1.16 to 1.46) and C2 (1.02 to 1.14) but causes a decrease at C1 (0.85 to 0.66) and C3 (0.97 to 0.74). These changes in Mulliken $\pi$ population are consistent with the CNDO/2 results of Inoue et al (29) and the $\pi$ electron densities of 48 are similar to those determined by Kollman, Table 3-4 (137).

Upon protonation total Mulliken populations determined by MINDO/3 decrease at N (7.19 to 6.91), C1 (5.77 to 5.68) and C3 (6.00 to 5.81) and increase at C2 (6.01 to 6.12). The total electron densities at N and C3 for 48 found here are in contrast with the STO-3G results (see Table 3-4). Although there are no STO-3G results for the parent enimine 47 with which to calculate the electron density changes, it would appear that the STO-3G method predicts that there is no positive charge on C3 for the iminium salt. This is also inconsistent with the $^{13}C$ nmr results for retinal iminium salts (20,29,30) and the $^{13}C$ nmr data discussed in the following section (129).

MINDO/3 bond lengths for 47 and 48 reveal that salt formation causes the formal double bonds to lengthen while the formal single bond shortens. These results are similar to those calculated by Kakitani and Kakitani (128) using a self-consistent HMO method for a retinal imine and its iminium salt. Although the MINDO/3 bond length changes are small they are indicative of the charge delocalization illustrated by the MINDO/3 electron density changes.

Although the MINDO/3 method incorrectly predicts that 48b is favoured over 48a the remaining results are in good agreement with previous calculations (29,128,137). In summary, MINDO/3 data predict that protonation causes a positive charge build up at C1 ($\sim$ +0.10) and C3 ($\sim$ +0.20) and an increase of negative charge at C2 ($\sim$ -0.10). These changes are accompanied by a small increase of the C=N and C=C bond lengths and decrease of the C-C bond length.

*Analysis of $^{13}C$ Chemical Shifts*

In a magnetic field the electrons shield the nucleus such that it experiences a field strength marginally less than the external field. The mathematical expression defining this shielding factor contains a term involving the atom electron density (144). Thus, as the atom electron density decreases the magnetic resonance frequency of the nucleus shifts to lower magnetic field strength. As a consequence, chemical shifts and particularly $^{13}C$ nmr chemical shifts have been used as a probe for charge density of organic ions.

The $^{13}C$ signals given in Tables 3-5 and 3-6 were assigned by various proton off-resonance and selective decoupling experiments. The separate resonances observed for each of the methyl carbons on nitrogen

Table 3-5

$^{13}C$ NMR Data for Aliphatic Imines and Iminium Salts

| | Chemical Shift (ppm) | | | | | | | | |
|---|---|---|---|---|---|---|---|---|---|
| Compound | C1 | C2 | C3 | $R^2$ | $R^3$ | C1' | C2' | C3' | C4' |
| 32[a] | 156.9 | 133.1 | 139.0 | - | 17.9 | 56.3 | 29.4 | - | - |
| 33[a] | 165.3 | 137.1 | 135.4 | 11.3 | 14.0 | 61.1 | 33.4 | 20.5 | 13.9 |
| 34[a] | 163.5 | 144.0 | 123.1 | 17.1 | - | 61.1 | 33.1 | 20.5 | 13.9 |
| 37[a] | 167.7 | 123.7 | 166.8 | - | 19.9 | 60.7 | 26.6 | - | - |
| 38[b] | 174.7 | 131.4 | 165.4 | 9.1 | 16.7 | 53.4 | 30.9 | 19.7 | 13.0 |
| 39[c] | 173.8 | 136.4 | 145.9 | 13.1 | - | 53.2 | 30.0 | 18.7 | 11.4 |

a - in ppm from TMS in $CDCl_3$

b in ppm from ext. TMS in $FSO_3D$

c in ppm from $\underline{C}F_3CO_2D$ (114.5) in TFA-d

Table 3-6

$^{13}C$ NMR Data for Aromatic Imines and Iminium Salts

| Compound | Chemical Shift[a] (ppm) | | | | | | | | | | | |
|---|---|---|---|---|---|---|---|---|---|---|---|---|
| | C1 | C2 | C3 | C4 | C5,9 | C6,8 | C7 | C1'/C1" | C2' | C3' | C4' | Others |
| 35[b] | 162.31 | 128.47 | 141.04 | 135.92 | 127.15[d] | 128.95[d] | 128.76 | 61.31 | 33.10 | 20.46 | 13.88 | |
| 40[c] | 172.08 | 120.48 | 159.21 | 135.22 | 131.01[d] | 130.80[d] | 134.43 | 53.78 | 31.85 | 20.63 | 13.84 | |
| 42 | 171.29 | 117.80 | 162.01 | 135.12 | 131.54 | 130.81 | 134.97 | 50.28/42.17[e] | - | - | - | |
| 43 | 170.78 | 115.02 | 162.01 | 127.96 | 134.17 | 116.34 | 166.03 | 49.84/41.73[e] | - | - | - | 56.71 |
| 44 | 171.22 | 116.70 | 162.38 | 132.56 | 131.69 | 131.54 | 146.96 | 50.06/42.02[e] | - | - | - | 21.92 |
| 45 | 171.22 | 118.31 | 160.26 | 133.80 | 132.85 | 130.88 | 140.53 | 50.42/42.31[e] | - | - | - | |
| 46 | 171.44 | 121.36 | 158.29 | 140.67 | 123.20 | 125.55 | 151.47 | 50.86/42.82[e] | - | - | - | |

a in ppm from TMS in $CD_3NO_2$. Numbering of carbons as in text.

b in ppm from TMS in $CDCl_3$.

c $CD_3NO_2$/TFA solvent.

d assignment could be reversed.

e N-$CH_3$ groups, assignment could be reversed.

for salts 42 to 46 again implies that rotation about the $C=N^+$ bond is slow on the nmr time scale while the magnetic equivalence of the ortho and meta ring carbons supports the conclusion reached from a consideration of the $^1H$ nmr spectra that rotation about the C3,C4 bond is rapid.

Comparison of the data for the imines 32 to 35 with that of their corresponding acid salts 37 to 40 shows the typical pattern of chemical shift changes which are associated with the conversion of retinal imines to their iminium salts (20,29,30). Upon protonation the C1 resonance of the imine exhibits a modest (6 to 10 ppm) downfield shift, the C2 resonance shifts upfield (8 to 10 ppm) and the signal due to C3 moves to substantially (20 to 30 ppm) lower field.

Examination of a series of cationic, neutral and anionic molecular species has led to an empirical correlation of $^{13}C$ chemical shift changes and atomic electron density. This relationship states that a positive or negative charge localized on a carbon atom will result in a chemical shift change of about 180 ppm/electron (147). The application of this relationship to the $^{13}C$ nmr data in Tables 3-5 and 3-6 reveals that protonation causes a positive charge build up of +0.11 to +0.17 at C3. This is in good agreement with the MINDO/3 results. Although the chemical shift and electron density changes at C1 and C2 are in qualitative agreement, a study of Lewis acid complexes of conjugated carbonyl compounds by Childs et al (139) has shown that these parameters do not correlate as well for C1 and C2.

The para substituted salts 42 to 46 could provide some indication of the change in charge delocalization induced by substituent changes. Delocalization of the positive charge onto the benzenoid system might

be expected, particularly when X is electron donating. If such an effect occurred then the C1 and C3 signals should shift upfield as X is changed from an electron-withdrawing to an electron-donating group. The chemical shift change for C1 as a function of X is very small but it is in the expected direction, however, the C3 signal shifts in the opposite downfield direction. In fact, the resonance frequency shifts for C2 and C3 mimic very closely the changes observed by Stothers and Dhami (140) for the analogous styrenes. They explained these alterations in terms of the contribution of the resonance forms 49 and 50 as X is changed from a donating to a withdrawing group respectively. The positions of the ring carbon resonance change dramatically as X is altered, but these changes are in line with those expected for substituted benzenes (146).

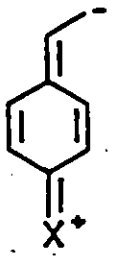


49

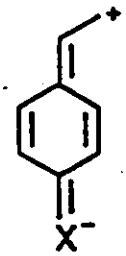


50

Thus salts 42 to 46 act principally as styrene analogs which have been substituted with an iminium function at C2. There seems to be some conjugative interaction with the ring but its magnitude appears to be independent of substituent. This suggests that the resonance form with a formal positive charge on the nitrogen is the major contributor to the ground state structure of α,β-unsaturated iminium salts.

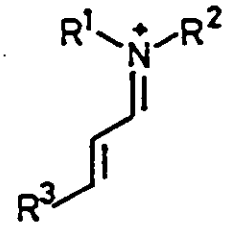

Solid state $^{13}C$ nmr spectra of the crystalline salts 42 to 46 were procured in order to provide a means of comparing the cation structures in the solution and solid phases (129,130). The spectra were obtained using CPMAS techniques (131) and were provided by courtesy of C.A. Fyfe at the University of Guelph. Spectral data are summarized in Table 3-7. Resolution varied from sample to sample with 43 providing the best results, Figure 3-2. The quaternary carbons were readily identified in the solid state spectrum by using a pulse sequence which suppresses the signals of carbons with directly bonded protons, Figure 3-2c (132). Methyl carbon resonances were not completely suppressed because of reduction of the local dipolar field caused by rapid internal motion of these groups.

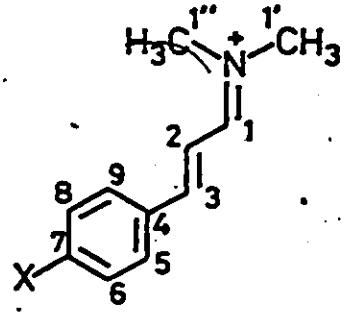

42 X=H , 43 X=$OCH_3$ , 44 X=$CH_3$

45 X=Cl , 46 X=$NO_2$

The solid state spectrum of 43 appears to be quite different from its solution spectrum, Figure 3-2. First, the resonances of

Table 3-7

Solid State $^{13}C$ NMR Data of Iminium Salts

| Compound | Chemical Shift[a] (ppm) | | | | | | | | | | |
|---|---|---|---|---|---|---|---|---|---|---|---|
| | C1 | C2 | C3 | C4 | C5,9[b] | | C6,8[b] | | C7 | C1'/C1"[b] | Others |
| 42 | 171.1 | 112.4 | 155.2 | 134.9 | 131.4 | | 131.4 | | 134.9 | 51.8/43.6 | |
| 43 | 174.8 | 115.0 | 164.6 | 128.4 | 141.4 | 131.4 | 122.4 | 115.0 | 167.7 | 54.2/43.6 | 56.4 |
| 44 | 171.5 | 119.3 | 160.7 | 131.4 | 131.4 | | 131.4 | | 146.9 | 50.1/43.0 | 22.2 |
| 45 | 169.5 | 116.4 | 155.2 | 129.3 | 129.3 | | 129.3 | | 129.3 | 46.9/39.2 | |
| 46 | 171.6 | 119.8 | 157.8 | 138.4 | 133.7 | 128.7 | 125.0 | | 151.3 | 48.7/39.6 | |

a in ppm from TMS

b assignment could be reversed

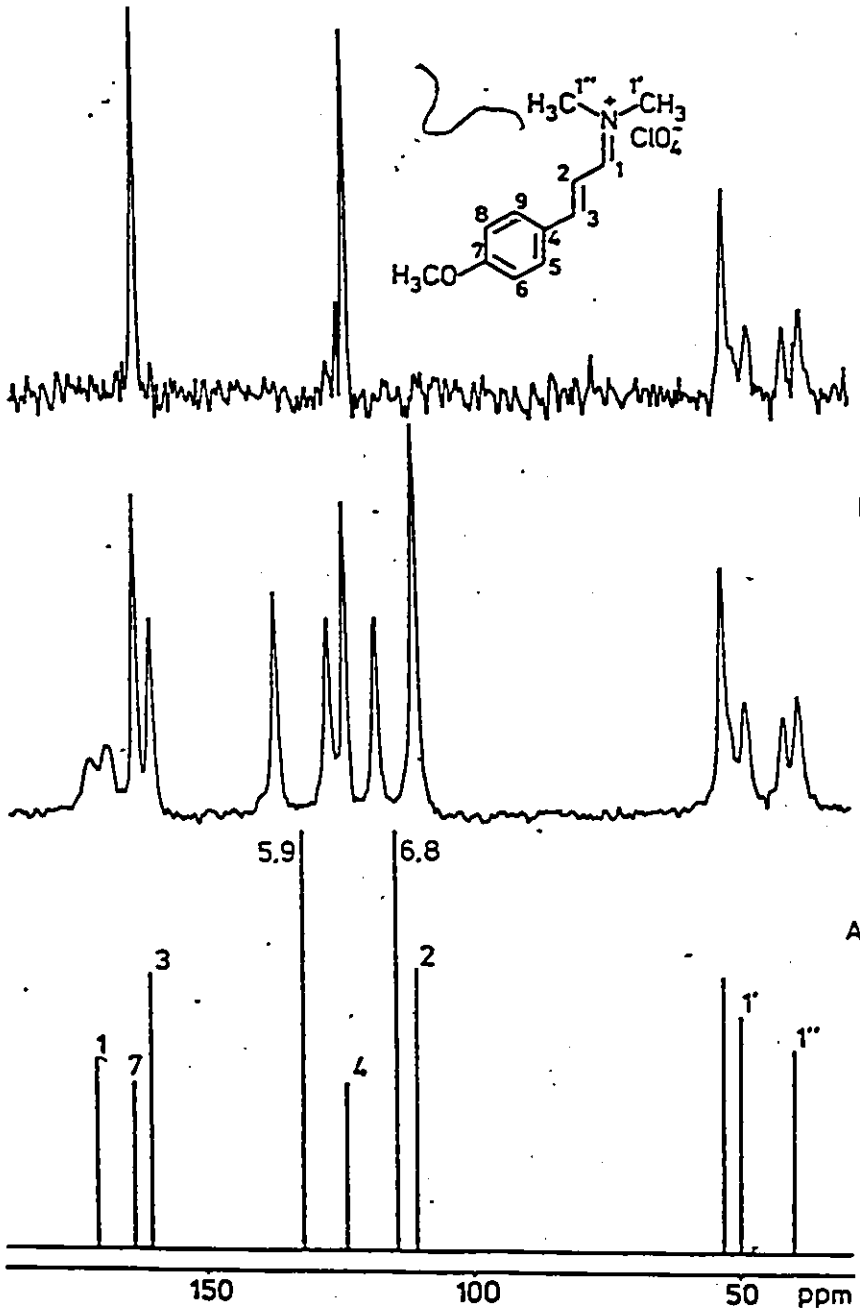


Figure 3-2: $^{13}C$ nmr spectra of trans-N,N-dimethyl-3-(p-methoxyphenyl)-2-propenylideniminium perchlorate, 43 (a) solution, (b) solid state, (c) suppressed.

carbons adjacent to nitrogen are doublets. This phenomenon, which has been observed previously in the solid state spectra of nitrogen containing compounds, is attributable to coupling with the nitrogen quadrupole (131). A second feature of the spectrum is the complexity of the signals due to the aromatic ring carbons. The suppressed spectrum, Figure 3-2c, indicates that the resonances due to the quaternary carbons C4 and C7 are still singlets. These resonances, and those due to the vinyl carbons, are coincident with the corresponding resonances of the cation in solution. This suggests that in the solid state, rotation about the C3,C4 and/or C7,$OCH_3$ bonds has been stopped so that C5 and C9, and C6 and C8 are no longer magnetically equivalent.

Except for the minor differences noted above the chemical shifts observed for the various carbons in the solution and solid state spectra of cations 42 to 46 are very similar. This is particularly evident for the vinyl carbon signals and suggests that there are no strong cation/anion interactions in the solid-state and that the cation structures in the two phases are analogous.

*Crystallographic Structure Determination*

Single crystals of 42 and 43, suitable for x-ray structure determination, were obtained by slow evaporation of solvent, $CH_2Cl_2$ and $CH_3OH$ respectively, from solutions of the salts. The structures were solved by R. Faggiani and C.J.L. Lock of the chemistry department at McMaster University. Both cations have N,C(1) and C(2),C(3) bond lengths, 1.29 Å and 1.35 Å respectively, indicative of double bonds but the lengths of the formal single C(1),C(2) and C(3),C(4) bonds (~ 1.45 Å) indicate that there is some degree of delocalization. None of the bond

angles are dramatically different from 120° and there is no apparent distortion of the ring. Structures of the cations are shown in Figures 3-3 and 3-4 and interatomic distances and angles are given in Table 3-8.

The crystal structures of 42 and 43 show that both cations exist in an s-trans conformation and confirm that they have a trans configuration. In both cases the backbone and rings of each cation are planar. The cation of 42 has a crystallographic plane of symmetry, although the temperature profiles suggest the possibility of slight distortion about the plane. There is some deviation from planarity in the cation of 43 but this deviation is small as illustrated by the torsional angles along the backbone and at the methoxy group which differ by no more than 5.3° from 0° or 180°.

Bond lengths and angles do not differ significantly in the two cations and the observed bond lengths agree well with those reported previously for iminium salts (141,142). The N,C(1) bond length for both 42 and 43 is the same within experimental error as that found for the unconjugated tetramethylmethyleniminium (141) and the conjugated cyclobutenylideniminium cations (142). Moreover, the C(2),C(3) bond length in both 42 and 43 (1.35 Å) is not significantly different than that expected for an isolated double bond. It would seem clear from the bond lengths of the two cations that the degree of conjugation in these systems is small. Thus the positive charge appears to reside mainly in the iminium moiety. Even in 43, where the methoxy group can interact conjugatively with the positively charged system, there is no apparent increase in conjugation. This observation is consistent with the $^{13}C$ nmr data discussed in the previous section.

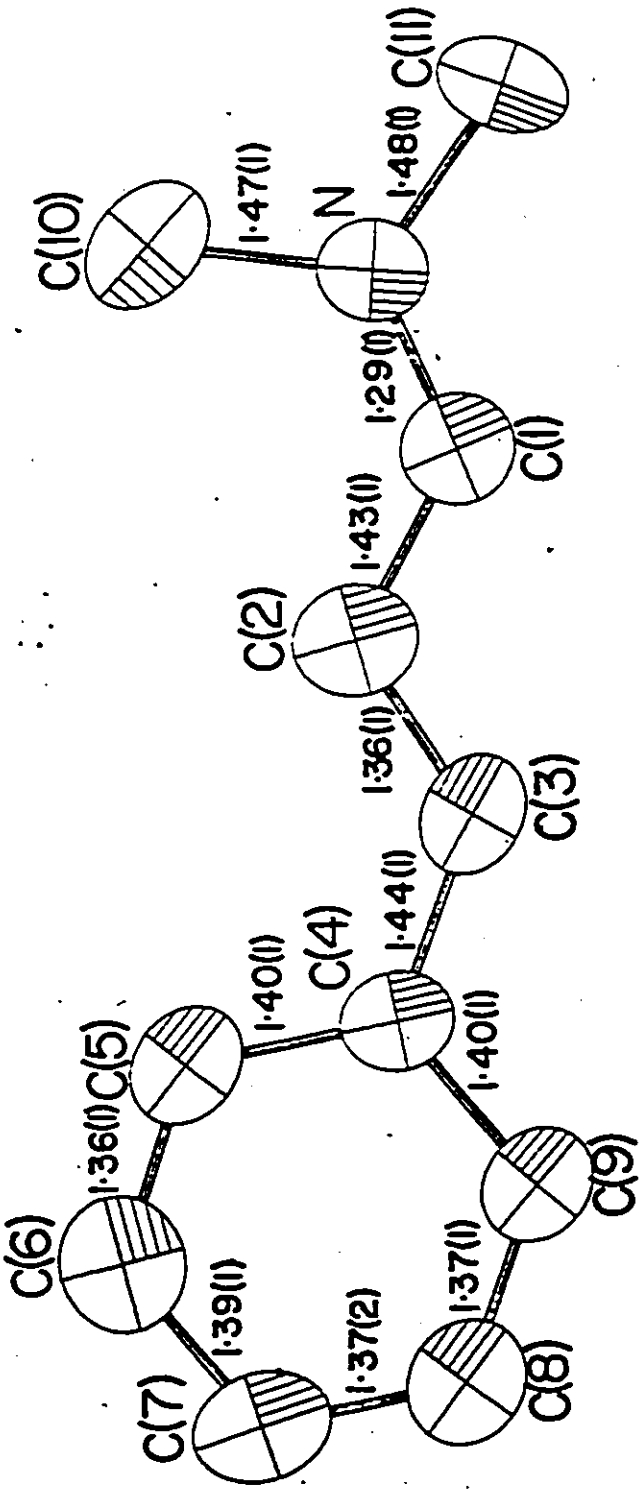


Figure 3-3: ORTEP diagram for the trans-N,N-dimethyl-3-phenyl-2-propenylidenimlnium cation, 42.

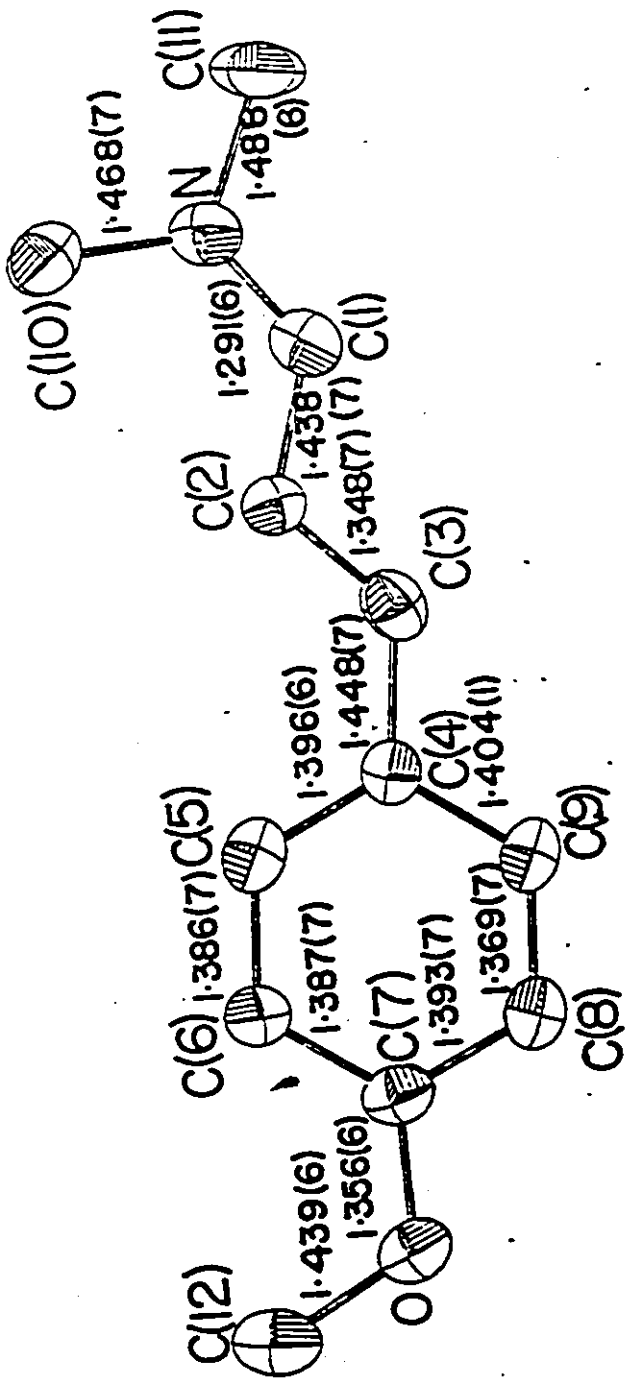


Figure 3-4: ORTEP diagram for the trans-N,N-dimethyl-3-(p-methoxyphenyl)-2-propenylideniminium cation, 43.

Table 3-8

Selected interatomic distances (Å) and angles (deg) for trans-N,N-dimethyl-3-phenyl-2-propenylideniminium perchlorate (42) and trans-N,N-dimethyl-3-(p-methoxyphenyl)-2-propenylideniminium perchlorate (43)

| | 1 | 2 | | 1 | 2 | | 1 | 2 |
|---|---|---|---|---|---|---|---|---|
| N-C(1) | 1.29(1) | 1.291(6) | C(1)-C(2) | 1.43(1) | 1.438(7) | C(2)-C(3) | 1.36(1) | 1.348(7) |
| C(3)-C(4) | 1.44(1) | 1.448(7) | C(4)-C(5) | 1.40(1) | 1.396(6) | C(5)-C(6) | 1.36(1) | 1.386(7) |
| C(6)-C(7) | 1.39(1) | 1.387(7) | C(7)-C(8) | 1.317(2) | 1.393(7) | C(8)-C(9) | 1.37(1) | 1.369(7) |
| C(9)-C(4) | 1.40(1) | 1.404(1) | N-C(10) | 1.47(1) | 1.468(7) | N-C(11) | 1.48(1) | 1.488(6) |
| C(7)-O | -- | 1.356(6) | O-C(12) | -- | 1.439(6) | Cl-O(1) | 1.404(7) | 1.427(4) |
| Cl-O(2) | 1.412(7) | 1.393(4) | Cl-O(3) | 1.385(7) | 1.419(4) | Cl-O(4) | -- | 1.413(4) |

| | 42 | 43 | | 1 | 2 | | 1 | 2 |
|---|---|---|---|---|---|---|---|---|
| C(10)-N-C(11) | 119.0(7) | 115.8(4) | C(10)-N-C(1) | 121.3(7) | 125.0(4) | C(11)-N-C(1) | 119.7(7) | 119.1(4) |
| N-C(1)-C(2) | 126.6(8) | 124.9(5) | C(1)-C(2)-C(3) | 117.8(8) | 117.8(4) | C(2)-C(3)-C(4) | 125.7(9) | 127.9(4) |
| C(3)-C(4)-C(5) | 122.3(8) | 122.8(4) | C(3)-C(4)-C(9) | 119.1(9) | 119.1(4) | C(9)-C(4)-C(5) | 118.6(9) | 118.0(5) |
| C(4)-C(5)-C(6) | 119.8(9) | 120.7(5) | C(5)-C(6)-C(7) | 122(1) | 119.7(5) | C(6)-C(7)-C(8) | 118(1) | 120.6(5) |
| C(7)-C(8)-C(9) | 122.1(9) | 119.0(5) | C(8)-C(9)-C(4) | 119.8(9) | 121.8(5) | C(6)-C(7)-O | -- | 124.6(4) |
| C(8)-C(7)-O | -- | 114.81(4) | C(7)-O-C(12) | -- | 118.1(4) | O(1)-Cl-O(2) | 108.3(4) | 110.7(3) |
| O(1)-Cl-O(3) | 110.7(3) | 108.6(2) | O(1)-Cl-O(4) | -- | 110.1(3) | O(2)-Cl-O(3) | 109.1(3) | 108.3(3) |
| O(2)-Cl-O(4) | -- | 108.7(3) | O(3)-Cl-O(4) | -- | 110.3(3) | | | |

The methoxy group lies in the plane of the ring and significant multiple bonding from the ring carbon to the oxygen atom is implied by the considerable difference in the two C-O bond lengths (c.f. C(7)-O 1.356(6) Å vs C(12)-O 1.439(6) Å). This seems to contradict the conclusion reached in the previous paragraph until it is remembered that the comparable bond lengths in deoxyanisoin, 51, and p,p-dimethoxybenzophenone, 52, indicate a similar interaction with the ring (143).

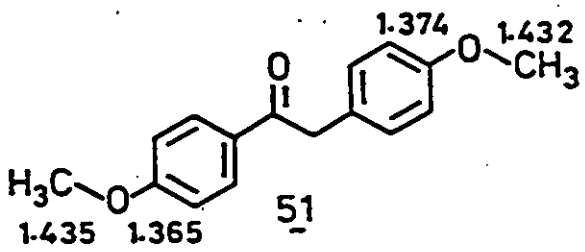


51

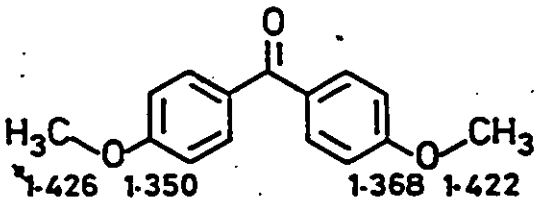


52

Crystal packings for 42 and 43 are shown in Figure 3-5. Despite the fact that the space groups and cells are different, both have similar layer structures with each layer containing both cations and anions. Cations in any given layer are oriented so that the dipoles are roughly in the same direction (for 42, roughly along c), but in adjacent layers they are in opposite directions. The differences in the structures arise from the amount of cation-cation overlap in adjacent

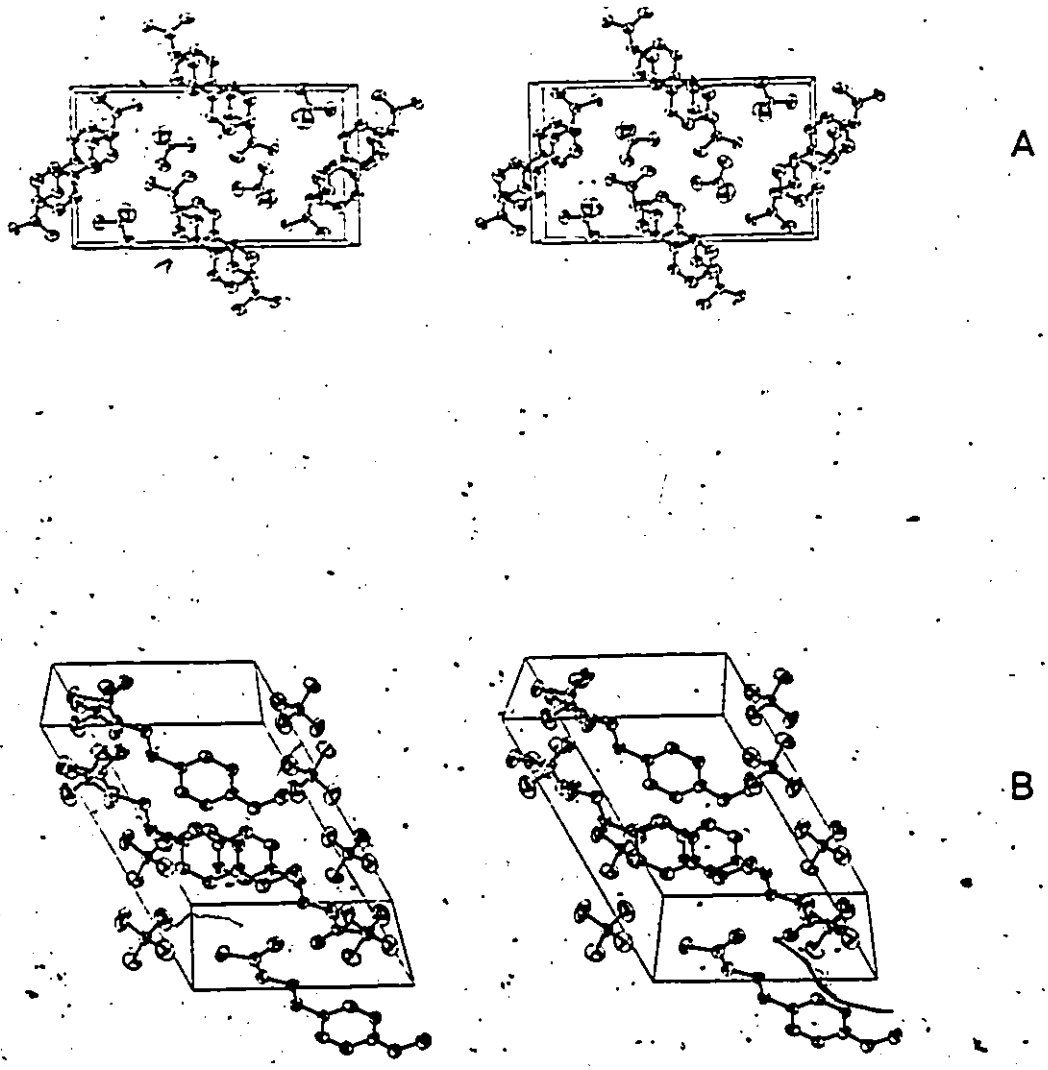


Figure 3-5: Crystal packings for (a) trans-N,N-dimethyl-3-phenyl-2-propenylideniminium perchlorate, 42 and (b) trans-N,N-dimethyl-3-(p-methoxyphenyl)-2-propenylideniminium perchlorate, 43.

layers. For 42 the cations lie almost directly over each other in the a direction, packed head-to-tail, whereas the cation-cation overlap is much smaller in 43. All contacts are at or above the sum of the van der Waals radii and there is no evidence of any strong interaction between anion and cation which might significantly distort the cation.

It must be remembered at this point that the comparison of solution and solid state $^{13}C$ nmr data showed that cation structures were analogous in the two phases. Thus, the structures determined in the solid state by x-ray crystallography should still exist in solution.

D. Conclusions

The iminium salts prepared for this work were found to be in a unique configuration. Double bond configurations were shown to be trans from the analysis of $^{1}H$ nmr coupling constants. This assignment, in the case of the C=C bond, was confirmed by x-ray crystallographic structure determination. The crystal structures showed that the salts exist in an s-trans conformation. It was concluded from the analysis of the solution and solid state $^{13}C$ nmr data that the cation structures in the two phases are analogous. This implies that in solution the cations exist predominantly in an s-trans conformation.

Calculations using MINDO/3 showed that upon protonation some positive charge was delocalized onto the carbon framework and that this was most significant at C3. This charge delocalization was accompanied by a small increase in the double bond lengths and decrease in the carbon, carbon single bond length. Changes in carbon chemical shifts upon salt formation were shown to imply the same amount of charge delocalization determined from the MINDO/3 data. However, the extent of this

delocalization was found to be independent of the aromatic ring substituent so that it was concluded that the ground state structure is best represented by the resonance form with a formal positive charge on nitrogen.

The bond lengths of the carbon chain determined from the crystal structures were found to be alternating single and double bonds consistent with the MINDO/3 and $^{13}C$ nmr data. No increase in conjugation or charge delocalization with change in ring substituent is evident from the crystallographic data. These observations support the conclusion that the positive charge is localized principally in the iminium moiety.

# CHAPTER 4

# PHOTOCHEMISTRY

Absorption of light by an iminium salt will lead to the formation of the lowest excited singlet state ($S_1$). This state can in principle lose its energy by a variety of pathways (see Scheme 1-1, p. 11). The energy can be dissipated by the emission of light (fluorescence), a non-radiative process such as isomerization, or intersystem crossing to the first excited triplet state ($T_1$). Energy loss from $T_1$ can also be accomplished by emission (phosphorescence) or a radiationless process such as isomerization.

For the acyclic α,β-unsaturated iminium salts discussed in this thesis isomerization about the multiple bonds could be a major dissipative pathway.

## A. Qualitative Observations

The absorption spectra of the iminium salts 37 to 46 were measured and the results are summarized in Table 4-1. All the aliphatic iminium salts (37 to 39) exhibit an intense absorption maximum at about 250 nm while the maxima for the aromatic salts (40 to 46) range from 323 nm to 384 nm depending on the ring substituent. The high intensity of these bands indicates that for all of the iminium salts, the transitions are of $\pi$-$\pi^*$ character. This is expected since the nitrogen lone pair is employed in bonding, eliminating the n-$\pi^*$ transition.

An attempt was made to measure the fluorescence of salt 42 at room temperature in 98% $H_2SO_4$ and at 77K in an acid glass (3:1, V:V,

Table 4-1

Electronic absorption data for the iminium salts

| Compound | Solvent | $\lambda_{max}$ (nm) | $\text{Log}\varepsilon_{max}$ |
|---|---|---|---|
| 37 | $H_2SO_4$ | 250 | 5.6 |
| 38 | $H_2SO_4$ | 262 | 4.8 |
| 39 | $H_2SO_4$ | 245 | 4.2 |
| 40 | $H_2SO_4$ | 340 | 4.9 |
| 41 | $H_2SO_4$ | 335 | 4.4 |
| 42 | TFA | 341 | 4.4 |
| 43 | TFA | 384 | 4.6 |
| 44 | TFA | 359 | 4.6 |
| 45 | TFA | 350 | 4.5 |
| 46 | TFA | 323 | 4.4 |

methane sulphonic: n-propane sulphonic acids). In both cases no fluorescence was observed ($\phi_f < 10^{-3}$).

Direct irradiation of any of the iminium salts in acid solution (TFA, $FSO_3H$ or $H_2SO_4$) led to the formation of several photoproducts. The reactions were followed by $^1H$ nmr spectroscopy directly on the irradiated solutions and typical spectra are shown in Figures 4-2 and 4-4. When the irradiations were carried out in deuterated media no incorporation into C-H bonds was observed for any of the iminium salts. A photostationary state appeared to be reached after 4 to 24 hours irradiation (time required was dependent on substituents). The similarity of the $^1H$ nmr spectra of the photoproducts compared with the original iminium salt (see Figures 4-1 and 4-3) suggest that they are all geometric isomers, equations 19 and 20. When irradiation was continued for prolonged time periods (> 24 hrs) some decomposition was observed but no attempt was made to identify these products. As will be shown in detail in the next section the principal photoproducts were identified from their $^1H$ nmr spectral data, Tables 4-2, 4-3 and 4-4. The compositions of these mixtures were determined by the integration of nmr resonances and the data are given in equations 19 and 20.

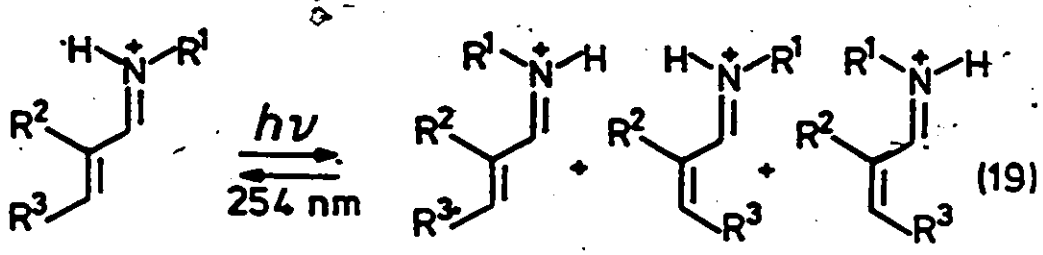


(19)

**37** $R^1$=t-Bu, $R^2$=H, $R^3$=$CH_3$ (50%) **53** (12%) **54** (28%) **55** (10%)
**38** $R^1$=n-Bu, $R^2$=$R^3$=$CH_3$ (25%) **56** (10%) **57** (44%) **58** (21%)
**39** $R^1$=n-Bu, $R^2$=$CH_3$, $R^3$=H (65%) **59** (35%)

Table 4-2

$^1$H nmr data for the aliphatic iminium salts and their principal photoproducts

| Compound | Chemical Shift[a,b] (ppm) | | | | | | | | | Coupling Constant (Hz) | | | |
|---|---|---|---|---|---|---|---|---|---|---|---|---|---|
| | H1 | H2 | H3 | $R^3$ | N-H | H1' | H2' | H3' | H4' | $J_{N,1}$ | $J_{1,2}$ | $J_{2,3}$ | $J_{3,CH_3}$ |
| 37 | 8.14dd | 6.48dd | 7.29dq | 2.03d | 9.2bd | - | 1.38s | - | - | 17.4 | 10.1 | 14.8 | 6.9 |
| 53 | 7.97t | 6.86dd | 7.4dq | 2.15d | 9.2bd | - | 1.50s | - | - | 12 | 12 | 15 | 7 |
| 54 | 8.55dd | 6.41t | 7.08dq | 2.09d | 9.2bd | - | 1.42s | - | - | 17.6 | 11 | 12 | 7 |
| 55 | 8.46t | 6.80t | 7.4dq | 2.11d | 9.2bd | - | 1.50s | - | - | 12 | 12 | 12 | 7 |
| 38 | 8.08d | 1.85s | 7.09q | 2.01d | 9.2bd | 3.69q | 1.66m | 1.28m | 0.83t | 17.1 | - | - | 7.3 |
| 56 | 7.92d | 1.87s | 7.12q | 2.05d | 9.2bd | 3.62q | 1.66m | 1.28m | 0.83t | 11.6 | - | - | 7 |
| 57 | 8.70d | 1.90s | 7.01q | 2.05d | 9.2bd | 3.85q | 1.66m | 1.28m | 0.83t | 17.1 | - | - | 7 |
| 58 | 8.53d | 1.79s | 6.94q | 1.96d | 9.2bd | 3.65q | 1.66m | 1.28m | 0.83t | 10.4 | - | - | 7 |
| 39[c] | 8.26d | 2.07s | 6.56s[d] | 6.47s[d] | 9.2bd | 3.85q | 1.68m | 1.32m | 0.85t | 17.6 | - | - | - |
| 59[c] | 8.10d | 2.28s | 6.58s[d] | 6.41s[d] | 9.2bd | 4.00q | 1.68m | 1.32m | 0.85t | 12 | - | - | - |

[a] bd = broad doublet, d = doublet, dd = doublet of doublets, q = quartet, dq = doublet of quartets, s = singlet, t = triplet, m = multiplet

[b] in ppm from $(CH_3)_4N^+BF_4^-$ (3.10 ppm) in TFA solution

[c] in ppm from $(CH_3)_4N^+BF_4^-$ (3.10 ppm) in $FSO_3H$ solution

[d] assignment could be reversed

Table 4-3

$^1$H nmr data for the aromatic N-n-butyliminium salts and their principal photoproducts

| Compound | Chemical Shift[a,b] (ppm) | | | | | | | | | | | Coupling Constant (Hz) | | |
|---|---|---|---|---|---|---|---|---|---|---|---|---|---|---|
| | H1 | H2 | H3 | Aryl | H | | N-H | H1' | H2' | H3' | H4' | $J_{N,1}$ | $J_{1,2}$ | $J_{2,3}$ |
| 40 | 8.25dd | 7.06dd | 7.75d | 7.32dd | 7.42d | 7.52d | 9.2bd | 3.70q | 1.68m | 1.32m | 0.85t | 17.2 | 10.3 | 15.5 |
| 60[c] | 8.25 | 7.20dd | 7.88d | 7.32dd | 7.42d | 7.61d | 9.2bd | 3.75q | 1.68m | 1.32m | 0.85t | - | 11.0 | 15.3 |
| 61 | 8.42dd | 6.58t | 7.90d | 7.24dd | 7.35d | 7.42d | 9.2bd | 3.70q | 1.68m | 1.32m | 0.85t | 17.2 | 10.3 | 10.3 |
| 41 | 8.43dd | 7.23dd | 7.83d | 7.73d | 8.20d | | 9.2bd | 3.77q | 1.71m | 1.33m | 0.85t | 16.5 | 9.8 | 15.9 |
| 63[d] | 8.43d | 7.39dd | 7.98d | 7.82d | 8.23d | | - | 3.84t | 1.71m | 1.33m | 0.85t | - | 10 | 14.6 |
| 64[d] | 8.45d | 6.80t | 7.92d | 7.48d | 8.22d | | - | 3.8t | 1.71m | 1.33m | 0.85t | - | 11 | 11 |
| 65[d] | 8.45d | 6.93t | 8.12d | 7.5d | 8.2d | | - | 3.8t | 1.71m | 1.33m | 0.85t | - | 11 | 11 |

[a] bd = broad doublet, d = doublet, dd = doublet of doublets, q = quartet, dq = doublet of quartets s = singlet, t = triplet, m = multiplet.

[b] in ppm from $(CH_3)_4N^+BF_4^-$ (3.10 ppm) in TFA solution.

[c] data obtained from thermal equilibrium mixture (see Chapter 5).

[d] TFA-d used as solvent in order to simplify low field end of spectrum for photostationary state mixture.

Table 4-4

$^1H$ nmr data for the aromatic N,N-dimethyliminium salts and their principal photoproducts

| Compound | Chemical Shift[a,b] (ppm) | | | | | | | | Coupling Constant (Hz) | |
|---|---|---|---|---|---|---|---|---|---|---|
| | H1 | H2 | H3 | Aryl H | | | H1'/H1"[c] | Other | $J_{1,2}$ | $J_{2,3}$ |
| 42 | 8.20d | 7.08dd | 7.79d | 7.34dd | 7.43d | 7.60d | 3.50s/3.59s | | 10.6 | 15.3 |
| 66 | 8.26d | 6.26t | 7.97d | 7.27dd | 7.35d | 7.44d | 3.53s/3.61s | | 10.4 | 11.1 |
| 43 | 8.09d | 6.92dd | 7.71d | 6.92d | 7.61d | | 3.45s/3.54s | 3.82s | 10.8 | 14.8 |
| 67 | 8.25d | 6.41t | 7.86d | 6.98d | 7.31d | | 3.48s/3.60s | 3.83s | 10.8 | 10.8 |
| 44 | 8.13d | 7.01dd | 7.74d | 7.16d | 7.44d | | 3.47s/3.56s | 2.26s | 10.8 | 14.8 |
| 68 | 8.26d | 6.47t | 7.92d | 7.18s | | | 3.50s/3.60s | 2.26s | 10.8 | 10.8 |
| 45 | 8.20d | 7.05dd | 7.73d | 7.30d | 7.52d | | 3.50s/3.59s | | 10.8 | 14.9 |
| 69 | 8.25d | 6.56t | 7.89d | 7.31d | 7.34d | | 3.53s/3.62s | | 10.5 | 11.0 |
| 46 | 8.36d | 7.29dd | 7.86d | 7.81d | 8.20d | | 3.60s/3.67s | | 10.2 | 15.5 |
| 70 | 8.30d | 6.79t | 7.97d | 7.50d | 8.21d | | 3.60s/3.67s | | 10.3 | 11.4 |

[a] d = doublet, dd = doublet of doublets, m = multiplet, s = singlet, t = triplet.

[b] in ppm from $(CH_3)_4N^+BF_4^-$ (3.10 ppm) in TFA solution.

[c] assignment could be reversed.

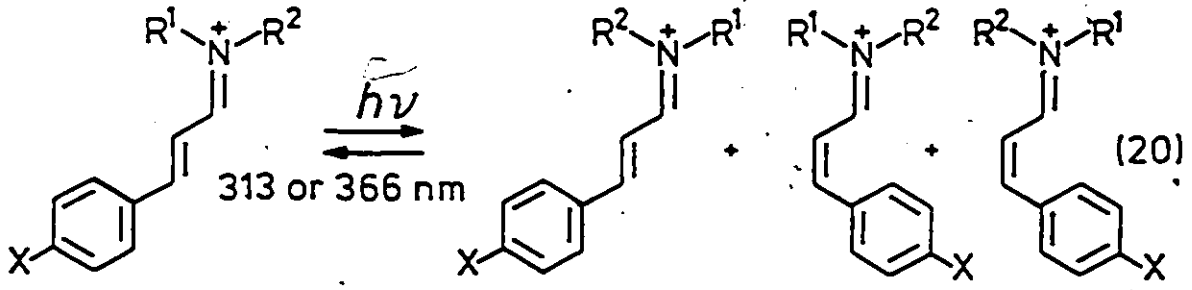


| | | | | |
|---|---|---|---|---|
| 40 $R^1$=H, $R^2$=n-Bu, X=H (53%) | 60 (<1%) | 61 (47%) | 62 (<1%) |
| 41 $R^1$=H, $R^2$=n-Bu, X=$NO_2$ (35%) | 63 (15%) | 64 (40%) | 65 (10%) |
| 42 $R^1$=$R^2$=$CH_3$, X=H (43%) | | 66 (57%) | |
| 43 $R^1$=$R^2$=$CH_3$, X=$OCH_3$ (48%) | | 67 (52%) | |
| 44 $R^1$=$R^2$=$CH_3$, X=$CH_3$ (53%) | | 68 (47%) | |
| 45 $R^1$=$R^2$=$CH_3$, X=Cl (38%) | | 69 (62%) | |
| 46 $R^1$=$R^2$=$CH_3$, X=$NO_2$ (59%) | | 70 (41%) | |

B. Identification of Photoproducts

The photoproducts were characterized by a detailed inspection of the $^1$H nmr spectra of the mixtures obtained upon irradiation. Since the analysis is complex, it will be outlined in stages starting with the aliphatic systems (equation 19) where the absence of aromatic proton resonances makes the analysis of the vinyl proton signals simpler. To start, cation 39, in which only isomerization about the $C=N^+$ bond can be detected, will be discussed, Table 4-2.

The vinyl proton region of the 400 MHz $^1$H nmr spectrum of 39 is illustrated in Figure 4-1. The spectrum exhibited a doublet at δ 8.26 for the resonance due to the C1 proton and singlets at δ 6.56 and 6.47 for the signals due to the two C3 protons. A broad doublet was also observed at about δ 9.2 for the nitrogen proton. This resonance was

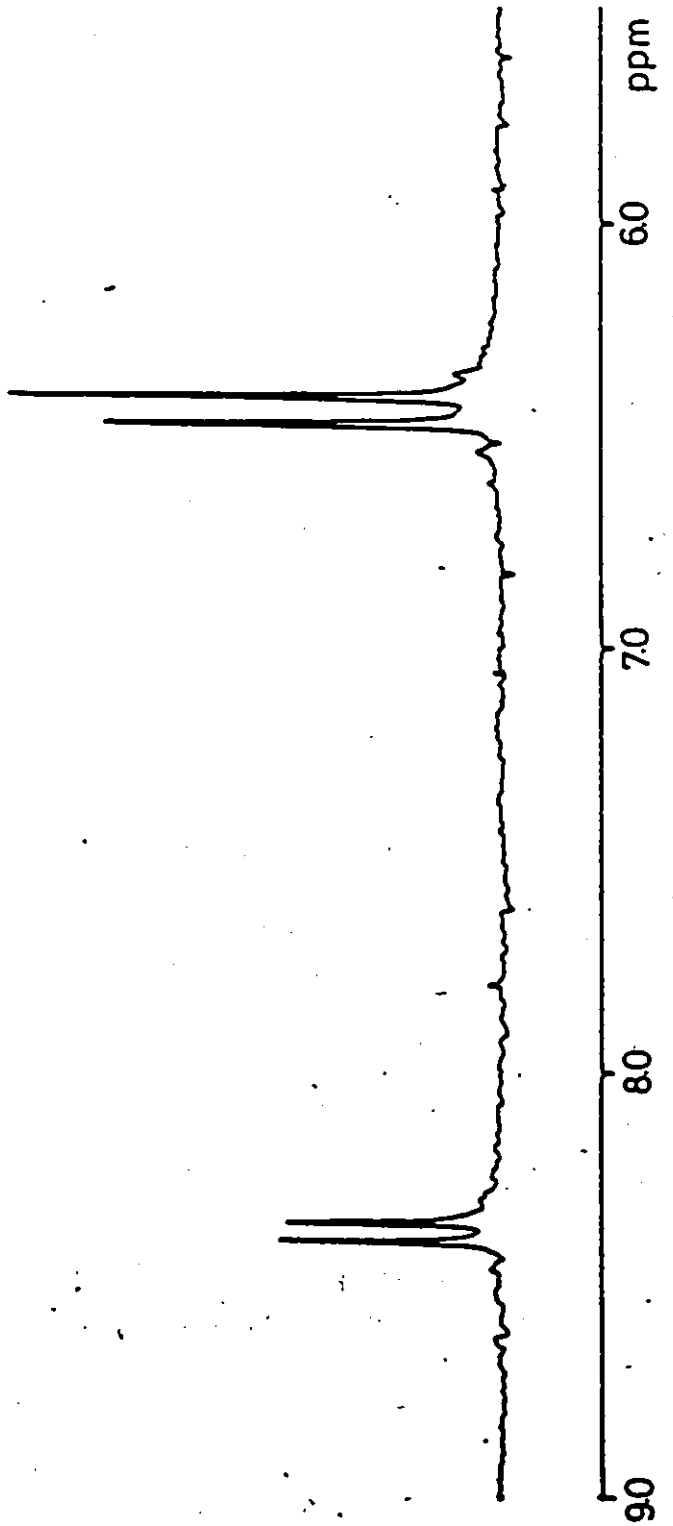


Figure 4-1: Vinyl region of the 400 MHz $^1H$ nmr spectrum of the trans-N-n-butyl-2-methyl-2-propenylideniminium cation 39, in TFA.

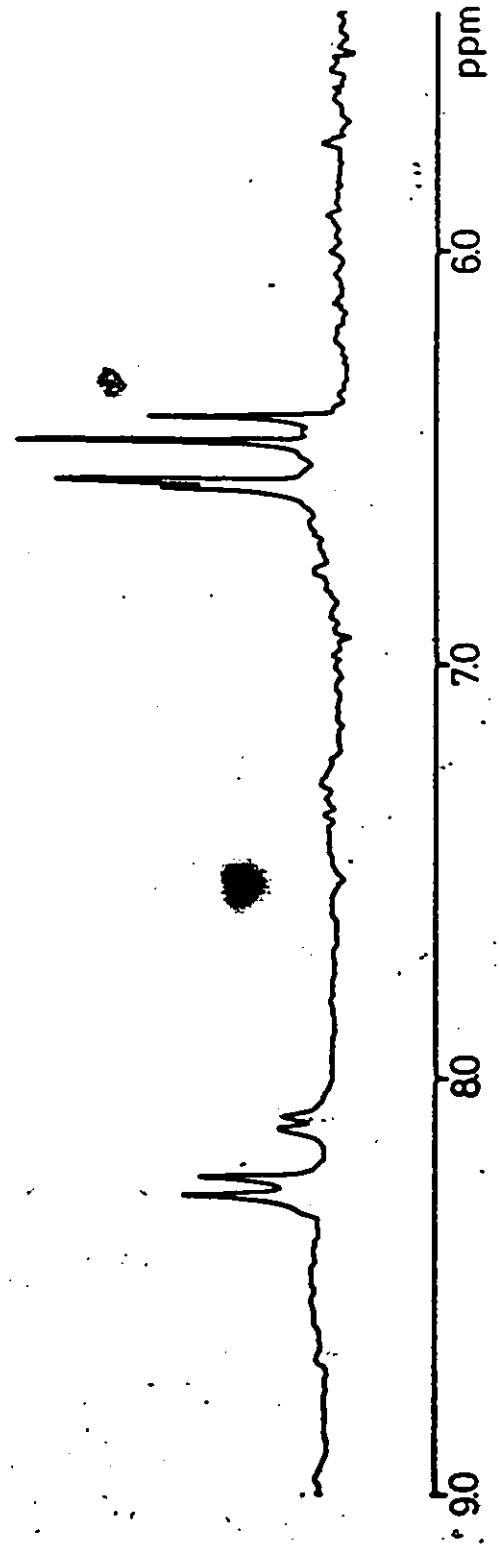


Figure 4-2: Vinyl region of the 400 MHz $^1H$ nmr spectrum of the photostationary state mixture formed by the irradiation of the trans-N-n-butyl-2-methyl-2-propenylideniminium cation 39, in TFA.

present in the spectra of all of the acid salts. In deuterated acid the doublet at δ 8.26 became a singlet indicating that the coupling was across the $C=N^+$ bond. The magnitude of this coupling constant ($J_{N,1}$) was 17.6 Hz, consistent with the assigned trans configuration (19,133,134). Figure 4-2 shows the vinyl region of the 400 MHz $^1H$ nmr spectrum for the photostationary state mixture containing 39 and a new cation. There was a doublet at δ 8.10 for the signal due to the C1 proton of this new cation and two new singlets at δ 6.58 and 6.41 for the resonances due to the C3 protons. The similarity of the spectrum of this photoproduct to that of 39 is apparent and indicated that the photoproduct is an isomer of 39. A value of 12 Hz for the $J_{N,1}$ coupling constant was indicative of a cis configuration about the $C=N^+$ bond (134), consistent with that anticipated for 59.

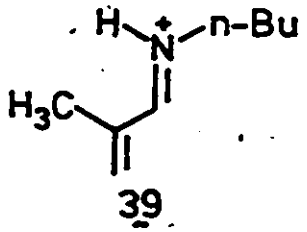


39

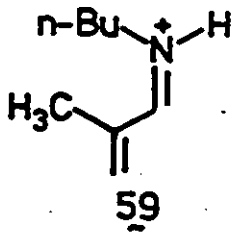


59

Cation 37 could exhibit isomerism about both the $C=N^+$ and C=C bonds and thus presents a more complex case. However, identification of the configurations about both $C=N^+$ and C=C bonds was possible by an analysis of proton,proton coupling constants, Table 4-2. The vinyl proton region of the 400 MHz $^1H$ nmr spectra of 37 and its photostationary state mixture are illustrated in Figures 4-3 and 4-4, respectively.

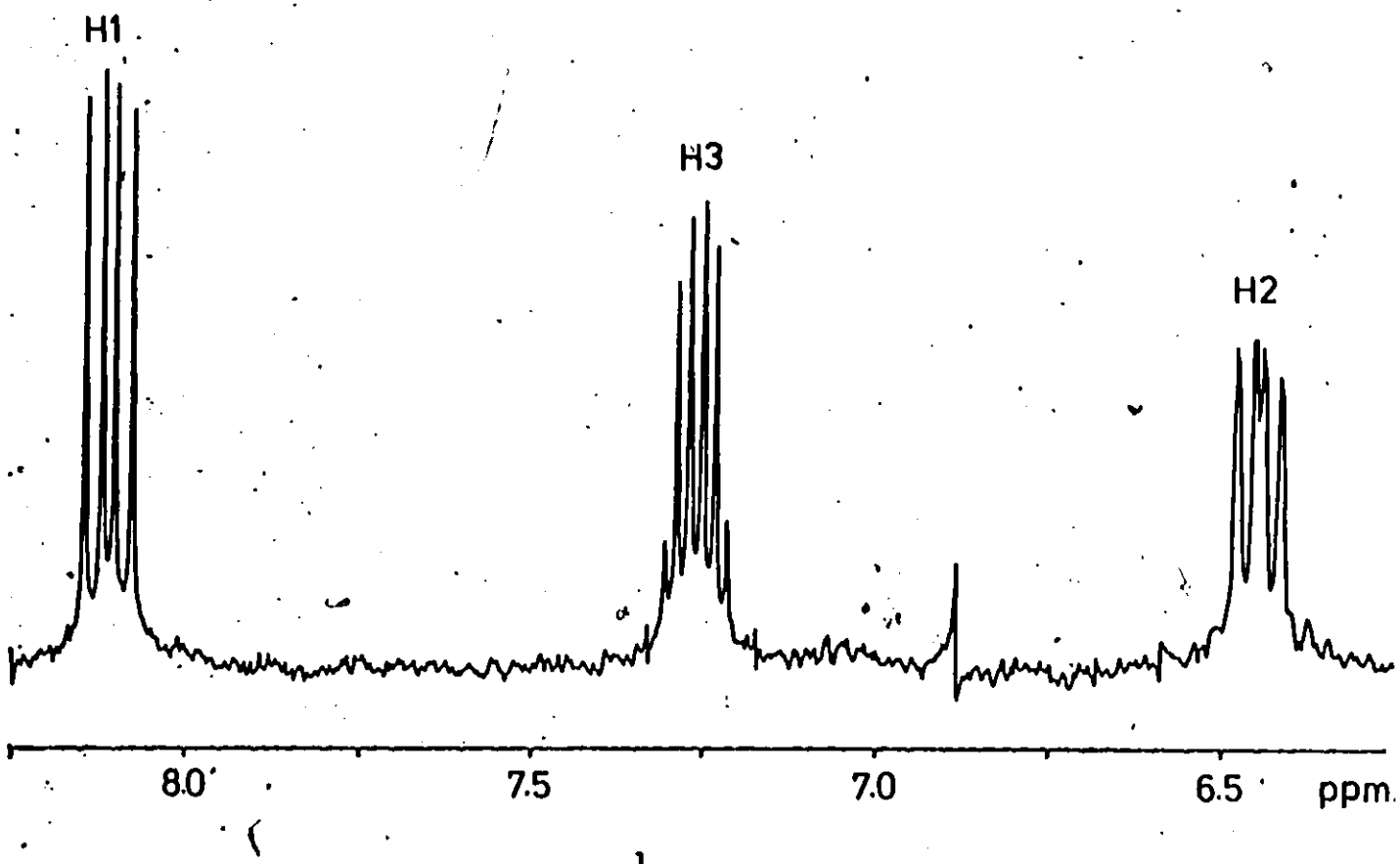


Figure 4-3: Vinyl region of the 400 MHz $^1$H nmr spectrum of the trans,trans-N-t-butyl-2-butenylideniminium cation 37, in TFA.

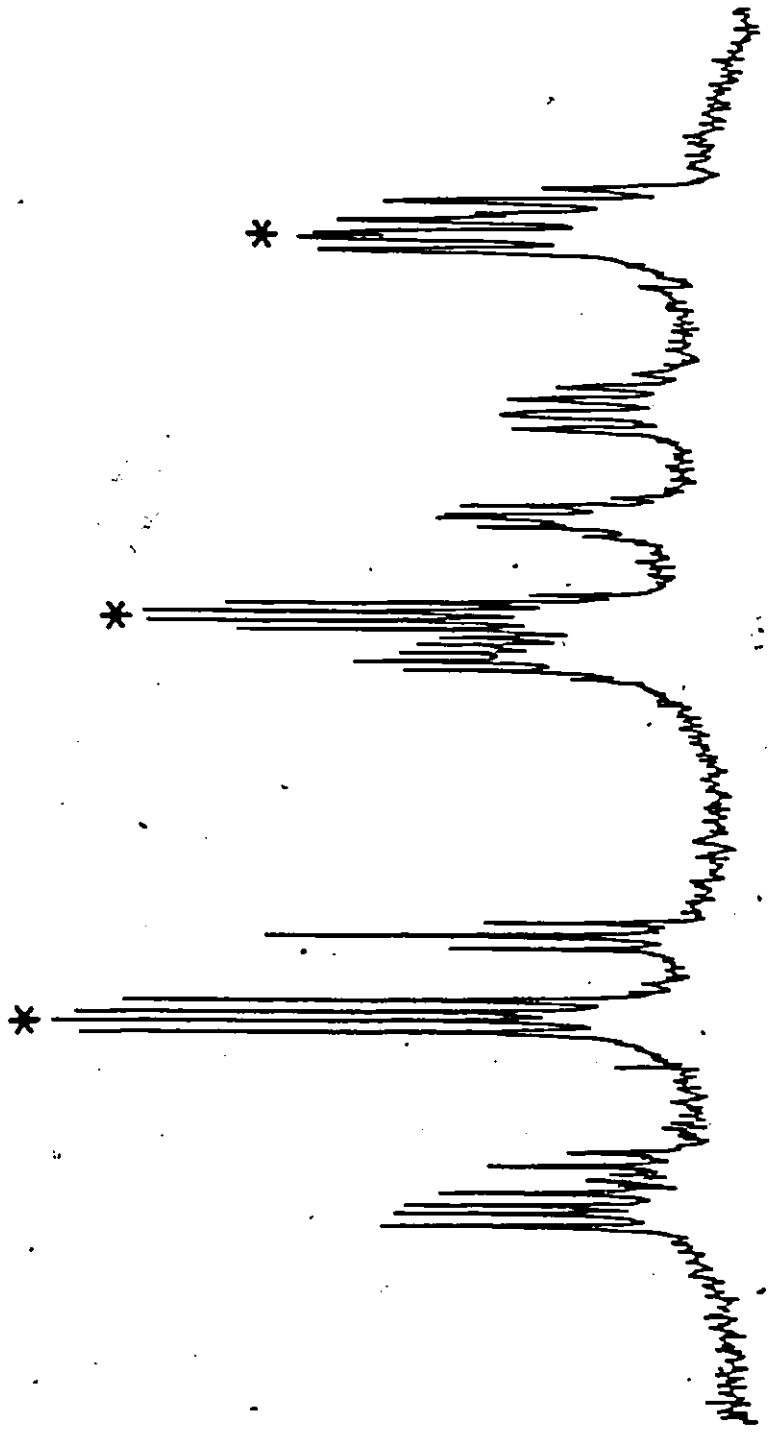


Figure 4-4: Vinyl region of the 400 MHz $^{1}H$ nmr spectrum of the photostationary state mixture formed by the irradiation of the trans,trans-N-t-butyl-2-butenylideniminium cation 37, in TFA.

The spectrum of 37 (Figure 4-3) showed a doublet of doublets ($J_{N,1}$ = 17.4 Hz, $J_{1,2}$ = 10.1 Hz) at δ 8.14 for the signal due to H1, a slightly overlapping doublet of quartets ($J_{2,3}$ = 14.8 Hz, $J_{3,CH_3}$ = 6.9 Hz) at δ 7.29 due to the resonance for H3 and another doublet of doublets at δ 6.48 for the signal due to H2. Long range coupling to the methyl group at C3 broadened the resonance due to H2.

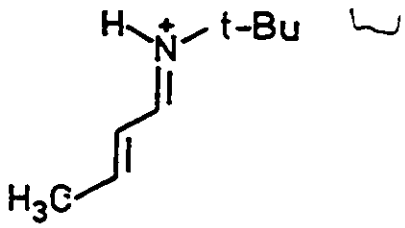


37

At first glance, the spectrum of the photostationary state mixture (Figure 4-4) appeared horrendously complex. However, the starting trans,trans-isomer 37 could still be identified as denoted by the asterisks.

More careful examination of the spectrum of the mixture in the region between δ 8.0 and 8.5, revealed the presence of four separate resonances. In deuterated acid media these signals all collapsed to doublets with very similar coupling constants ($J_{1,2}$ ~ 10 Hz). This indicated that they are due to the C1 proton of the four possible geometric isomers. Two of these resonances (δ 8.14 and 8.55 ) had coupling constants across the $C=N^+$ bond of about 17 Hz, indicative of a trans configuration (19,133,134). This implied that the resonance at δ 8.55 could be due to the proton of the trans,cis-isomer, 54. The two remaining signals (δ7.97 and 8.46) had a coupling constant ($J_{N,1}$ = 12 Hz) consistent with a cis configuration about the $C=N^+$ bond

(134). These resonances could be due to the Cl proton of the cis,trans- and cis,cis-isomers, 53 and 55 respectively.

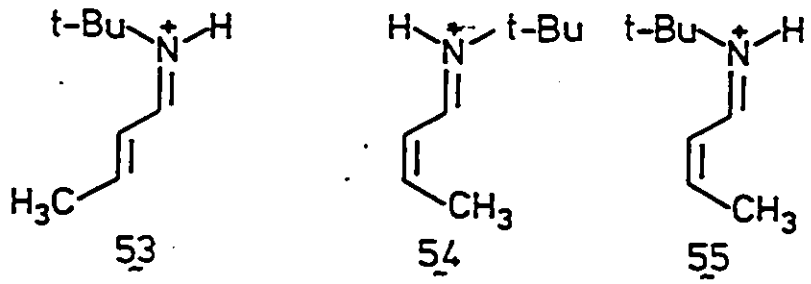


53 54 55

Figure 4-5 illustrates the experiments which confirmed the identification of the trans,cis-isomer, 54. Spin decoupling of the resonance at δ 8.55 (Figure 4.5a) gave partial collapse of the triplet centered at δ 6.41 identifying this as the corresponding resonance for H2. Irradiation of the resonance for the methyl group centred at δ 2.09 (Figure 4-5b) caused a sharpening of the triplet due to H2 at δ 6.41 and the multiplet at δ 7.08 collapsed to a doublet with a coupling constant ($J_{2,3}$) of 12 Hz. Such a value of $J_{2,3}$ is consistent with a cis configuration about the C=C bond (135). These two experiments clearly indicated that the resonances at δ 8.55, 7.08 and 6.41 are due to H1, H3 and H2, respectively, of a single isomer and the observed coupling constants indicated that this isomer had a trans,cis configuration such as 54.

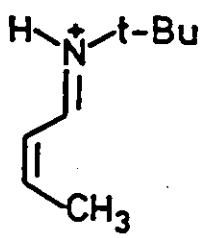


54

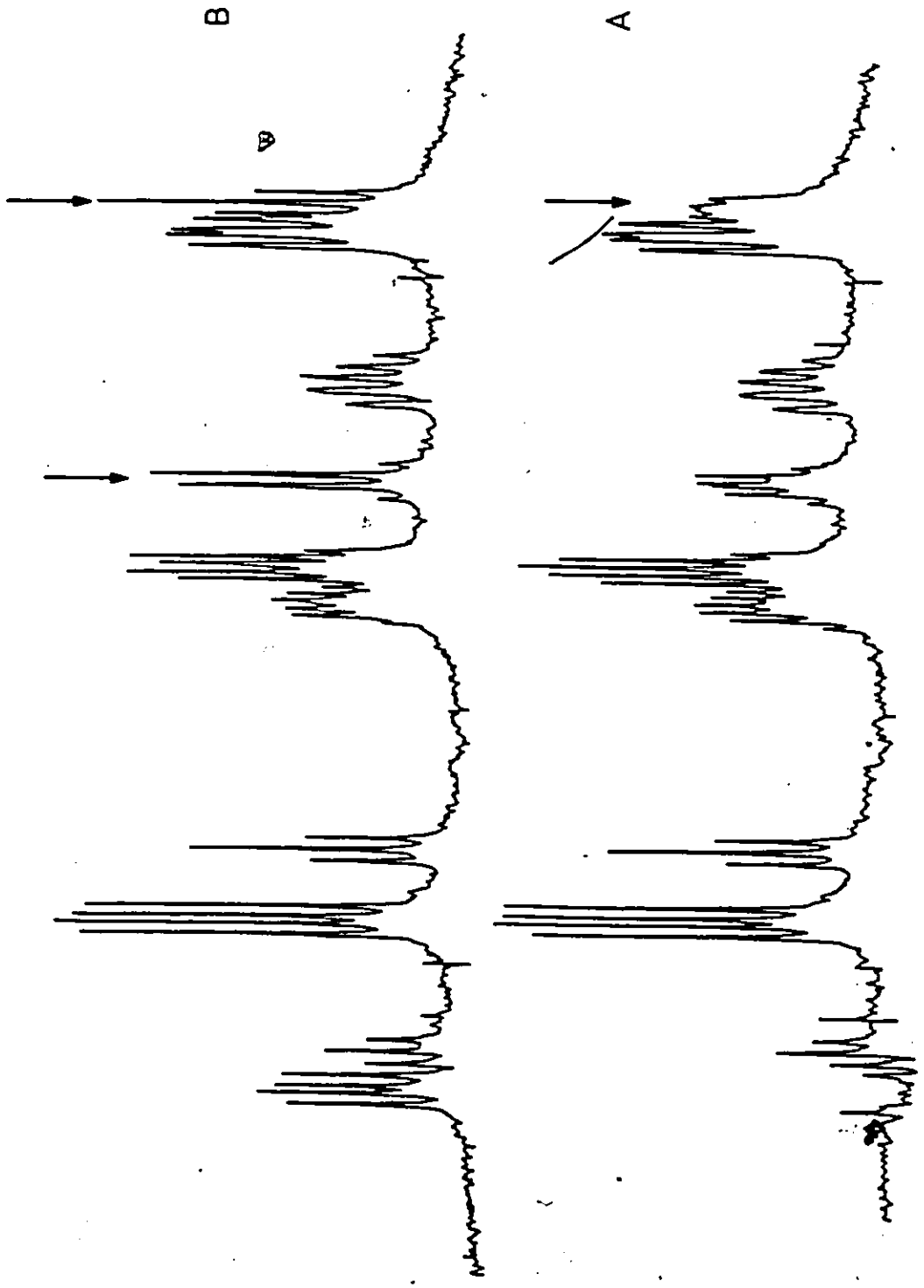


Figure 4-5: Double resonance experiments used to identify the trans,cis-N-t-butyl-2-butenylideniminium cation 54.

Identification of the cis,trans- and cis,cis-isomers was accomplished by the double resonance experiments shown in Figure 4-6. Spin decoupling of the resonance at δ 7.97 (Figure 4-6a) caused partial collapse of the downfield side of the multiplet centred at about δ 6.8. This indicated that the resonances at δ 8.46 and 6.86 are coupled to each other and that they are due to H1 and H2, respectively, of the same isomer. On the other hand, irradiation of the signal at δ 8.46 (Figure 4-6b) caused partial collapse of the upfield side of the multiplet centred at about δ 6.8. Thus the resonances at δ 8.46 and 6.80 are due to H1 and H2 of another isomer.

Figure 4-6c illustrates the effect of simultaneously decoupling the two methyl groups at δ 2.11 and 2.15. A sharpening of the multiplet at δ 6.8 occurred and collapse of the multiplet at about δ 7.4 gave two overlapping doublets. The higher intensity doublet, which was assumed to correspond to the resonance at δ 7.97, is coupled to a C2 proton with a constant ($J_{2,3}$) of 15 Hz. The magnitude is consistent with a trans configuration about the C=C bond (135). Thus, the resonances at δ 7.97, 7.4 and 6.86 are due to H1, H3 and H2, respectively, of the cis,trans-isomer, 53. The remaining lower intensity doublet, which must correspond to the signal at δ 8.46, is coupled to a C2 proton with a coupling constant ($J_{2,3}$) of 12 Hz. This is consistent with a cis configuration about the C2,C3 bond (135). Therefore, the signals at δ 8.46, 6.80 and 7.4 were attributed to H1, H2 and H3 respectively, of the cis,cis-isomer, 55.

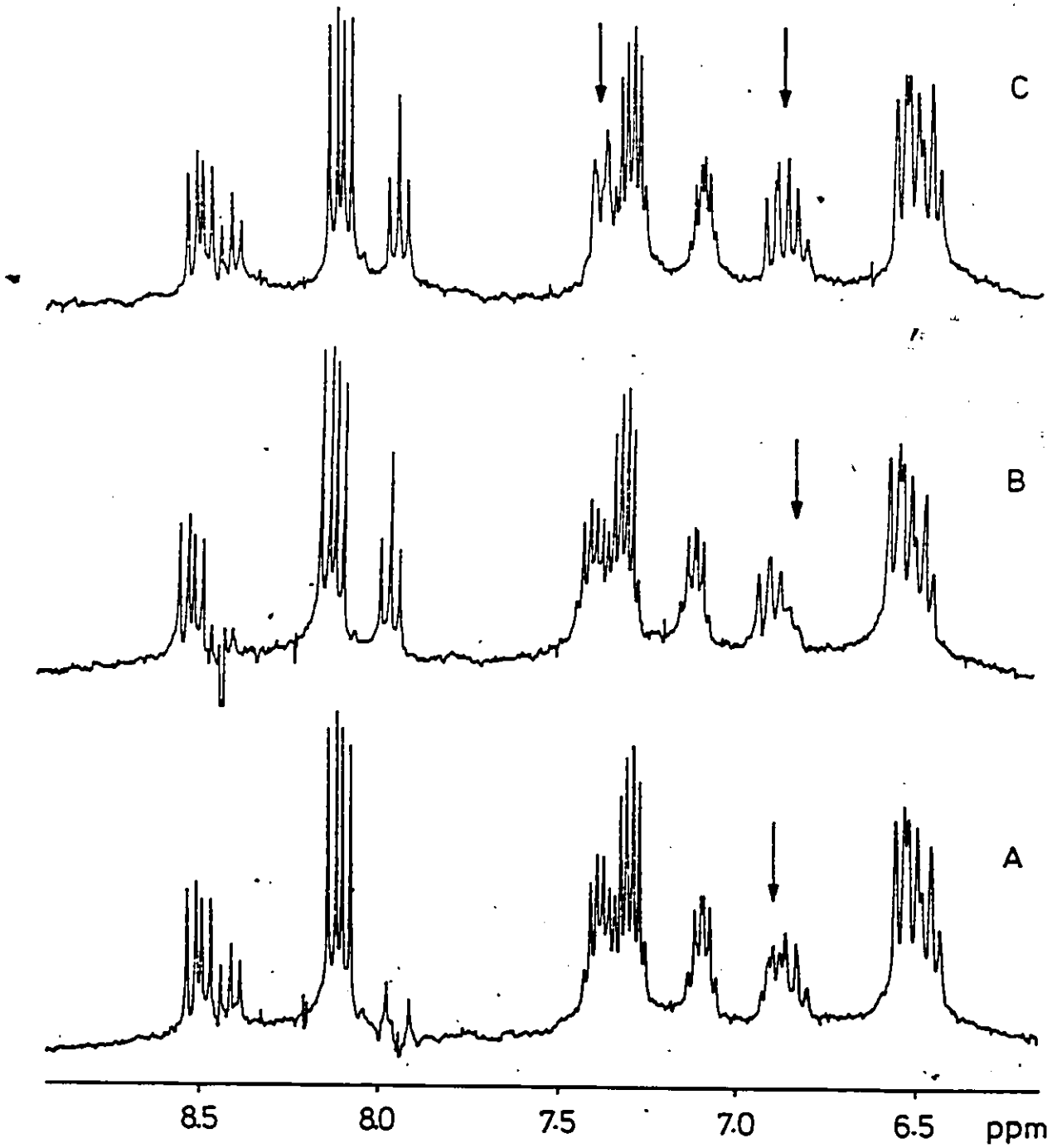


Figure 4-6: Double resonance experiments used to identify the cis,trans- and cis,cis-N-t-butyl-2-butenylideniminium cations, 53 and 55 respectively.

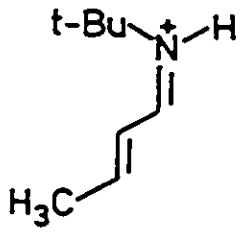

53

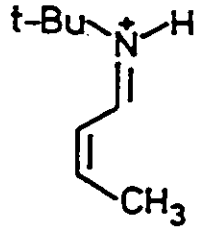

55

The vinyl region of the 400 MHz $^1$H nmr spectrum of 38 showed a doublet ($J_{N,1}$ = 17.1 Hz) at δ 8.08 due to the signal for H1 and a quartet ($J_{3,CH_3}$ = 7.3 Hz) at δ 7.09 for the resonance due to H3. Long range coupling to the C2 methyl group broadened this latter signal. In comparison with 37 and its photoproducts, a less complex spectrum was obtained for the photostationary state mixture but the lack of coupling across the C1,C2 and C2,C3 bonds, caused by methyl substitution at C2, complicated isomer identification.

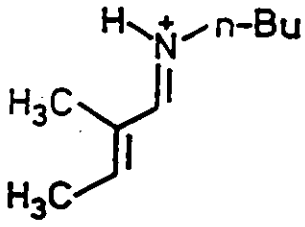

38

The spectral region from δ 7.90 to 8.70 for the mixture contained four doublets. Resonances which occurred at δ 8.08 and 8.70 had a coupling constant of about 17 Hz. These must be due to H1 of the trans,trans- and trans,cis- isomers, 38 and 57 respectively. The other two resonances in this region (δ 7.92 and 8.53) were split by a 12 Hz coupling indicative of a cis configuration about the C=N$^+$ bond (134). Based on the observation, obtained from the identification of the photoproducts formed by irradiation of 37 and 39, that the C=N$^+$

bond cis-isomers had resonances due to H1 which were shifted to higher field relative to the corresponding $C=N^+$ bond trans-isomers, the resonances at δ 7.92 and 8.53 were assigned tentatively to the C1 proton of the cis,trans- and cis,cis- isomers, 56 and 58 respectively. The remaining resonances (H3, C2 and C3 methyl groups) were related to the above signals by their relative intensities.

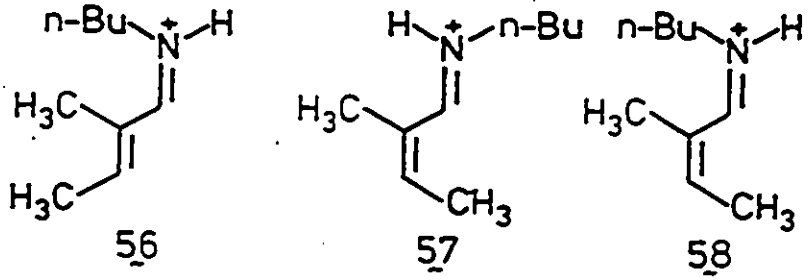


56 57 58

The photoproducts formed by the irradiation of cations 40 to 46 (see equation 20) were identified by a similar analysis of proton, proton coupling constants, Tables 4-3 and 4-4. Cations 40 and 41 have potentially three other geometric isomers. In the photomixture formed from 40 there were no detectable amounts (< 1%) of the cis,trans- and cis,cis-isomers, 60 and 62 respectively. However, the corresponding isomers 63 and 65 formed by the irradiation of 41 were produced in substantial amounts (15% and 10% respectively). The lack of any $C=N^+$ bond cis-isomers from the irradiation of 40 was not due to their thermal instability as will be discussed in Chapter 5. Salts 42 to 46 had only one photoproduct each since symmetric substitution at nitrogen made $C=N^+$ bond isomerization unobservable. Thus, the identities of their isomeric photoproducts were easily established on the basis of coupling constants.

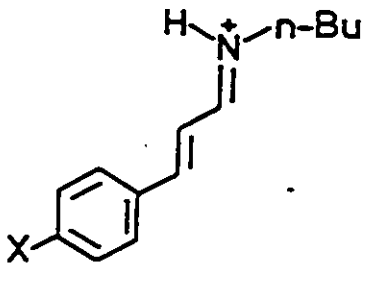

40 X=H
41 X=$NO_2$

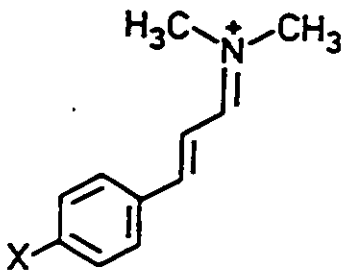

42 X=H . 43 X=$OCH_3$
44 X=$CH_3$ . 45 X=Cl
46 X=$NO_2$

It can be concluded that for all of the α,β-unsaturated iminium salts examined the principal photoproducts are geometric isomers. This, coupled with the lack of any emission, indicates that isomerization about the formal double bonds is the major dissipative pathway of the excited state. The observation of photoinduced $C=N^+$ bond isomerization is especially significant for, as far as I am aware, this is the first unambiguous evidence for such an occurrence (134).

C. Quantitative Measurements

The quantum yields of isomerization for a number of the isomer interconversions discussed in the previous two sections have been measured.

The yield for the photoisomerization about the $C=N^+$ bond of 39 (39 → 59) in TFA was measured at 25°C using a relative method, Table 4-5. Low pressure mercury lamps, which emit 98% of their light intensity at a wavelength of 253.7 nm, were used as a light source. Shorter wavelength light was absorbed by the quartz used in the equipment and the

Table 4-5

Quantum yields of isomerization for the aliphatic salts in $H_2SO_4$, $FSO_3H$ and TFA solution

| Reaction | Quantum Yield[a,b] | | | | | |
|---|---|---|---|---|---|---|
| | $H_2SO_4$ | | $FSO_3H$ | | TFA | |
| | Aerated | Degassed | Aerated | Degassed | Aerated | Degassed |
| 37 → 54 | 0.17 ± 0.02 | 0.18 ± 0.02 | 0.32 ± 0.04 | - | 0.32 ± 0.04 | - |
| 38 → 57 | 0.16 ± 0.02 | 0.15 ± 0.02 | 0.32 ± 0.03 | - | 0.31 ± 0.03 | 0.22 ± 0.03[c] |
| 39 → 59 | 0.12 ± 0.01 | 0.11 ± 0.01 | 0.12 ± 0.01 | 0.12 ± 0.01 | 0.11 ± 0.01 | - |

[a] measured relative to the photodecomposition of potassium ferrioxalate (152) at 253.7 nm, reactions have been corrected for back reaction (153).

[b] errors were estimated at ± 10%.

[c] value may be low due to solvent evaporation in the degassing experiment.

low intensity bands at longer wavelengths were ignored. The irradiations were carried out using a photochemical reactor with the samples in 5-mm-i.d. quartz tubes. Ferrioxalate actinometry was used to monitor the photon flux (152). For this case and all those described below the percent conversion was monitored by a $^1H$ nmr assay technique directly on the irradiated mixture. In all cases the conversion was less than 10% and was corrected for back reaction (153).

Quantum yields for C=C bond isomerization in 37 (37 → 54) and 38 (38 → 57) in TFA were measured at 25°C relative to the conversion of trans- to cis-pent-3-en-2-one in isopentane (165), Table 4-5. The same experimental set up described above was used but in these cases the samples were in 5-mm-o.d. quartz nmr tubes. The quantum yields for the conversions of 37 → 54, 38 → 57 and 39 → 59 were also measured in $H_2SO_4$ and $FSO_3H$ (or deuterated analogs) at 25°C relative to the conversion of trans- to cis-pent-3-en-2-one in isopentane (165), Table 4-5. Again samples were contained in quartz nmr tubes.

Most of the quantum yields in the various acid media were checked for the effect of dissolved oxygen. Degassing was achieved by bubbling dry nitrogen through the samples prior to irradiation. These data are contained in Table 4-5.

Since the sample concentrations were high, there could have been a significant layering effect. This was checked in the case of the conversion of 39 → 59 in $H_2SO_4$. The quantum yield was remeasured using the larger quartz tubes and ferrioxalate actinometry (152), only this time the samples were stirred during the irradiation by bubbling argon through them. There was no change in the quantum yield. It was concluded that there was no layering effect and this was assumed to apply to the

other systems and the other solvents.

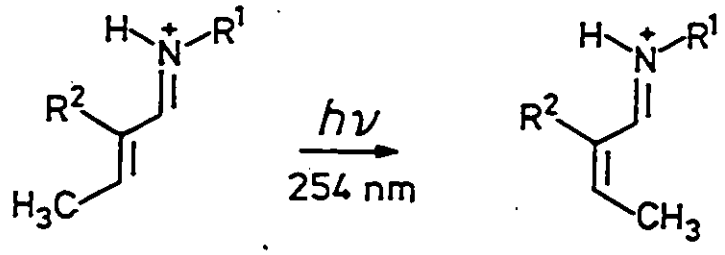


37 $R^1$=t-Bu , $R^2$=H
38 $R^1$=n-Bu , $R^2$=$CH_3$

54
57

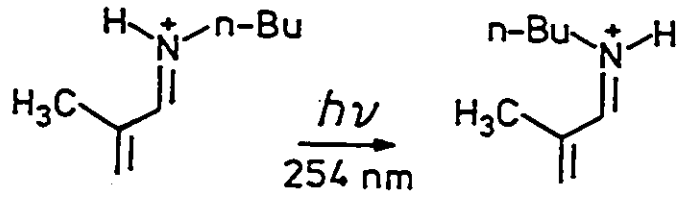


39

59

The quantum yields for C=C bond isomerization of various phenyl substituted salts in TFA were measured at 25°C by a relative method. An optical bench setup was employed. The light source was a super high pressure mercury lamp and the wavelengths (313 nm or 366 nm), with 20 nm bandwidths, were selected using a monochromator. After irradiation, a portion of the sample was transferred to an nmr tube and the percent conversion was determined from the 400 MHz $^1$H nmr spectrum of the mixture. In all cases the percent conversion was less than 10% and was corrected for back reaction (153). The yields for all of the reactions were measured relative to the photodecomposition of potassium ferrioxalate (152) and are summarized in Table 4-6.

Table 4-6

Quantum yields of isomerization for the aromatic salts in TFA solution

| Reaction | Excitation λ (nm) | Quantum Yield[a,b] |
|---|---|---|
| 40 → 61 | 313 | 0.58 ± 0.06 |
| 42 → 66 | 313 | 0.60 ± 0.06 |
| 42 → 66 | 366 | 0.75 ± 0.08 |
| 66 → 42[c] | 313 | 0.45 ± 0.05 |
| 43 → 67 | 366 | 0.59 ± 0.04 |
| 44 → 68 | 313 | 0.52 ± 0.05 |
| 45 → 69 | 313 | 0.58 ± 0.09 |
| 46 → 70 | 313 | 0.27 ± 0.02 |
| 70 → 46[c] | 313 | 0.33 ± 0.03 |

[a] errors are standard deviation of 3-4 runs.

[b] measured relative to the photodecomposition of potassium ferrioxalate (152), reactions have been corrected for back reaction (153).

[c] calculated using equation 21.

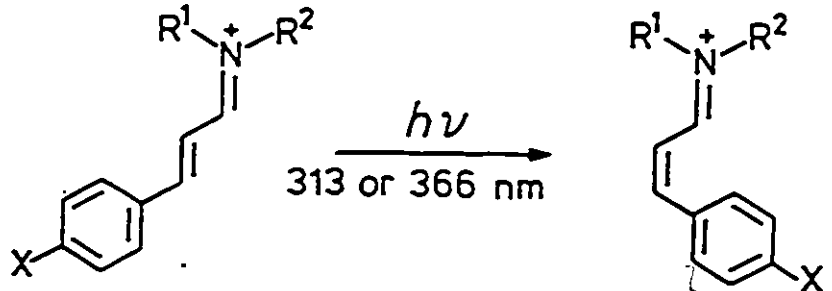


| | |
|---|---|
| 40 $R^1$=H, $R^2$=n-Bu, X=H | 61 |
| 42 $R^1$=$R^2$=$CH_3$, X=H | 66 |
| 43 $R^1$=$R^2$=$CH_3$, X=$OCH_3$ | 67 |
| 44 $R^1$=$R^2$=$CH_3$, X=$CH_3$ | 68 |
| 45 $R^1$=$R^2$=$CH_3$, X=Cl | 69 |
| 46 $R^1$=$R^2$=$CH_3$, X=$NO_2$ | 70 |

All of the above quantum yields are for the forward (trans → cis) reaction. A value for the reverse (cis → trans) reaction was desired. Since the cis-isomers could not be isolated from the irradiated mixtures nor synthesized independently (154) the yield for the reverse process had to be estimated from the photostationary state data.

At the photostationary state the rates of the forward and reverse isomerization reactions are equal. The relative rate of a photochemical process is the product of three terms - the concentration ($C_x$) of the reactant, the molar extinction coefficient ($\varepsilon_x$) of the reactant and the quantum yield ($\phi_{x \to y}$) for the reaction. Thus, at the photostationary state of a single cis/trans isomerization, equation 21 holds.

$$\phi_{t \to c} C_t \varepsilon_t = \phi_{c \to t} C_c \varepsilon_c \qquad (21)$$

where $\phi_{t \to c}$ and $\phi_{c \to t}$ are the quantum yields for the conversion of the trans- to cis- and cis- to trans-isomers respectively, $C_t$ and $C_c$ are the photostationary state concentrations of the trans- and cis-isomers

respectively and $\varepsilon_t$ and $\varepsilon_c$ are the molar extinction coefficients at the appropriate wavelength for the trans- and cis-isomers respectively.

The quantum yields of the reverse process for 42 (66 → 42) and 46 (70 → 46) were estimated (see Table 4-6) using equation 21 and data given in the previous section. In the case of 42 and 66 the yield of the forward reaction (42 → 66) was measured as described previously and the molar extinction coefficient at 313 nm[†] of 42 was determined from its absorption spectrum. The extinction coefficient for the cis-isomer 66 was estimated from the absorption spectrum of the photostationary state mixture. The relative concentrations of 42 and 66 at the photostationary state were determined from the 400 MHz $^1$H nmr spectrum of the mixture. The only unknown remaining in equation 21 is the quantum yield for the conversion of 66 to 42 and this can be calculated by a slight manipulation of the equation. A similar analysis was used to estimate the quantum yield for the conversion of 70 to 46.

A preliminary experiment to examine the photoisomerizations of 41 was carried out. Since the photostationary state formed by the irradiation of 41 contained significant amounts of the cis C=N$^+$ bond isomers it was thought that a good estimate for the quantum yield of isomerization about the C=N$^+$ bond (41 → 63) might be obtained. The relative amounts of each isomer were monitored by a $^1$H nmr assay technique directly on the irradiated sample. The sample was contained in a 5-mm-o.d. medium-walled nmr tube and was irradiated with a broad

---

[†]The molar extinction coefficients at 313 nm for 42 and 66 are 5750 and 6220 respectively while the corresponding values for 46 and 70 are 28200 and 32500. Units are $cm^{-1}$ $M^{-1}$.

band of light centred at 300 nm.

By analogy to the conversions of 40 → 61 and 42 → 66 it was assumed that the quantum yield for C=C bond isomerization in 41 (41 → 64) was the same as for the conversion of 46 → 70 ($\phi$ = 0.27 ± 0.02). The conversion of 41 to 64 was monitored up to 21% conversion. At this point there was still no detectable amount of the cis,trans-isomer 63. This result implied that the concentration of 63 in the mixture was less than 2% and so the yield for the conversion of 41 → 63 must be less than 0.03.

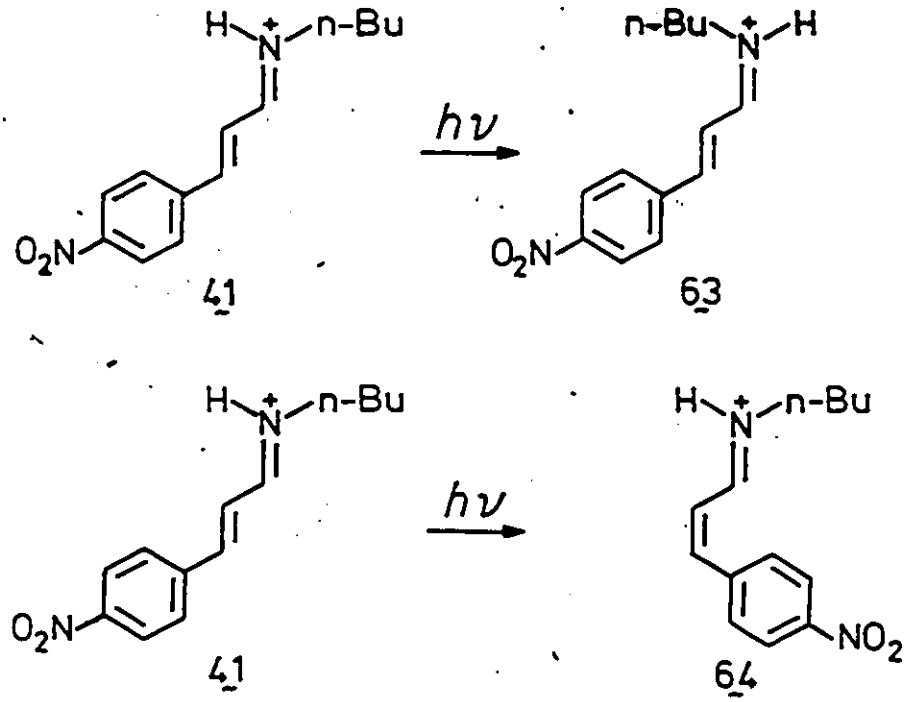


*Multiplicity of Excited State*

Since the α,β-unsaturated iminium salts do not fluoresce, the identity of the excited state must be deduced from an examination of the quantum yields of isomerization. Any changes in these yields caused by quenching or triplet sensitization could also aid in the

identification.

To differentiate between singlet and triplet photochemistry, a comparison of the results obtained by direct irradiation in the presence or absence of a triplet quencher is usually made. Triplet chemistry alone is observed by the use of triplet sensitization experiments. A quenching experiment involving molecular oxygen was carried out and the results are summarized in Table 4-5. These data indicate that the magnitudes of the quantum yields are not dependent on dissolved oxygen. Reaction from a singlet or short lived triplet state is consistent with these results (155).

Sensitization experiments were not carried out. Due to the solvents employed here the choice of sensitizers is limited to species such as europium salts (156). Energy transfer efficiencies between two cationic species are not well defined so that a great deal of fundamental work needed to be done before these experiments could be performed. Standard photochemical solvents (eg $CH_3OH$, $CH_3CN$), in which the more common sensitizers could have been used, could not be employed because it was found that the cis-isomers are thermally unstable in them, and undesirable electron transfer processes might also take place (94-99).

In salt 39 the quantum yield of isomerization about the $C=N^+$ bond is 0.11 $\pm$ 0.01 while the quantum yields for C=C bond isomerization in 37, 38 and 40 are 0.32 $\pm$ 0.04, 0.31 $\pm$ 0.03 and 0.58 $\pm$ 0.06 respectively. For these latter salts isomerization about the $C=N^+$ bond is also observable. However, isomerization about this bond was not detected in the C=C bond quantum yield measurements, since the percent conversions were less than 10%. The amount of cis $C=N^+$ bond isomers formed must be

below the nmr detection limit of 1% to 2%. This implies that the quantum yield for $C=N^+$ bond isomerization in 37, 38 and 40 must be less than 0.10. Such a large difference in the efficiencies of isomerization about the two multiple bonds suggests that these two processes are not coupled. That is, isomerization occurs about only one bond per quantum absorbed. Isomerization can occur from $S_1$ and $T_1$ but from studies of photoisomerizations of 1,3-dienes it is generally believed that reaction from $S_1$ results in isomerization about only one bond per quantum whereas reaction from $T_1$ can result in the isomerization of two bonds per quantum (157).

Although the excited state from which photoisomerization is occurring cannot be determined with certainty, the preceding quenching data and the relative magnitudes of the yields for $C=N^+$ and C=C bond isomerizations infer that a singlet state is involved.

*Substituent Effects*

In salt 39 $C=N^+$ bond photoisomerization is a relatively efficient reaction ($\phi = 0.11 \pm 0.01$ in TFA) (134). It is interesting to note that the quantum yield is very similar to that measured for $C=O^+$ bond isomerization ($\phi = 0.15 \pm 0.03$ in $FSO_3H$) in the methoxy allyl cation 71 (158-160). Isomerizations about the $C=N^+$ or $C=O^+$ bonds of these protonated iminium salts or enones are clearly one of the major pathways by which the excited states of these cations are deactivated. This result suggests that such a reaction might be important in the visual pigments.

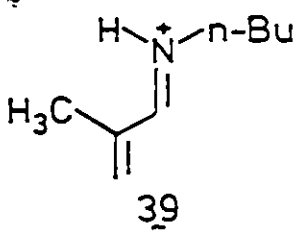

39

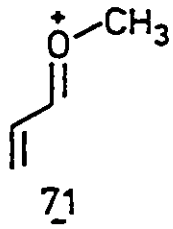

71

In the previous section it was estimated that for salts 37, 38 and 40, in which both $C=N^+$ and C=C can be observed, the quantum yield for $C=N^+$ bond isomerization is less than 0.10. This value is substantially lower in the case of salt 41 ($\phi < 0.03$). These results clearly indicate that a methyl or aryl substituent at C3 lowers the quantum yield for $C=N^+$ bond isomerization. This implies that for a retinal iminium salt system, which is conjugated extensively, the yield for $C=N^+$ bond isomerization might be very low.

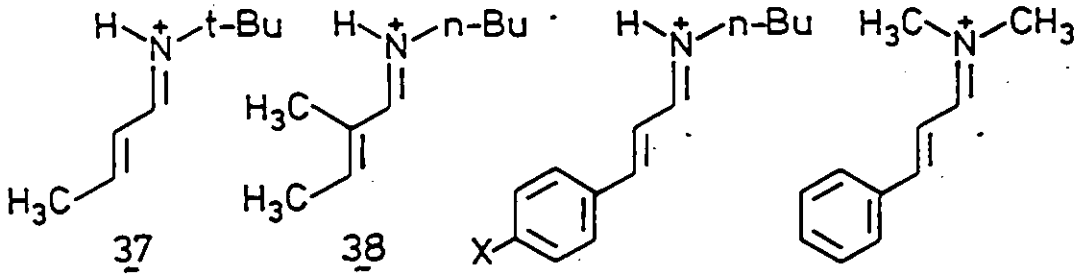

37 38 40 X=H 41 X=$NO_2$ 42

In salts 37 and 38 the quantum yields for C=C bond isomerization, 0.32 ± 0.04 and 0.31 ± 0.03 respectively, are identical within experimental error. This indicates that minor substituent changes at C2 and nitrogen have either no effect on the yield for C=C bond isomerization or their effects cancel. The former conclusion is more probable. An extension of the conjugated chain, such as in salt 40, causes an increase of the quantum yield for C=C bond isomerization (0.58 ± 0.06)

and, as discussed above, this appears to be accompanied by a decrease in the yield for the isomerization about the $C=N^+$ bond. Salt 42, which is very similar to 40, has a comparable quantum yield for C=C bond isomerization ($0.60 \pm 0.06$), again implying that minor substituent changes at nitrogen have no effect on the yield for C=C bond isomerization. These latter two quantum yields are very similar in magnitude to that measured for rhodopsin ($\phi = 0.67$, references 73 and 77).

The wavelength dependence of the quantum yield for C=C bond isomerization was determined for salt 42, Table 4-6. The quantum yield was measured at 313 nm and 366 nm and even though these wavelengths are widely separated, the energy is still being absorbed into the lowest energy absorption band. The value determined at 366 nm ($0.75 \pm 0.08$) appears to be higher than that measured at 313 nm ($0.60 \pm 0.06$). However, the two values are within two standard deviations of each other and so are not statistically different. It was concluded that for excitation into the lowest energy absorption band the quantum yield for C=C bond isomerization is wavelength independent. This result is in good agreement with the quantum yield measurements for rhodopsin (73,77) but in contrast with those obtained for retinal iminium salts in solution (31,35).

*Possible Isomerization Mechanisms*

Photochemical isomerization in the α,β-unsaturated iminium salts could proceed by an intra- or intermolecular mechanism. Quantum yields for isomerization are not dependent on acid strength (compare the results in $FSO_3H$ and TFA in Table 4-5) and irradiation in a deuterated

medium does not produce any detectable deuterium incorporation. Electron transfer induced isomerizations would be expected to yield a thermodynamic equilibrium mixture of isomers. The photostationary state mixtures are not equilibrium mixtures (see Chapter 5). Therefore an electron transfer pathway can be discarded. These results all imply that an intramolecular mechanism is involved.

There are three conceivable intramolecular pathways. The first is a photon-induced disrotatory ring closure followed by a thermal ring opening, Scheme 4-1. Such a process can result in isomerization about either $C=N^+$ or C=C bonds depending on the direction of ring opening. The ring closure has been observed in the direct irradiation of 1,3-dienes but the conjugated olefin must be in the s-cis conformation (157). In Chapter 3 it was shown that the α,β-unsaturated iminium salts exist predominantly in the s-trans conformation (129). A minor conformational component could not account for the high quantum yields of isomerization since rotation about the C1,C2 bond is restricted in the excited state (161). Thus, this mechanism can be eliminated as a viable isomerization pathway.

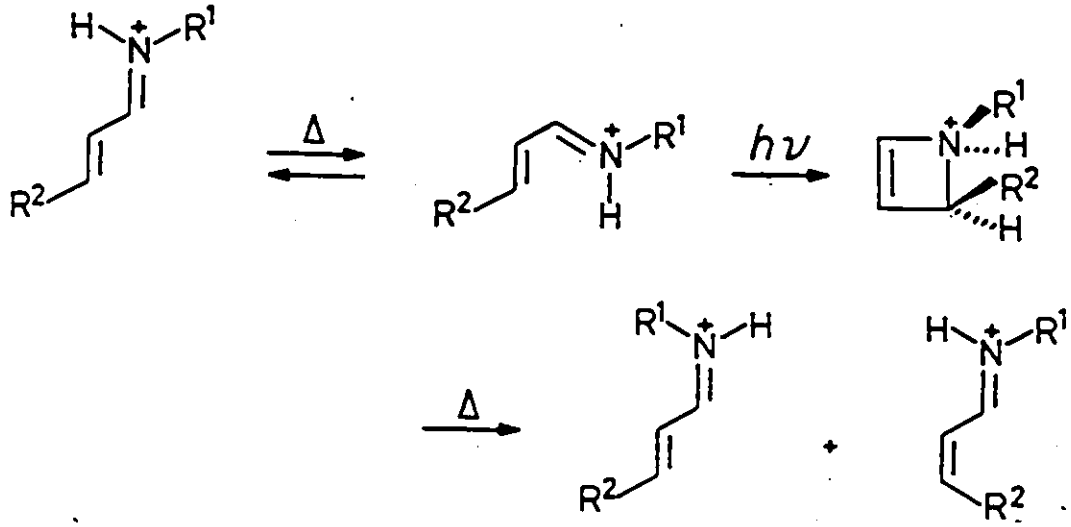

Scheme 4-1

A second pathway involving concerted cyclopropyl ring formation is illustrated in Scheme 4-2. Excitation of one geometric isomer can lead to two different intermediates. If the thermal cyclopropyl ring opening is governed by orbital symmetry considerations then ring opening results in the formation of either a new isomer or the starting one (157). To be consistent with the large difference observed for the quantum yields for $C{=}N^{+}$ and C=C bond isomerizations, the rate of interconversion of these intermediates must be slow compared with their rate of decay to the ground state.

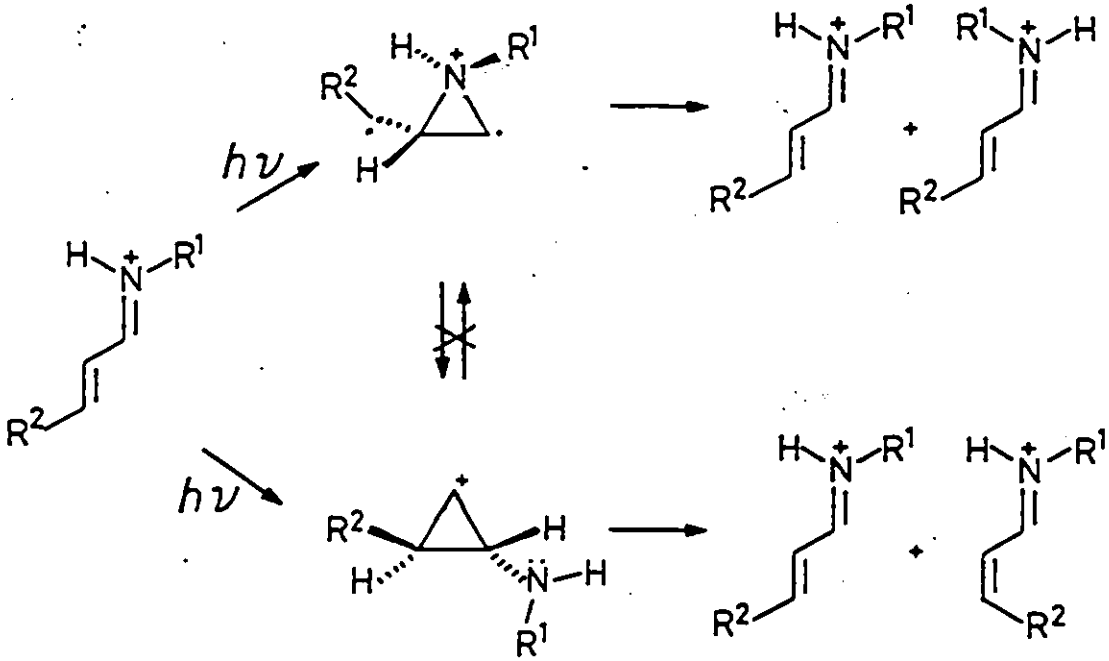

Scheme 4-2

For C=C bond isomerization in the cyclopropyl mechanism (Scheme 4-2) the intermediate has either a cationic (illustrated) or radical centre at C2. In either case this suggests that substituents at C2 might affect the yield for C=C bond isomerization. However, the data discussed in the previous section showed that a change of substituent at C2 had no effect on the quantum yield of isomerization about the C=C bond.

The final mechanism involves the formation of a twisted excited state intermediate by the rotation of one of the multiple bonds, Scheme 4-3. Again, excitation of one of the geometric isomers can lead to two different intermediates which must not interconvert at a rate comparable to their decay to ground state. Decay of these intermediates can lead to either a new isomer or back to the original one.

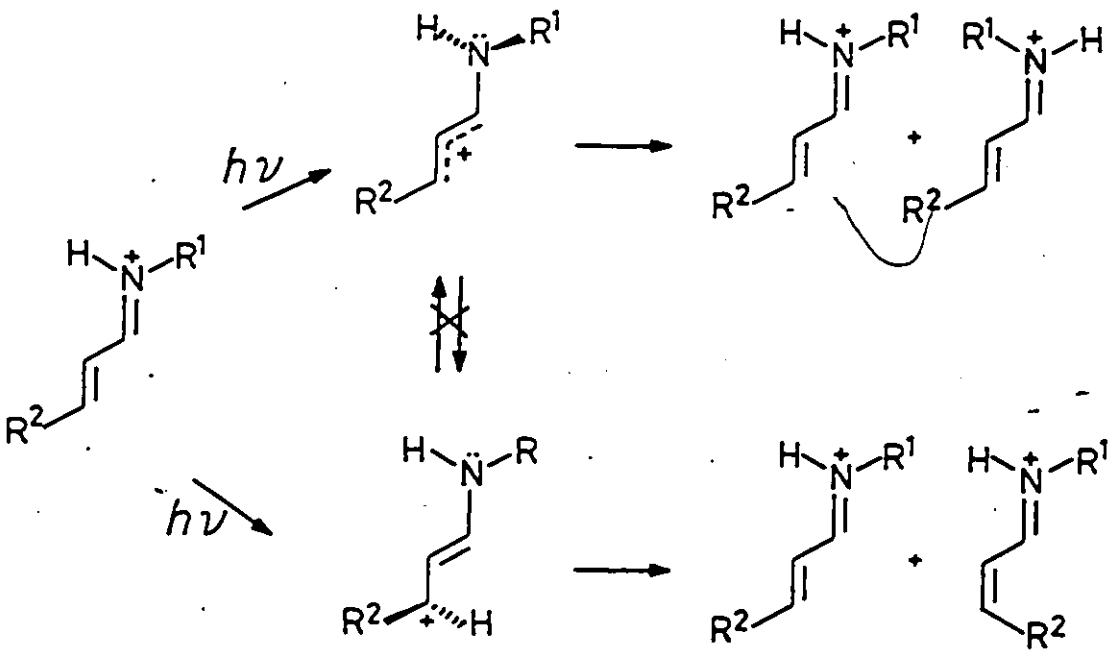


Scheme 4-3

In this mechanism the intermediate can be composed of either cationic and neutral segments (illustrated) or radical cationic and radical segments. The former electron distribution is consistent with the calculations of Salem and Bruckmann (87,88). They proposed, from their theoretical calculations, that in the first excited singlet state of conjugated iminium salts there is a shift of the positive charge from the nitrogen onto the carbon framework. This charge polarization is most pronounced when one of the C=C bonds is twisted by 90° although even in the "planar" excited state there is a substantial change in charge distribution.

For the α,β-unsaturated iminium salts examined here this change in charge distribution implies that in the excited state there is a large increase of the positive charge at C3. This should be most pronounced in the twisted intermediate such that C3 could have nearly a full positive charge in the case of C=C bond isomerization. As the electron demand of the substituent at C3 changes, the energy of this intermediate should change dramatically. In fact the entire potential energy surface for the excited state might be altered. Thus, a change in the excited state energy partitioning might be expected.

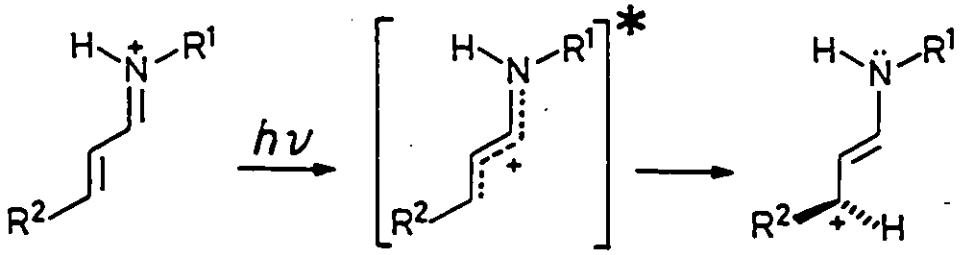

The absorption data for salts 42 to 46 (see Table 4-1) support a shift in positive charge for the "planar" excited state. The methoxy substituted salt 43, which is best able to stabilize a positive charge at C3, has the lowest energy transition ($\lambda_{max}$ = 384 nm) while the destabilized nitro substituted salt 46, has the highest energy transition ($\lambda_{max}$ = 323 nm).

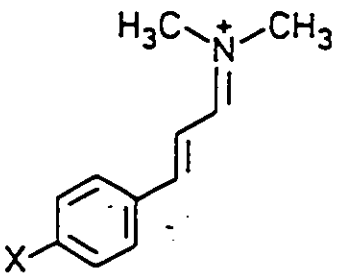

42 X=H , 43 X=$OCH_3$
44 X=$CH_3$ , 45 X=Cl
46 X=$NO_2$

In salts 42 to 45 the quantum yields for C=C bond isomerization range from 0.52 ± 0.05 to 0.60 ± 0.06, Table 4-6. These values are identical within experimental error and calculation of the yield for the reverse reaction in 42 (66 → 42, $\phi$ = 0.45 ± 0.05) shows that the sum of the two quantum yields is 1.0. This suggests that all of the energy might be channelled into C=C bond isomerization. Salt 46, however, has a significantly lower quantum yield (0.27 ± 0.03) and calculation of the yield for the reverse process (0.33 ± 0.03) indicates that only 60% of the excited state energy is accounted for by isomerization about the C=C bond. The low estimated value for the quantum yield of isomerization about the $C=\overset{+}{N}$ bond in 41 ($\phi$ < 0.03) implies that the remaining energy is not all funnelled into $C=N^+$ bond isomerization. Where this energy is going cannot be established at the present time. This electronic

dependence of the magnitude of the quantum yield for C=C bond isomerization is completely consistent with a large shift of positive charge, in the singlet excited state, from the iminium moiety onto the carbon framework.

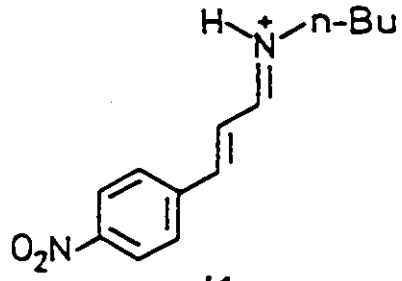

41

The bond rotation mechanism (Scheme 4-3) is the only one which is consistent with a large shift in charge distribution. Thus, the above results strongly suggest that this mechanism is the operative pathway for isomerization of the iminium salts.

*Viscosity Dependence*

The viscosity dependence of the quantum yields of isomerization of salts 37 to 39 is illustrated by the data in Table 4-5. At 25°C the viscosities of the solvents used vary over a wide range - 20.0 cP for 96% $H_2SO_4$ (162), 1.56 cP for $FSO_3H$ (163) and 0.854 cP for TFA (164). These values are for the pure solvents and will be altered by the presence of solute, but they should give a good idea of the viscosity differences involved.

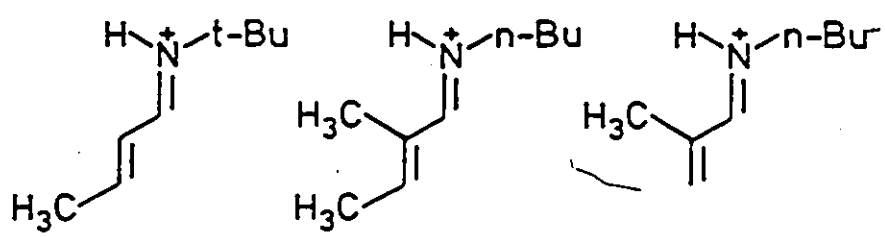

37 38 39

For salt 39 the quantum yield for $C=N^+$ bond isomerization varies from 0.12 ± 0.01 in $H_2SO_4$ and $FSO_3H$ to 0.11 ± 0.01 in TFA. These values are identical within experimental error. The quantum yields for C=C bond isomerization in 37 and 38 show a marked viscosity dependence. In $FSO_3H$ and TFA the quantum yields are 0.32 ± 0.04 and 0.31 ± 0.03 for 37 and 38 respectively whereas in the more viscous $H_2SO_4$ the corresponding values are 0.17 ± 0.02 and 0.16 ± 0.02. A similar viscosity dependence of the yield for C=C bond isomerization in protonated enones has been reported (160). This dependence of the quantum yield of isomerization about the C=C bond may be due to a redistribution of the solute/solvent interactions caused by an alteration of the charge distribution (134,160).

In the ground state of the α,β-unsaturated iminium salts most of the positive charge is localized in the iminium moiety so that, while the crystallographic data indicate that there are no specific cation/anion interactions, the strongest solute/solvent interactions are expected to be around the $C=N^+$ bond. The charge distribution in the excited state appears to be different. Electronic absorption data and the electronic dependence of the quantum yields of isomerization are consistent with an increase of positive charge at C3. A natural consequence of this effect is that the amount of positive charge on nitrogen is diminished. Thus, in the excited state the solute/solvent interactions might be weakened around the $C=N^+$ bond but increased at the C=C bond in comparison to the ground state interactions.

Solute/solvent interactions could inhibit torsional motion about the multiple bonds in the excited state. This effect would be most pronounced in solvents of high viscosity and at bonds where the interactions are the strongest. The observation that only the yield for C=C bond isomerization shows a viscosity dependence is consistent with the idea that there is a large change in the charge distribution on going from the ground state to the first excited state. There are, however, some implications which, at this time, cannot be fully explained. Since the yield for C=C bond isomerization has diminished, does this mean that energy is now being channelled into other decay pathways? The viscosity independence of the quantum yield for $C=N^+$ bond isomerization in 39 seems to imply that no extra energy is going into this reaction. The lack of emission, even at 77K in a rigid glass, indicates that isomerization and fluorescence are not coupled as is the case in trans-stilbene (157). The only explanation which appears to be consistent with all of these results is that the decay ratio of the twisted excited state intermediate has been altered significantly. Why this should occur in the case of C=C bond isomerization only cannot be explained without further experimentation.

D. Conclusions

Upon direct irradiation in acid solution, α,β-unsaturated iminium salts undergo efficient cis/trans isomerizations. From an analysis of $^1H$ nmr data the principal photoproducts have all been identified as geometric isomers. The unambiguous identification of photoisomerization about a $C=N^+$ bond is particularly significant since, to my knowledge, it is the first report of such an occurrence.

Prolonged irradiation results in the formation of a photostationary state among the isomers and no other major photoproducts are formed. Since no emission was detected it appears that isomerization is the only major decay pathway of the excited state. Although the multiplicity of the excited state could not be determined with certainty all of the experimental data is consistent with a singlet state.

In the one case where the quantum yield for $C=N^+$ bond isomerization could be measured without ambiguity this reaction was shown to be efficient. However, charge stabilizing substituents at C3 appear to lower this yield dramatically. The quantum yield for C=C bond isomerization, on the other hand, is increased when such substituents are placed at C3.

An isomerization mechanism involving rotation about a single multiple bond per quantum absorbed is consistent with the experimental data. As proposed by Salem and Bruckmann (87,88) such a mechanism requires an extensive change in charge distribution in the excited state. Particularly in the case of C=C bond isomerization a significant positive charge increase at C3 is a consequence of this mechanism. The electronic and viscosity dependence of the quantum yields for C=C bond isomerization and the electronic absorption data all support this dramatic charge polarization.

# CHAPTER 5

## THERMAL CHEMISTRY

Stereomutation about the acyclic double bonds of the α,β-unsaturated iminium salts can also occur in the ground state. A quantitative investigation of these reactions and an evaluation of the possible mechanistic pathways was undertaken and the results are presented here.

### A. Qualitative Observations

For the aliphatic α,β-unsaturated iminium salts 37 to 39 there were no observable thermal isomerizations at temperatures up to 60°C in any of the acid media (134). The heating of solutions of either the starting all-trans isomers or their photostationary state mixtures did not give any detectable changes in their $^1$H nmr spectra. Prolonged heating (> 24 hours) of these salts resulted in a general decomposition. Since it appeared that no useful information could be obtained, further investigation of these salts was abandoned.

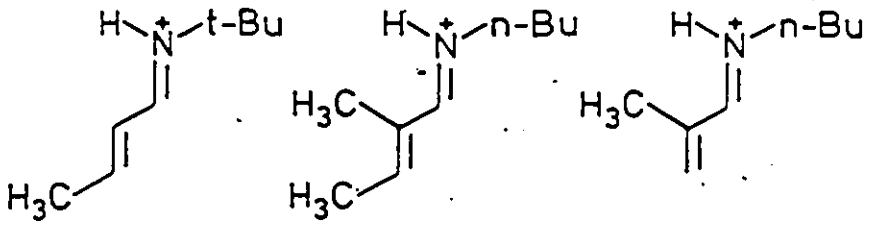


37 38 39

In contrast to the aliphatic systems, the aromatic salts 40 and 41 gave a mixture of the starting trans,trans-isomers and the cis,trans-

isomers 60 and 63 respectively, when heated at 100°C in TFA, equation 22. The same mixtures were obtained by warming the photostationary state mixtures formed from the irradiation of 40 and 41. These observations suggested that the isomers were in thermal equilibrium at 100°C. Due to the complexity of the reaction mixtures in these two cases, the experimental data were difficult to interpret quantitatively.

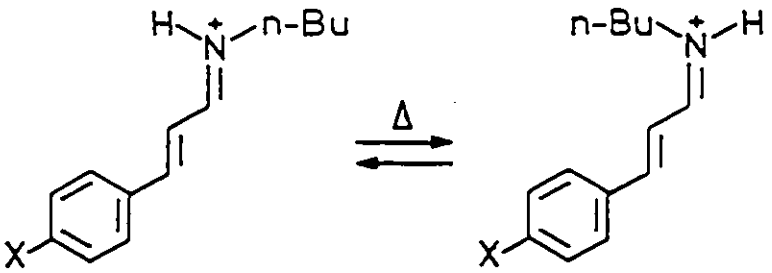


(22)

40 X=H (72%) 60 (28%)
41 X=$NO_2$ (79%) 63 (21%)

The $^1H$ nmr spectra of the iminium salts 42 to 46 showed no changes after prolonged heating at 100°C in TFA solution. This was not surprising since the $C=N^+$ isomerization observed in 40 and 41 can not be detected in salts 42 to 46 due to symmetric substitution at nitrogen. In all cases, warming of the photostationary state mixture at 100°C in TFA resulted in the conversion of the cis- to the trans-isomers. equation 23. The half-lives of these isomerizations appeared to vary greatly.

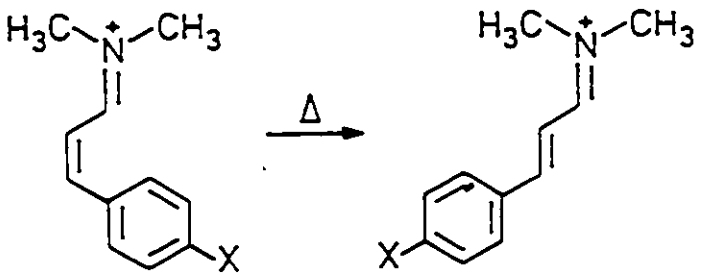

(23)

| | |
|---|---|
| 66 X=H | 42 |
| 67 X=$OCH_3$ | 43 |
| 68 X=$CH_3$ | 44 |
| 69 X=Cl | 45 |
| 70 X=$NO_2$ | 46 |

B. Quantitative Measurements

The isomerizations of salts 66 - 70 to 42 - 46 respectively were examined quantitatively. In each case a photostationary state mixture was generated by the irradiation of the appropriate trans-isomer in TFA. The reactions of the cis- to trans-compounds were measured by heating the samples in a constant temperature bath at 100 ± 0.5°C. After varying lengths of time the compositions of the solutions were determined using $^1H$ nmr spectroscopy. Two independent runs were made for each reaction.

In each case good first-order kinetics were observed. Values of the first-order rate constants are summarized in Table 5-1 along with other pertinent data.

*Substituent Effects*

The data in Table 5-1 show that the magnitudes of the rate constants of isomerization for salts 66 to 70 vary over a wide range. The fastest reaction (67 → 43) has a half-life of about 6 minutes while

Table 5-1

Isomerization rate constants at 100 ± 0.5°C for the para substituted iminium salts in TFA

| Reaction | X[c] | $k^a$ $s^{-1}$ ($x10^6$) | Log($k/k_o$) | $\sigma^{+b}$ |
|---|---|---|---|---|
| 66 → 42 | H | 1.6 | 0 | 0 |
| 67 → 43 | $OCH_3$ | 2000 | 3.1 | -0.78 |
| 68 → 44 | $CH_3$ | 4.6 | 0.45 | -0.31 |
| 69 → 45 | Cl | 2.0 | 0.084 | 0.11 |
| 70 → 46 | $NO_2$ | 19 | 1.1 | 0.79 |

[a] estimated error is ± 10%

[b] from reference 166

[c] para substituent on phenyl ring

the slowest (66 → 42) has a half-life of about 7200 minutes or 120 hours. It is clear that the para ring substituents have a profound effect on the rates of isomerization about the C=C bonds of these salts. This dependence is by no means a simple one since both a p-methoxy group and a p-nitro group accelerate the reaction relative to the unsubstituted system.

The Hammett equation, in its many variations, has been used to obtain information about reaction mechanisms (167). Equation 24 gives the form of the relationship used here.

$$\mathrm{Log}(k/k_0) = \sigma\rho \qquad (24)$$

where k and $k_0$ are reaction rate constants, $\sigma$ is a substituent parameter determined from a standard reaction and $\rho$ is a constant of proportionality. Thus if a linear free energy relationship exists between the standard reaction and the one under examination a plot of $\mathrm{Log}(k/k_0)$ vs $\sigma$ should yield a straight line of slope $\rho$.

Both the magnitude and sign of $\rho$ can provide mechanistic information. A positive $\rho$ means that electron-withdrawing substituents accelerate the rate, implying that there is an increase of electron density at the reaction site during the course of the reaction. On the other hand, a negative $\rho$ implies that there is a decrease in electron density at the reaction site. The magnitude of $\rho$ shows how sensitive the reaction is to the effect of the substituent. A $|\rho| < 1$ indicates that the reaction is less sensitive than the standard reaction while the reaction is more sensitive if $|\rho| > 1$. The slope of the Hammett plot sometimes changes as the substituents are varied. That is two straight lines of different slopes are obtained. This usually implies that the reaction mechanism

is changing in response to the varying electron demand of the substituents (167).

When the reaction site is in direct conjugation with the substituent, $\sigma$ constants, which are based on the ionization of substituted benzoic acids, often do not give a good correlation. For this reason $\sigma^+$ and $\sigma^-$ constants were introduced. These constants are employed if an electron deficient or electron rich reaction site, respectively, is in direct conjugation with the substituents. Since the substituents in salts 66 to 70 were in direct conjugation with an electron deficient centre the $\sigma^+$ constants are the most appropriate.

The Hammett $\sigma^+$ plot of the rate constants of isomerization for salts 66 to 70 is illustrated in Figure 5-1. This plot is somewhat different than that normally encountered. It has a distinct upward curve with the slope changing from positive to negative. The values for the methoxy and methyl substituted salts, 67 and 68 respectively, lie on a steeply negative slope ($\rho$ = -5.6). This suggests that there is a significant increase in positive charge in the C3/phenyl moiety during the course of the isomerization process in these systems. The data for salts 66, 69 and 70, however, lie on a much less steep positive slope ($\rho$ = 1.3). Thus during the stereomutation of these latter three salts the electron density in the C3/phenyl moiety would seem to increase. These data clearly indicate that there are at least two mechanistic pathways operating in the isomerizations of salts 66 to 70 (167). It is instructive at this point to discuss the possible mechanisms.

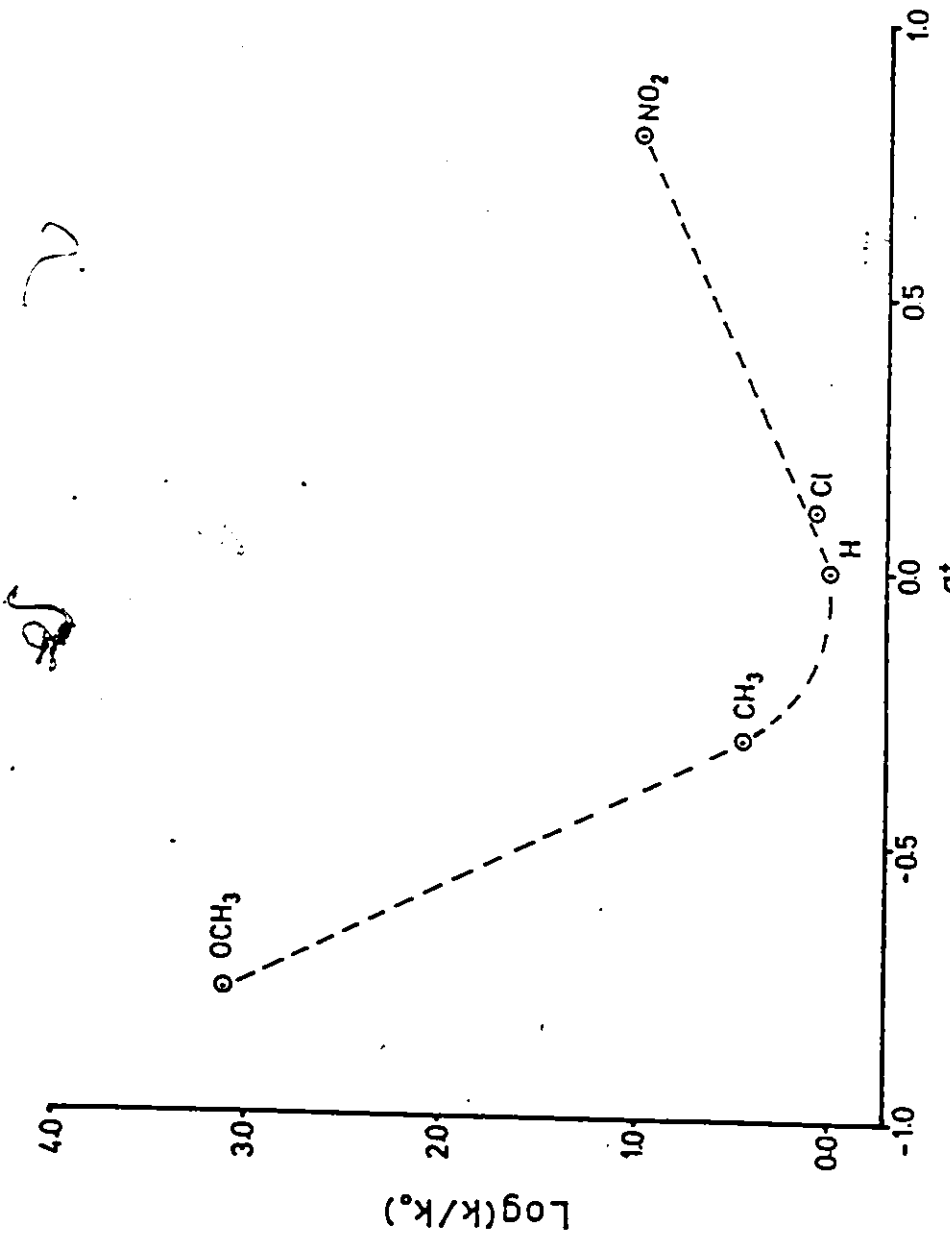


Figure 5-1 Hammett $\sigma^+$ plot for the rate constants determined in TFA.

*Possible Isomerization Mechanisms*

Four broad types of mechanisms were considered for these isomerizations. Two of these pathways, bond rotation (equation 25) and azetinium formation (equation 26), are intramolecular processes while the other two mechanisms, C2 protonation (equation 27) and Michael addition (equation 28) are intermolecular processes. The electron demand at the C3/phenyl end of the cations might be expected to vary substantially with these mechanisms.

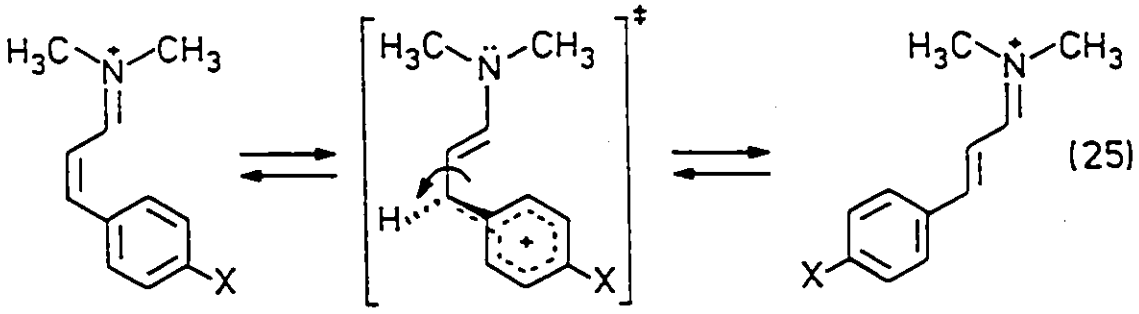

(25)

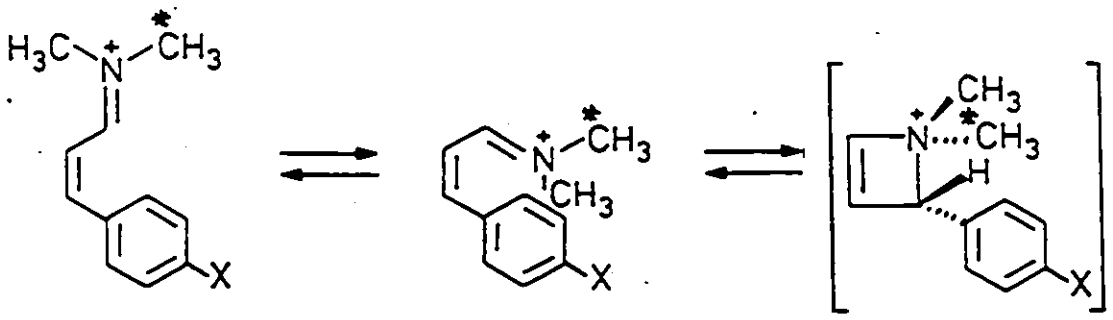

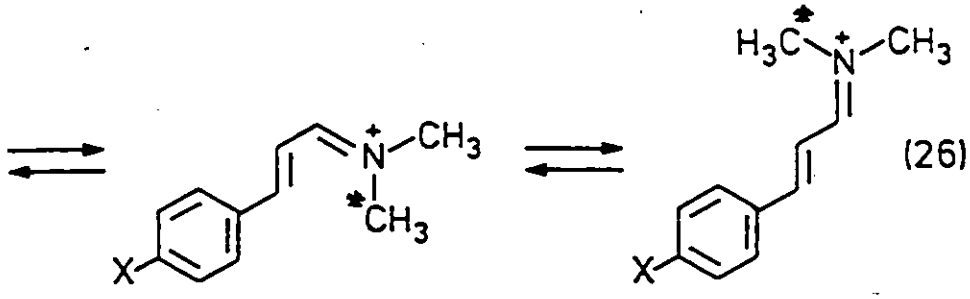

(26)

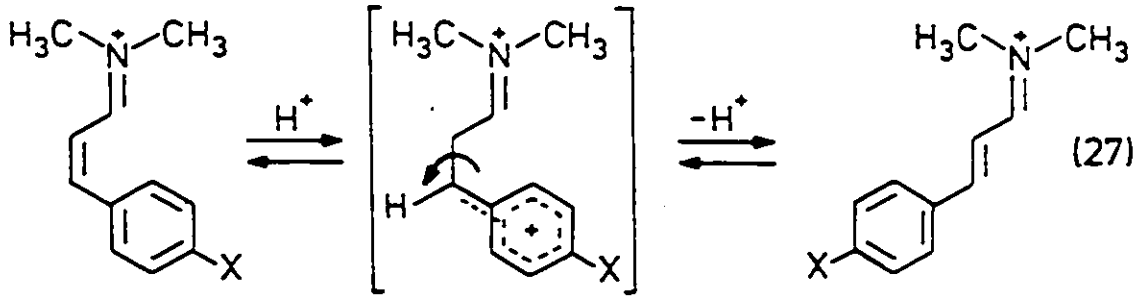


(27)

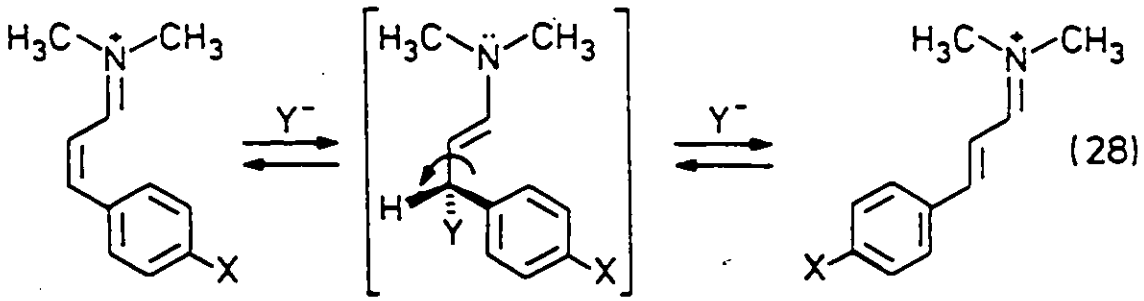


(28)

As was concluded in Chapter 3 there is some positive charge at C3 in the ground state of α,β-unsaturated iminium salts. Some of this charge should be delocalized into the phenyl ring. For the bond rotation mechanism (equation 25) it is expected that the charge distribution transition state is substantially different from that of the ground state. That is a good correlation with $\sigma^+$ might be anticipated. However, what might the slope of this plot be? It is attractive to localize the positive charge at the C3/phenyl end of the system such that the charge on the ring will be enhanced in the transition state. Thus the Hammett $\sigma^+$ plot would have a negative slope. Other charge distributions are possible.

To investigate the change in charge distribution in this pathway the isomerization about the C=C bond in the parent system 48a was examined using MINDO/3. The results of these calculations are

summarized in Table 5-2. These data include the activation energy required to go from the planar cation to the 90° twisted transition state and the total Mulliken populations at C3 for the two species. Figure 5-2 illustrates the activation energy calculated by MINDO/3.

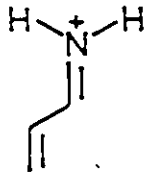

48a

The total Mulliken population at C3 for 48a is 5.81 whereas the twisted transition state has a value of 5.34. Thus the positive charge at C3 increases from 0.19 to 0.66 on going from the ground state to the transition state. This implies that the barrier to isomerization via this mechanism should be strongly dependent on the substituent at C3. In fact, this pathway should be facilitated by the presence of good positive charge stabilizing substituents at C3. These substituents are expected to have a larger effect on the energy of the transition state than on the ground state. Thus, a good correlation with $\sigma^+$ with a negative $\rho$ is anticipated. The activation barrier calculated by MINDO/3 (43.7 kcal/mol) for C=C bond isomerization in 48a is high, but, as just mentioned, this barrier should be greatly diminished by proper substitution at C3.

A mechanism involving protonation at C2 should also place significant positive charge on the C3/phenyl moiety in the isomerization intermediate, equation 27. Again positive charge stabilizing substituents at C3 would facilitate reaction by this pathway and a good correlation

Table 5-2

MINDO/3 activation energies and Mulliken populations for the bond rotation and azetinium formation mechanisms

| Mechanism | Activation Energy kcal/mol | Mulliken population at C3 (total) | |
|---|---|---|---|
| | | Planar cation | Transition state |
| Bond Rotation | 43.7 | 5.81 | 5.34 |
| Azetinium Formation | 62.0[a] | 5.83 | 5.77 |

[a] for formation of transition state from s-cis iminium salt 48b.

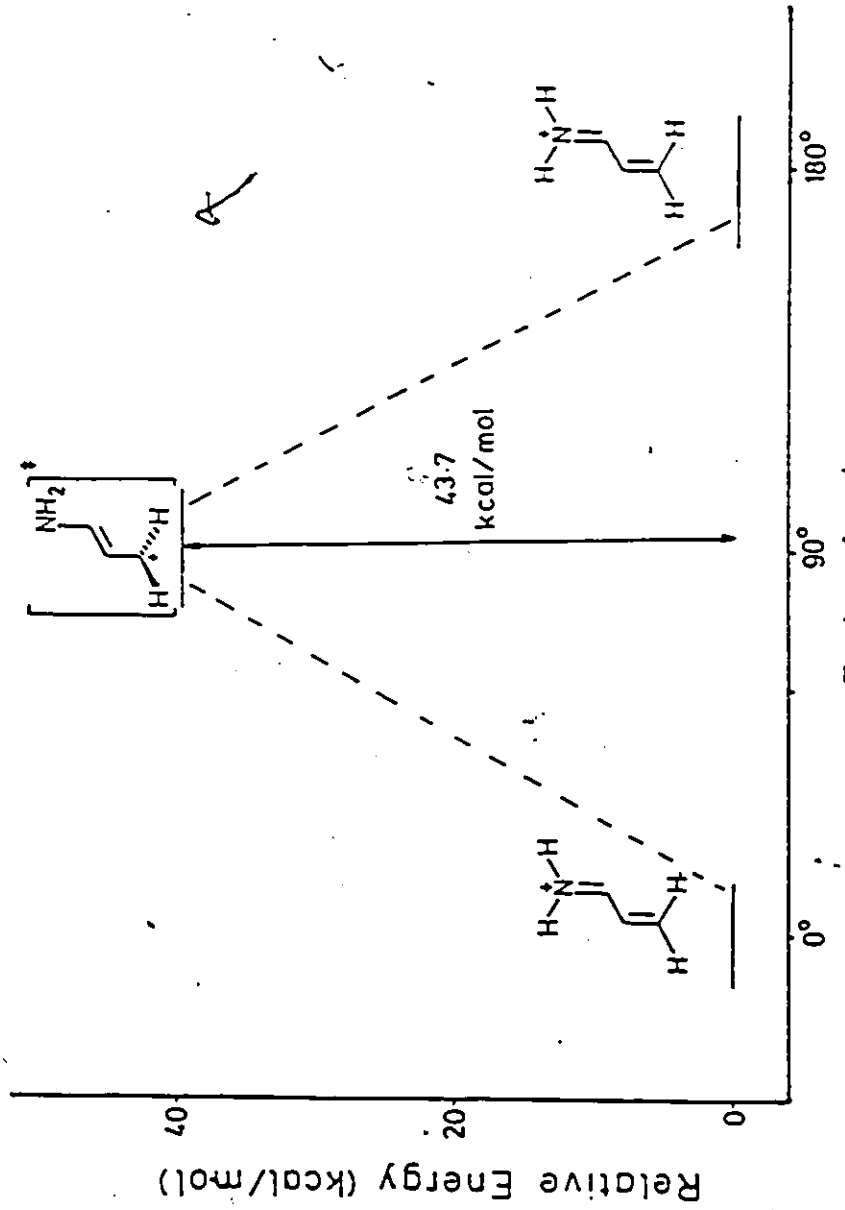


Figure 5-2 MINDO/3 activation barrier for C=C bond rotation of the parent α,β-unsaturated iminium cation, 48a.

with $\sigma^+$ with a negative slope is expected. This mechanism could be ruled out for the stereomutation of protonated enones (124) but cyanine dyes are known to protonate at C2 (109,168).

Isomerization via azetinium formation involves a thermally allowed conrotatory ring closure and re-opening, equation 26. Ring closure must occur from the s-cis conformation. Both $C=N^+$ and C=C bond isomerizations would be expected to occur simultaneously if the ring closure and re-opening are concerted. However, in the cases discussed here, $C=N^+$ bond isomerization cannot be detected. A similar mechanism involving an oxete has been suggested to be involved in the stereomutation of protonated enones (124).

From a qualitative argument using the Hammond postulate (169), it would appear that the geometry of the transition state for azetinium formation more closely resembles the four-membered ring. In the azetinium ion, C3 is no longer conjugated to the formally positively charged nitrogen. Thus the electron density in the C3/phenyl moiety might be expected to increase on going from the iminium salt to the transition state. If this is the case, a correlation with $\sigma^+$ is still expected but with a positive value.

To examine the energy requirements and charge distribution in this mechanism the energy surface for the conversion of the parent azetinium ion 72 to the s-cis iminium cation 48b was determined by the MINDO/3 method. In these calculations the N,C3 bond length was used as the reaction coordinate. The calculated transition state geometry was similar to that determined by Dewar and Kirschner (170) for the conrotatory ring opening of cyclobutene. Some of these results are

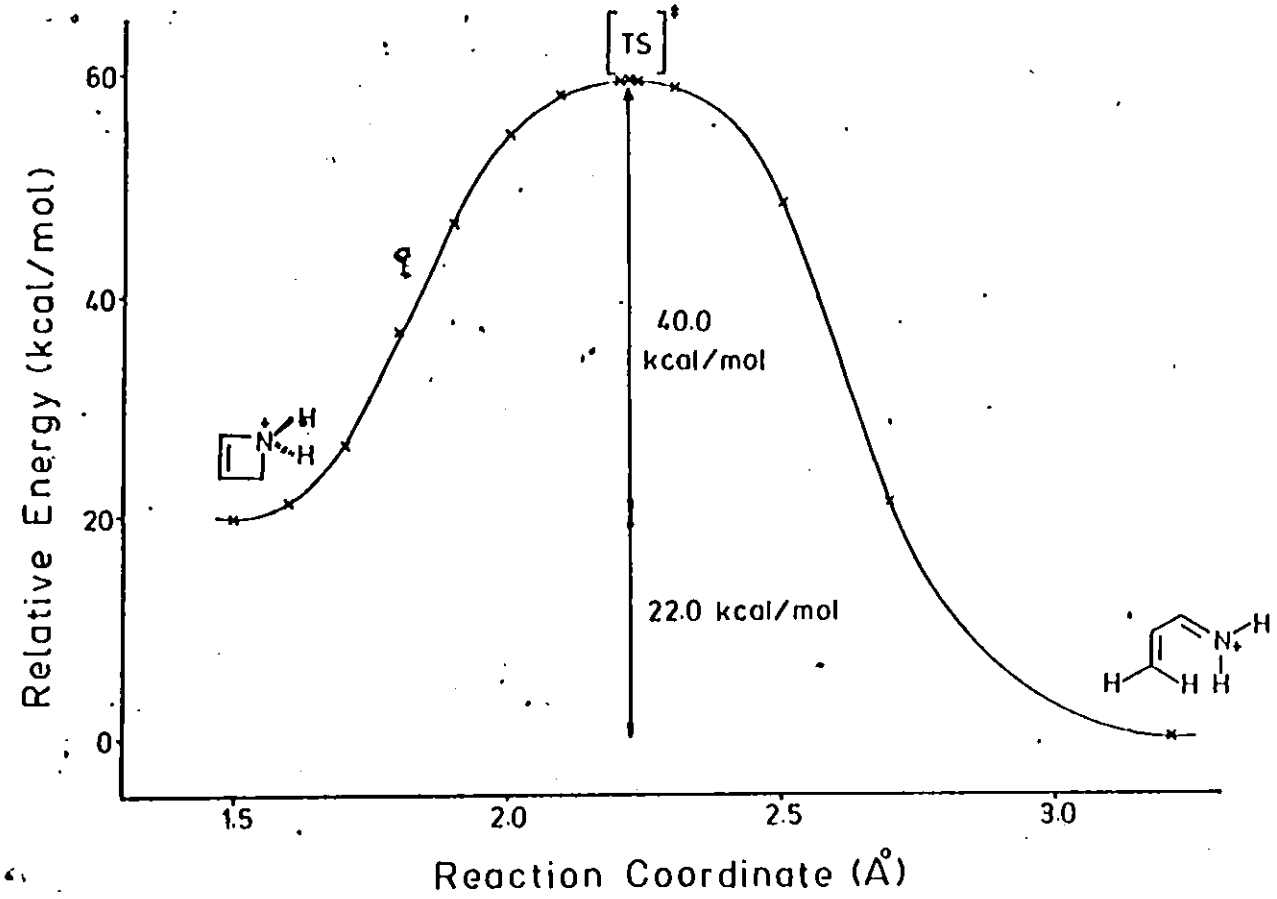


Figure 5-3 MINDO/3 energy surface for the conrotatory ring opening of the parent azetinium ion, 72.

given in Table 5-2. Figure 5-3 illustrates the MINDO/3 energy surface for the reaction.

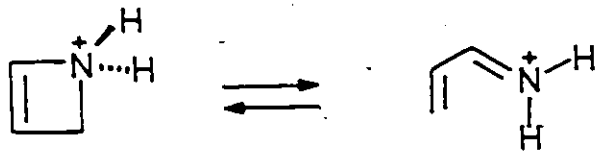

72 48b

The total Mulliken populations at C3 show a slight decrease on going from 48b (5.83) to the transition state (5.77) for the concerted ring closure. That is the positive charge increases from 0.17 to 0.23. This change in positive charge is opposite to that anticipated from the qualitative argument above. However, the positive charge at C3 of the azetinium ion 72 is only 0.11. This latter result indicates that the changes in the total Mulliken populations at C3 for this mechanism are small. The MINDO/3 method may not be able to accurately determine the relative Mulliken populations at all the points on the energy surface. The calculated activation energy is very high (62.0 kcal/mol) but, by analogy to substituted butadienes (171) this is expected to be lowered by substituents at both nitrogen and C3.

It is suggested from these calculations that C=C bond stereomutation via the azetinium mechanism would have a small $\sigma^+$ dependence. The magnitude of the slope of the Hammett plot is expected to be small. It may, in fact, be positive but no definite conclusion can be reached since this is subject to the accuracy of the Mulliken populations determined by the MINDO/3 method.

The fourth mechanism, which has been suggested as a possible pathway for the enzyme-catalysed isomerization of a retinal iminium salt

(125), involves the Michael addition of a nucleophile, equation 28. Attack of a nucleophile at C3 is similar to the reverse of the hydrolysis of para substituted t-cumyl chlorides, which is the reaction used to define the $\sigma^+$ constants (172). Thus an excellent correlation with $\sigma^+$ and a positive $\rho$ value are expected.

The substituent dependence of the acid-catalysed nucleophilic attack on benzaldehydes in semicarbazone formation could be considered as a further close analogy to the Michael addition mechanism. In the case of the substituted benzaldehydes, a good correlation with $\sigma^+$ was reported with a $\rho$ of 1.5 (173).

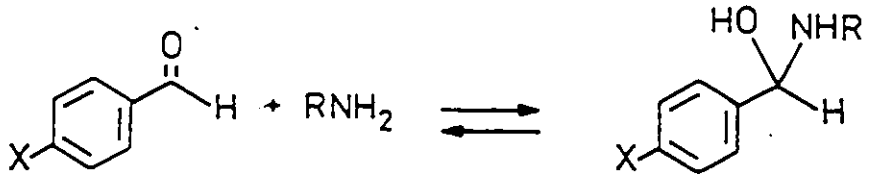


The problem is how to differentiate among these four possible mechanisms. The bond rotation and C2 protonation mechanisms both predict a negative $\rho$ for a Hammett $\sigma^+$ plot and as such are consistent with the data obtained for salts 67 and 68 (see Figure 5-1). On the other hand, the data for salts 66, 69 and 70 give a positive $\rho$. Thus azetinium formation and Michael addition are viable pathways for these latter salts.

*Effect of Solvent Acidity*

The effect of solvent acidity on these reactions was investigated to further define the reaction mechanisms.

In the bond rotation mechanism the rate-limiting step is the

formation of the 90° twisted transition state. The rate of formation of this species is dependent both on the solvating power of the solvent and the ability of the molecule to stabilize a large positive charge at the C3/phenyl end of the molecule. Small alterations in the medium are not expected to change seriously its solvating ability and as such should not alter significantly the rate of isomerization by this mechanism.

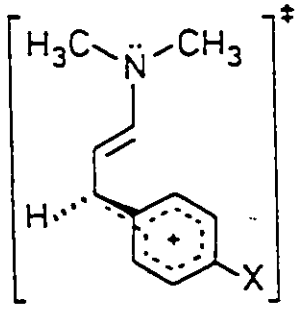

The rate-determining step in the C2 protonation mechanism is expected to be the addition of a proton at C2. In the expression defining the concentration of this intermediate there will be a term for the acid strength of the medium. Thus the rate of formation of this dication should be proportional to solvent acidity. A change in this parameter should be reflected by a corresponding change in the rate of isomerization.

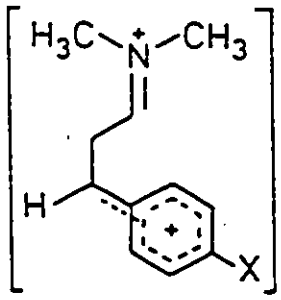

Azetinium formation is a concerted intramolecular process and as such is anticipated to be largely independent of small changes in the bulk properties of the solvent. Thus a small increase in solvent acidity is not expected to alter the rate of isomerization by this pathway.

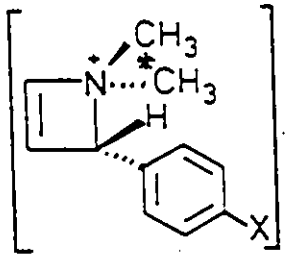

In the case of Michael addition, the rate-limiting step is the attack of a nucleophile at C3. For a pure solvent, the best nucleophile present is the solvent anion, which is formed by self ionization of the solvent.

$$2CF_3CO_2H \rightleftharpoons CF_3CO_2H_2^+ + CF_3CO_2^-$$

The concentration of this anion in the case of pure TFA is about $2x10^{-7}M$ (164). An increase in the concentration of protons by the addition of a strong acid (eg. $H_2SO_4$) should shift this equilibrium to the left and so decrease the nucleophile concentration. Therefore, the Michael addition mechanism is expected to show a decrease in the rate of isomerization with an increase in solvent acidity.

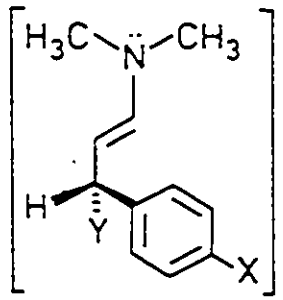

The rate constants for the isomerizations of salts 66 to 70 were measured in a solvent mixture of 0.015M $H_2SO_4$ in TFA, Table 5-3.

The acid strengths of the two solvents were measured at 25°C using 2,4-dinitroaniline and the $H_o$ acidity scale. The values obtained were -4.0 and -5.1 for TFA and $H_2SO_4$/TFA respectively. The $H_o$ value of $H_2SO_4$/TFA agreed well with that reported previously (174) but the value for TFA was substantially lower than the accepted value of -2.8 (164,175). Regardless of this discrepancy, the $H_o$ values measured here indicate clearly that the addition of $H_2SO_4$ has increased the acidity of the solvent on the $H_o$ scale. The absolute values of $H_o$ are not important in this relative experiment.

Two additional problems, which arise, are the temperature dependence of $H_o$ and the presence of anions which might act as nucleophiles. The isomerizations occurred at 100°C whereas the above $H_o$ values were determined at 25°C. As far as I am aware, the temperature dependence of the $H_o$ acidity function in TFA has not been examined. However, it has been measured at temperatures up to 90°C for various $H_2SO_4/H_2O$ mixtures (176). A significant decrease in the acid strength was observed in these mixtures when the temperature was increased, but their relative acidities did not change. Thus it was anticipated that

Table 5-3

Isomerization rate constants at 100 ± 0.5°C for the para substituted iminium salts in TFA and 0.015M $H_2SO_4$/TFA

| Reaction | X[a] | $k^b$ $s^{-1}$ ($x10^{-6}$) | | $Log(k/k_o)^c$ | | $\sigma^{+d}$ |
|---|---|---|---|---|---|---|
| | | TFA | $H_2SO_4$/TFA | TFA | $H_2SO_4$/TFA | |
| 66 → 42 | H | 1.6 | 0.94 | 0 | -0.24 | 0 |
| 67 → 43 | $OCH_3$ | 2000 | 6200 | 3.1 | 3.6 | -0.78 |
| 68 → 44 | $CH_3$ | 4.6 | 29 | 0.45 | 1.2 | -0.31 |
| 69 → 45 | Cl | 2.0 | 0.94 | 0.084 | -0.25 | 0.11 |
| 70 → 46 | $NO_2$ | 19 | 3.1 | 1.1 | 0.27 | 0.79 |

[a]para substituent on phenyl ring

[b]estimated error is ± 10%

[c]determined using $k_o = 1.6x10^{-6}$ $s^{-1}$

[d]from reference 166

the acidity of the $H_2SO_4$/TFA mixture would still be greater than that of TFA at 100°C.

The only anions introduced into the solutions were $ClO_4^-$, $HSO_4^-$ (from added $H_2SO_4$) and $BF_4^-$ (from the internal standard, see Chapter 6). These anions are poor nucleophiles. In all probability trifluoroacetate was still the best nucleophile in solution.

Comparison of the rate constants of isomerization can be made by examining the data given in Table 5-3. It can also be represented graphically. Figure 5-4 illustrates a Hammett plot of $Log(k/k_o)$ vs $\sigma^+$ for both sets of data. The plot for the solvent mixture has been modified to show the change in the rate constants. In order to maintain a common reference point in the evaluation of $Log(k/k_o)$, the $k_o$ value was taken as the rate constant of isomerization for the unsubstituted salt 66 in TFA. Such a non-standard reference point does not alter the shape of the plot but it allows the data to be compared with the values obtained in TFA.

The new plot has a shape similar to the previous Hammett plot. Again the values for salts 67 and 68 lie on a steeply negative slope ($\rho$ = -4.9) whereas the data for 66, 69 and 70 lie on a less steep positive slope ($\rho$ = 1.8). The curvature of the new plot is again indicative of a change in mechanism with the variation in the electron demand of the substituents. A comparison of the first-order rate constants given in Table 5-3 shows that the rates of isomerizations for salts 67 and 68 are accelerated in the $H_2SO_4$/TFA solvent mixture, while the rates for the other three salts are retarded in this medium. These results are consistent with isomerization occurring by protonation at C2

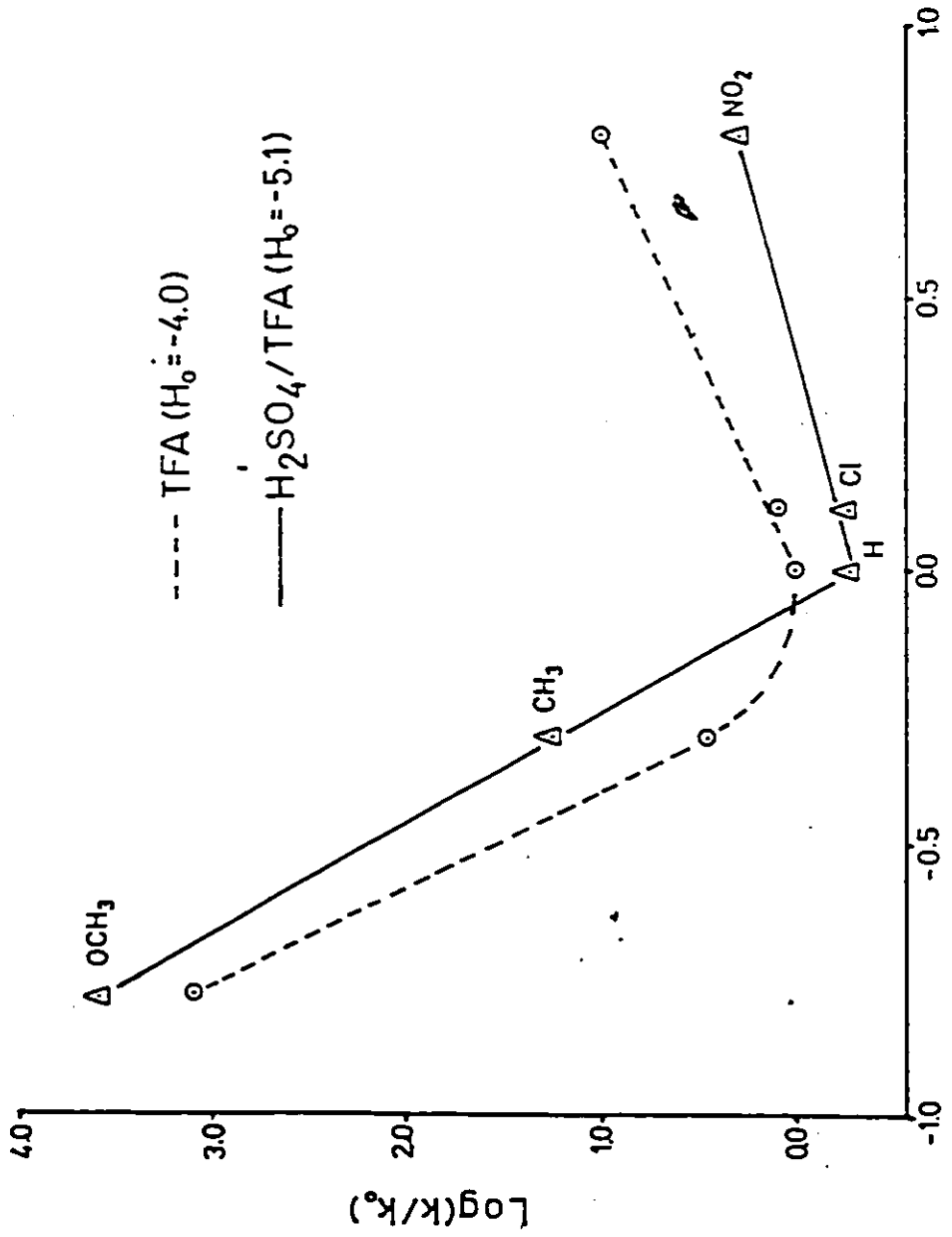


Figure 5-4 Hammett $\sigma^+$ plot for the rate constants determined in TFA and $H_2SO_4$/TFA

in the case of 67 and 68 and by Michael addition of a nucleophile for 66, 69 and 70. The two intramolecular mechanisms are incompatible with the observed changes upon alteration of the solvent acidity and so can be ruled out on this basis.

*Deuterium Exchange*

The study of the isomerization in deuterated acid could provide further evidence as to which of the isomerization mechanisms are operating. The bond rotation and azetinium formation pathways, which are intramolecular processes, should not lead to exchange. For this reason the following discussion concentrates on the other two mechanisms.

If the isomerization involves protonation at C2, then exchange of the C2 proton would be expected to accompany isomerization when the reaction is carried out in deuterated acid. It is also possible that exchange could be faster than the rate of isomerization since exchange could occur in both the cis- and trans-isomers. In the case of cyanine dye 20, deuterium incorporation at C2 has been observed in aqueous $D_2SO_4$ solvent (109).

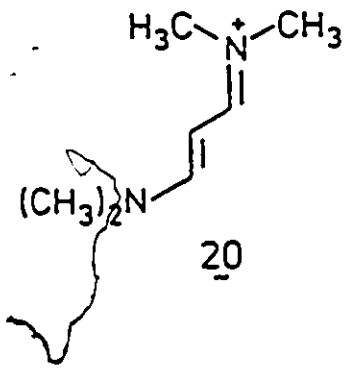


20

For the simple Michael addition mechanism, no exchange is expected when deuterated media are used. It is possible, however, that

further protonation of the enamine intermediate could occur. This could take place on one of two sites - nitrogen or C2. Protonation at nitrogen is expected to be much faster than at C2 (177). Thus deuterium incorporation may or may not occur during a Michael addition type isomerization.

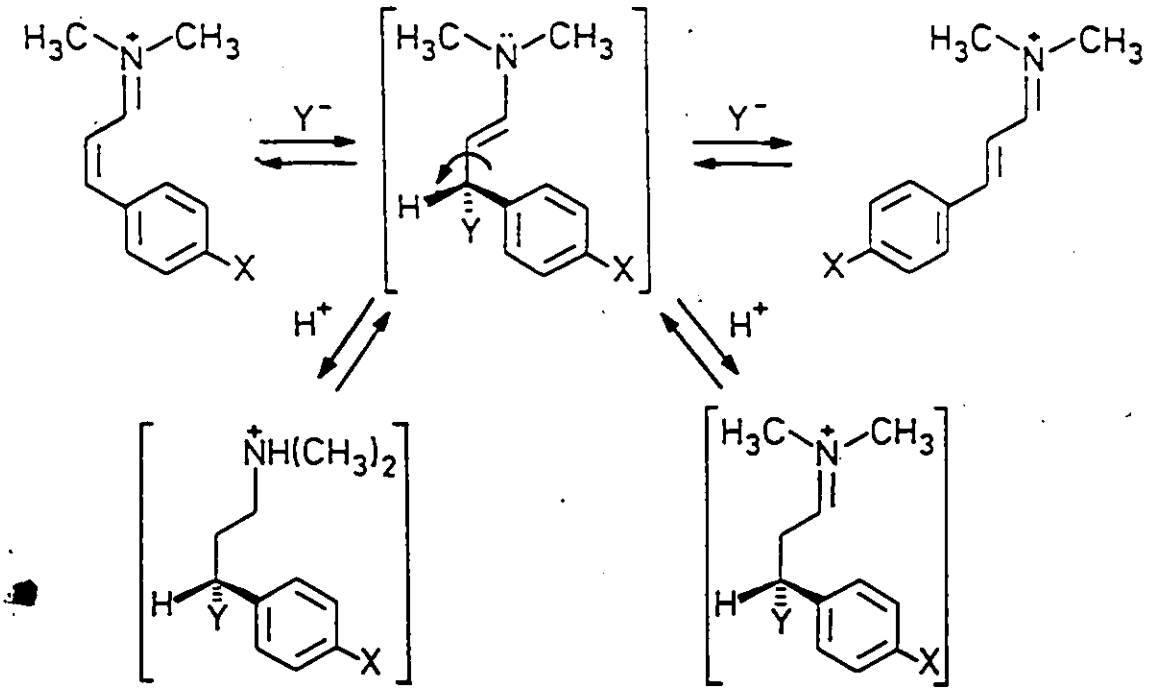

The isomerizations of salts 66 - 70 to 42 - 46 respectively, were monitored in both TFA-d and $D_2SO_4$/TFA-d at 100°C. There was no detectable deuterium incorporation at C2 or any other position during the course of these isomerizations.

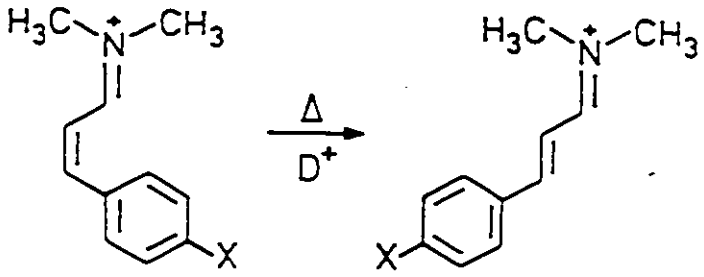

| | | |
|---|---|---|
| 66 | X=H | 42 |
| 67 | X=$OCH_3$ | 43 |
| 68 | X=$CH_3$ | 44 |
| 69 | X=Cl | 45 |
| 70 | X=$NO_2$ | 46 |

In the case of salts 66, 69 and 70 this result is consistent with both the Michael addition and azetinium formation mechanisms. The latter mechanism was ruled out by the acid dependence experiment. Although 66 may be a borderline case, these salts appear to isomerize exclusively by a Michael addition pathway.

The lack of exchange for salts 67 and 68 raises a dichotomy. The Hammett $\sigma^+$ correlation suggested that either a bond rotation or a C2 protonation mechanism was involved. Protonation at C2 is consistent with the acid strength experiment but the results of the deuterium exchange experiment seem to contradict this conclusion and suggest that a bond rotation mechanism is involved. Is it possible that there is an as yet unconsidered mechanism which is consistent with all of the above results?

Protonation at nitrogen would give a dication which is expected to have a low barrier to isomerization about the C2,C3 bond (178), equation 29. This mechanism would increase the positive charge at the C3/phenyl end of the molecule during the course of the reaction and as such would give a good correlation with $\sigma^+$ with a negative slope. As

well, it can explain the acid dependence and deuterium exchange data.

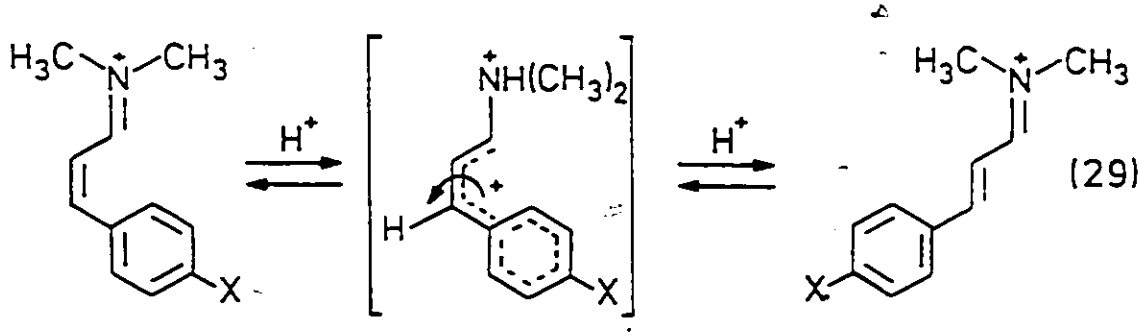


(29)

Although, to my knowledge, there is no precedence for nitrogen protonation in iminium salts, it has been shown to occur in the case of amidinium salts (180). Exchange of the N-H protons and the equilibration of the resonances due to the N-$CH_3$ protons of amidinium salt 73 occurred in $H_2SO_4/H_2O$ mixtures of high acid strength. Both of these processes were found to be acid-catalysed and a mechanism involving protonation at nitrogen was proposed (180). A similar acid dependence of the barrier to rotation about the $C=N^+$ bond in cyanine dyes has been reported (109).

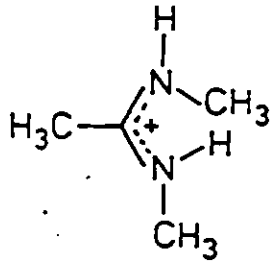


73

At first, the addition of a proton at the formally positively charged nitrogen seems odd, but it must be remembered that the π-electron density at this site is high (see Tables 3-3 and 3-4 and reference 137).

Table 5-4

Rate constants of deuterium exchange at 100 ± 0.5°C for the C2 proton in TFA-d and $D_2SO_4$/TFA-d

| Compound | X[a] | $k^b$ $s^{-1}$ ($x10^6$) | |
|---|---|---|---|
| | | TFA-d | $D_2SO_4$/TFA-d |
| 42 | H | <0.2 | <0.2 |
| 43 | $OCH_3$ | 72 | 340 |
| 44 | $CH_3$ | <0.5 | <0.5 |
| 45 | Cl | <0.2 | <0.2 |
| 46 | $NO_2$ | <0.5 | <0.5 |

[a]para substituent on phenyl ring

[b]estimated error is ± 10%

The dication which is formed on nitrogen protonation is similar to that produced by C2 protonation. In fact, the energies of these two species might well be similar.

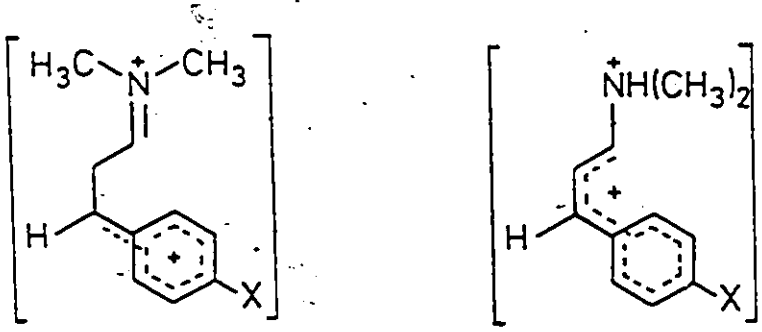

Prolonged heating of the trans-isomers 42 to 46 in either acid medium at 100°C resulted in deuterium exchange at C2 only in the case of 43. The rates of these processes were monitored quantitatively by $^1H$ nmr spectroscopy and the first-order rate constants are given in Table 5-4. Deuterium incorporation for 43 was accelerated in the stronger acid medium, although the rate was still at least an order of magnitude slower than the rate of isomerization (see Table 5-3).

The observation of deuterium incorporation at C2 of 43 is consistent with the previous statement that the energies of the dications formed by nitrogen and C2 protonation are similar. In order to show that nitrogen protonation is indeed possible further experimentation is necessary.

## C. Conclusions

In summary the aromatic substituted α,β-unsaturated iminium salts undergo cis to trans isomerizations about their C=C bonds. As the para ring substituents vary, the mechanism of isomerization changes.

In the case of electron-withdrawing substituents isomerization occurs by Michael addition of a nucleophile. A mechanism involving protonation at nitrogen was proposed for salts with electron-donating substituents.

# EXPERIMENTAL

# CHAPTER 6

## EXPERIMENTAL METHODS

### A. Materials

All of the reagents employed were commercially available. $FSO_3H$ was purified by a double distillation. The first distillate was purged with dry nitrogen and redistilled. This acid was then stored in sealed glass ampules in 0.5 ml aliquots. TFA was purified by distillation from $cH_2SO_4$ and stored in a dry glass container which was kept in a dry box. Both $FSO_3D$ and TFA-d were obtained commercially and used without further purification. The methane sulphonic and n-propyl sulphonic acids used in the fluorescence measurements were vacuum distilled twice and stored in reacti-flasks.

The trans-pent-3-en-2-one, obtained commercially, contained some of the cis-ketone and mesityl oxide. This material was purified by preparative GLC. The purified ketone was collected in a glass "U" tube cooled in a dry ice/acetone bath (-78°C). Analysis by analytical GLC showed the trans-ketone to be 99.5% pure.

### B. Instrumental Techniques

*$^1H$ nmr Spectra*

All $^1H$ nmr spectra were obtained at 90 MHz on a Varian EM390 spectrometer or at 400 MHz on a Bruker WH400 spectrometer. This latter spectrometer is situated at the Southwestern Ontario Regional nmr Centre at the University of Guelph, Guelph, Ontario.

For the neutral imines 32 to 36, $CDCl_3$ was used as solvent and resonances were referenced to internal TMS. $FSO_3H$, 96% $H_2SO_4$ and TFA were employed as solvents to obtain the spectra of the aliphatic iminium salts 37 to 39. The chemical shifts were not medium dependent. In the case of the aromatic iminium salts 40 to 46 only TFA solvent was used. Tetramethylammonium tetrafluoroborate ($(CH_3)_4N^+BF_4^-$, $\delta$ 3.10) was used as internal standard in all acid solvents. The various resonances were assigned by the use of spin decoupling experiments. Sample concentrations ranged from 0.25M to 0.75M. Data are summarized in Tables 3-1 and 3-2.

The spectra of all photostationary state mixtures were acquired at 400 MHz and the signals of all photoproducts (53 to 70) were assigned by spin decoupling experiments (see Chapter 4) directly on these mixtures. Data are given in Tables 4-2, 4-3 and 4-4.

*Solution $^{13}C$ nmr Spectra*

All spectra were obtained at 22.6 MHz on a Bruker WH90 spectrometer or at 20.1 MHz on a Bruker WP80 spectrometer. For the neutral imines, 32 to 36, $CDCl_3$ was used as solvent and the signals were referenced to internal TMS. The spectra of the iminium salts 37 and 38 were obtained in $FSO_3D$ solvent and the resonances were referenced to external TMS whereas the spectrum of 39 was acquired in TFA-d solution and the solvent was used as internal reference ($\underline{C}F_3CO_2D$, $\delta$ 114.5). In the case of salt 40 0.75M TFA in $CD_3NO_2$ was employed as solvent and $CD_3NO_2$ ($\delta$ 62.77) was used as internal reference. The spectra of the dimethyliminium perchlorate salts, 42 to 46, were all acquired in $CD_3NO_2$ solvent with

internal TMS as a reference. Resonances for all compounds were assigned by various broadband, off-resonance and selective decoupling experiments. All concentrations were in the range of 0.25M to 0.75M. Data are summarized in Tables 3-5 and 3-6.

*Solid State $^{13}C$ nmr Spectra*

The $^{13}C$ CPMAS spectra of the iminium salts 42 to 46 were acquired at 25.1 MHz on a Bruker CXP100 spectrometer with a home built probe and spinner assembly. This instrument is situated in the laboratory of C.A. Fyfe at the University of Guelph, Guelph, Ontario and the spectra are provided by his courtesy. Proton spin locking and decoupling fields of approximately 40 k Hz were used. The spinner design was of the Andrew-Beams type utilizing Kel-F spinners driven by air and operated at spinning rates of about 3 k Hz. Data are given in Table 3-7.

*Electronic Absorption Spectra*

The absorption spectra were obtained on either a Cary 14 or a Pye Unicam SP8-100 UV-VIS spectrophotometer. Spectra of the acid salts 37 to 42 were acquired in 96% $H_2SO_4$ solution while TFA was employed for the salts 42 to 46. Concentrations of approximately $10^{-5}$M were used in all cases and data are summarized in Table 4-1.

*Infrared Spectra*

A Perkin-Elmer 283 IR spectrophotometer was used to obtain the IR spectra for all imines and iminium salts. Spectra of the neutral imines 32 to 36 were obtained either in $CCl_4$ solution (0.20 M to 0.25 M) or as thin films. In both cases NaCl windows were used. The KBr disc technique was employed for the iminium salts 42 to 46. Data are

summarized in Table 6-1.

*Gas Chromatography*

An Aerograph model A-90-P gas chromatograph was used for all of the preparative GLC work. The column used was a $\frac{1}{4}$" dia. x 6' long copper tube packed with 15% SE-30 on Chromosorb W. Column temperature was maintained at 100°C and the helium carrier gas flow rate was set at 30 ml/min. For the analytical work a Varian model 3700 gas chromatograph equipped with an FI detector was employed. Peak areas were obtained using a coupled Varian CDS 111 data system. In this case a $\frac{1}{8}$" dia. x 6' long copper column packed with 15% Carbowax on Chromosorb W was employed. A column temperature of 75°C and a nitrogen gas flow rate of 20 ml/min were maintained throughout the analysis.

C. Synthesis

The imines 32 to 36 were synthesized by a slight modification of the method of Kieczykowski et al (148) and the corresponding iminium satls 37 to 41 were prepared by dissolving the imines in $FSO_3H$, $H_2SO_4$ or TFA. In the syntheses of imines 32, 33 and 35 minor isomeric impurities of approximately 5% (see Chapter 3), which could not be separated, were formed. As a consequence their corresponding iminium salts 37, 38 and 40 were contaminated with these impurities. The dimethyliminium perchlorate salts 42 to 46 were prepared from the appropriate para-substituted cinnamaldehydes (149) by the method of Leonard and Paukstelis (150). The syntheses are given below.

Elemental analyses, yields and some other physical data are summarized in Table 6-1. $^1H$ nmr data are given in Tables 3-1 and 3-2

Table 6-1

Some physical data and elemental analyses for the imines and iminium salts

| Compound | mp °C | % Yield | Str. Freq. $cm^{-1}$ | | Mol Form. | Analysis[b] | | | | | |
|---|---|---|---|---|---|---|---|---|---|---|---|
| | | | | | | Calc. | | | Found | | |
| | | | $\nu_{C=N}$ | $\nu_{C=C}$ | | %C | %H | %N | %C | %H | %N |
| 32 | a | 60 | 1659 | 1630 | $C_8H_{15}N$ | 76.74 | 12.07 | 11.19 | 76.78 | 12.37 | 10.93 |
| 33 | a | 55 | 1650 | 1634 | $C_9H_{17}N$ | 77.63 | 12.31 | 10.06 | 77.88 | 12.41 | 9.98 |
| 34 | a | 10 | 1643 | 1621 | $C_8H_{15}N$ | 76.74 | 12.07 | 11.19 | 76.81 | 11.91 | 11.03 |
| 35 | a | 75 | 1635 | 1618 | $C_{13}H_{17}N$ | 83.37 | 9.15 | 7.48 | 83.02 | 9.22 | 7.91 |
| 36 | 63-4 | 50 | 1640 | 1625 | $C_{13}H_{16}N_2O$ | 67.22 | 6.94 | 12.06 | 67.54 | 7.00 | 12.39 |
| 42 | 132-3 | 95 | 1655 | 1611 | $C_{11}H_{14}NClO_4$ | 50.88 | 5.43 | 5.39 | 50.88 | 5.52 | 5.28 |
| 43 | 155-6 | 50 | 1662 | 1581 | $C_{12}H_{16}NClO_5$ | 49.75 | 5.57 | 4.83 | 49.73 | 5.72 | 4.60 |
| 44 | 150-1 | 75 | 1663 | 1615 | $C_{12}H_{16}NClO_4$ | 52.66 | 5.89 | 5.12 | 52.32 | 6.05 | 4.97 |
| 45 | 144-5 | 69 | 1660 | 1618 | $C_{11}H_{13}NCl_2O_4$ | 44.92 | 4.45 | 4.76 | 45.08 | 4.53 | 4.82 |
| 46 | 165-6 | 60 | 1670 | 1620 | $C_{11}H_{13}N_2ClO_6$ | 43.36 | 4.30 | 9.19 | 43.51 | 4.37 | 8.96 |

[a] Liquids

[b] Analyses were determined by either the Schwarzkopf Microanalytical Laboratory, 56-19 37th Ave., Woodside, N.Y. 11377 or Guelph Chemical Laboratories Ltd., 500 York Rd., Guelph, Ontario Canada N1E 3J4.

while $^{13}C$ nmr data are given in Tables 3-5, 3-6 and 3-7. Electronic absorption data for the iminium salts are summarized in Table 4-1.

*trans,trans-N-t-butyl-2-butenylidenimine, 32*

Crotonaldehyde (2 mls, 24.2 mmoles) in dry ether (10 mls) was added dropwise (30 min) to a cooled (0°C) stirred mixture of t-butylamine (4 mls, 38.1 mmoles) in dry ether (30 mls) and anhydrous $K_2CO_3$ (2 gms, 14.4 mmoles). After addition was complete the mixture was warmed to room temperature and left for four hours. This mixture was filtered to remove $K_2CO_3$ and the ether was evaporated. The resulting residue was vacuum distilled (bp = 38-40°C/20 mm) to obtain imine 32. Yield was 2 mls, (1.7 gms, 60%).

*trans,trans-N-n-butyl-2-methyl-2-butenylidenimine, 33 and trans-N-n-butyl-2-methyl-2-propenylidenimine, 34*

Tiglaldehyde (2 mls, 20.7 mmoles) in dry ether (10 mls) was added dropwise (30 min) to a cooled (0°C) mixture of n-butylamine (4 mls, 40.5 mmoles) in dry ether (30 mls) and anhydrous $K_2CO_3$ (2 gms, 14.4 mmoles). When addition was complete the mixture was warmed to room temperature and left overnight. The mixture was filtered and the ether was removed. The residue was vacuum distilled to give imine 33 (bp = 76.8°C/20 mm). Yield was 1.8 mls (1.5 gms, 55%).

Imine 34 was prepared in an analogous manner except that the tiglaldehyde was replaced with methacrolein (2 mls, 24.2 mmoles). The residue was vacuum distilled to give imine 34 (bp = 32.4°C/20 mm) in a yield of 0.35 mls (0.30 gms, 10%).

*trans,trans-N-n-butyl-3-phenyl-2-propenylidenimine, 35*

Imine 35 was synthesized by the same procedure as imine 32. Cinnamaldehyde (2 mls, 15.9 mmoles) replaced the crotonaldehyde. The residue was vacuum distilled to give 35 (bp = 150°C/2 mm) in 75% yield (2.5 mls, 2.1 gms).

*trans,trans-N-n-butyl-3-(p-nitrophenyl)-2-propenylidenimine, 36*

Imine 36 was synthesized by the same procedure as imine 32. The crotonaldehyde was replaced by p-nitrocinnamaldehyde (0.5 gms, 2.8 mmoles), which was synthesized by the aldol condensation of acetaldehyde and p-nitrobenzaldehyde (149). Due to the small amount of aldehyde the amount of the other reagents were reduced appropriately. The imine was purified by column chromatography (neutral alumina, eluted with 10% ether/petroleum ether) (mp = 63-4°C). Yield was 0.33 gm, 50%.

*Protonation Methods*

The iminium salts 37 to 41, which correspond to the imines 32 to 36, were prepared by one or all of the protonation procedures given below.

An appropriate amount of imine was placed into a medium-walled nmr tube, swirled to distribute it onto the walls of the tube and quickly frozen there by cooling in liquid nitrogen. If the imine was to be dissolved in $FSO_3H$ this tube was placed in a dry ice-acetone bath (-78°C) and previously cooled (-78°C) acid was added by pasteur pipette. The solution was stirred with a thin glass rod to facilitate mixing. If the imine was to be dissolved in $H_2SO_4$ or TFA the nmr tube was placed in an ice bath (0°C) and acid, cooled previously (0°C), was

added by pipette. Homogeneity of the solution was again ensured by stirring with a glass rod.

*trans-N,N-dimethyl-3-(p-X-phenyl)-2-propenylideniminium perchlorates*, 42 (X=H), 43 (X=$OCH_3$), 44 (X=$CH_3$); 45 (X=Cl), 46 (X=$NO_2$)

All of the dimethyliminium perchlorate salts were prepared by the following general procedure (150), which is illustrated for salt 42. The para-substituted cinnamaldehydes were synthesized by aldol condensation of the corresponding benzaldehydes with acetaldehyde as described in the literature (149).

Cinnamaldehyde (2 mls, 15.9 mmoles) and dimethylammonium perchlorate (2.30 gm, 16.0 mmoles) were dissolved in methanol (15 mls) and left to stir overnight. The resulting yellow crystals were isolated by vacuum filtration and recrystallized from methanol to constant melting point (mp = 132-3°C). Yield was 3.9 gm, 95%.

D. MINDO/3 Calculations

The MINDO/3 program was obtained from the Quantum Chemistry Program Exchange (Program #279) centred at the Chemistry Department of Indiana University. With minor modifications the program was made compatible with the computing facilities available at McMaster University. However, none of the program parameters were altered. All calculations were performed on either a CDC 6400 or a Cyber 170-730 computer.

The species calculated here were all fully optimized and the inclusion of 3X3 CI made little or no difference to their heats of formation. The energy surface for the ring opening of the azetinium ion 72 was calculated using the N,C3 bond length as the reaction coordinate

(170). After each change in this bond length the geometry was re-optimized.

E. Crystal Structure Determinations

*Collection of the Data*

Crystals of 42 and 43, suitable for single crystal x-ray analysis, were obtained by the slow evaporation of solvent, $CH_2Cl_2$ and $CH_3OH$ respectively, from solutions of the salts.

Precession photographs showed that the crystal of 42 was orthorhombic and that of 43 was triclinic. Unit cell parameters were obtained from a least-squares fit of $\chi$, $\phi$ and $2\theta$ for 15 reflections in the range $16.2° < 2\theta < 31$ for 42 and $16.2° < 2\theta < 34.8$ for 43 recorded on a Syntex $P2_1$ diffractometer with the use of graphite-monochromatic MoK radiation ($\lambda$ = 0.71069 Å). Crystal data and other numbers related to data collection are summarized in Table 6-2. The density of the crystals was measured by floatation in a t-butylchloride/carbon tetrachloride mixture. Reflection intensities were measured on a Syntex $P2_1$ diffractometer with the use of a coupled $\theta$ (crystal) - $2\theta$ (counter) scan. The methods of selection of scan rates and initial data treatment have been described (181,182). Corrections were made for Lorentz-polarization effects but not for absorption. This will make a maximum error in $F_o$ of < 1.0% for 42 and < 0.5% for 43.

*Solution of the Structures*

The solution was similar for the two structures. Chlorine atoms were found from three-dimensional Patterson syntheses and a series of full-matrix least-squares refinements and electron density differences

Table 6-2

Crystal data for $(C_{11}H_{14}N^+)(ClO_4^-)$, 42, and $(C_{12}H_{16}NO^+)(ClO_4^-)$, 43

| | 42 | 43 |
|---|---|---|
| Compound | $(C_{11}H_{14}N^+)(ClO_4^-)$ | $(C_{12}H_{16}NO^+)(ClO_4^-)$ |
| F.W. | 259.69 | 289.72 |
| Crystal size(mm) | parallelepiped, 0.17x0.17x0.27 | needle, 0.10x0.10x0.50 |
| Systematic absences | h0ℓ ℓ=2n+1<br>hk0 h+k=2n+1 | none |
| Space group | Pmcn | $P\bar{1}$ |
| Unit cell (Å and deg) | a=6.595(1)<br>b=18.288(4)<br>c=10.216(2) | a=6.862(1) α=119.05(1)<br>b=9.830(2) β=114.99(2)<br>c=13.376(3) γ=90.79(2) |
| Volume ($Å^3$) | 1232.3(4) | 687.1(2) |
| Z | 4 | 2 |
| $\rho_{calc}$(g $cm^{-3}$) | 1.400 | 1.400 |
| $\rho_{obs}$(g $cm^{-3}$) | 1.42(2) | 1.37(2) |
| Linear absorp. coeff. ($cm^{-1}$) | 3.09 | 2.99 |
| Max 2θ, reflectns. collected | 45°,h,k,±ℓ | 45°,±h,±k,ℓ |
| Standard reflectns. (e.s.d.%) | 1,5,0(1.2) 1,3,1(1.2) | 0,2,3(2.7) 2,4,-6(2.3) |
| Temp. (°C) | 22 | -35 |
| No. of independent reflectns. | 869 | 1765 |
| No. with I>0 | 833 | 1670 |
| No. with I<0, rejected | 36 | 95 |
| Final $R_1^a$, $R_2^a$ | 0.0688, 0.0772 | 0.079, 0.0757 |
| Final shift/error max.(ave.) | 0.054 | 0.076 |
| X (Secondary extinction) | 0.00211 | 0.00304 |
| Final difference map | | |
| Highest peak($e/Å^3$); location | 0.266; 0.25, 0.75, 0.20 | 0.542; 0.68, 0.92, 0.19 |
| Lowest valley($e/Å^3$); location | -0.237; 0.15, 0.75, 0.50 | -0.301; 0.08, 0.90; 0.16 |
| Weighting | $w=(\sigma^2+0.00062F_o^2)^{-1}$ | $w=(\sigma^2+0.00025F_o^2)^{-1}$ |
| Error in an observation of unit wt. | 1.720 | 0.8880 |

[a] $R_1 = \Sigma||F_o|-|F_c||/\Sigma|F_o|$ ; $R_2 = \{\Sigma w(|F_o|-|F_c|)^2/(\Sigma wF_o^2)\}^{\frac{1}{2}}$

Table 6-3

Atomic positional parameters for trans-N,N-dimethyl-3-phenyl-2-propenylideniminium perchlorate, 42

| Atom | x | y | z |
|---|---|---|---|
| Cl | 2500 | 1579(1) | 1432(2) |
| O(1) | 2500 | 811(4) | 1424(7) |
| O(2) | 2500 | 1825(4) | 123(7) |
| O(3) | 791(11) | 1844(3) | 2060(6) |
| C(1) | 2500 | -1386(4) | 2797(9) |
| C(2) | 2500 | -686(5) | 3409(8) |
| C(3) | 2500 | -663(5) | 4743(9) |
| C(4) | 2500 | -9(5) | 5529(7) |
| C(5) | 2500 | -691(6) | 4976(9) |
| C(6) | 2500 | 1290(6) | 5798(10) |
| C(7) | 2500 | 1228(6) | 7122(9) |
| C(8) | 2500 | 543(6) | 7651(9) |
| C(9) | 2500 | -73(5) | 6892(8) |
| C(10) | 2500 | -917(6) | 599(8) |
| C(11) | 2500 | -2278(5) | 1084(8) |
| N | 2500 | -1514(3) | 1558(7) |

Table 6-4.

Atomic positional parameters for trans-N,N-dimethyl-3-(p-methoxyphenyl)-2-propenylideniminium perchlorate, 43

| Atom | x | y | z |
|---|---|---|---|
| Cl(1) | -305(3) | -832(2) | 1904(1) |
| O(1) | 1464(7) | 104(5) | 2013(4) |
| O(2) | 518(10) | -1192(5) | 2871(4) |
| O(3) | -1845(8) | 80(5) | 2081(5) |
| O(4) | -1384(8) | -2301(4) | 661(4) |
| C(1) | 3770(9) | 7300(6) | 876(5) |
| C(2) | 4064(8) | 6194(6) | 1306(4) |
| C(3) | 5438(9) | 6803(6) | 2591(5) |
| C(4) | 5983(8) | 5942(6) | 3253(5) |
| C(5) | 5135(9) | 4272(6) | 2594(5) |
| C(6) | 5688(8) | 3502(6) | 3272(5) |
| C(7) | 7072(8) | 4405(6) | 4623(5) |
| C(8) | 7952(9) | 6073(6) | 5301(5) |
| C(9) | 7388(9) | 6817(6) | 4619(5) |
| C(10) | 857(9) | 5308(7) | -1380(5) |
| C(11) | 2218(11) | 8203(7) | -596(5) |
| C(12) | 6993(10) | 2052(7) | 4744(6) |
| N | 2394(8) | 6920(5) | -298(4) |
| O | 7696(6) | 3781(4) | 5383(3) |

Table 6-5

Temperature factors ($\AA^2$) for non-hydrogen atoms ($\times 10^3$) for $(C_{11}H_{14}N^+)(ClO_4^-)$, 42

| Atom | $U_{11}$ | $U_{22}$ | $U_{33}$ | $U_{12}$ | $U_{13}$ | $U_{23}$ |
|---|---|---|---|---|---|---|
| Cl | 96(2) | 53(2) | 49(1) | | | 0(1) |
| O(1) | 236(11) | 49(5) | 99(6) | | | 6(4) |
| O(2) | 167(9) | 94(6) | 70(5) | | | 25(4) |
| O(3) | 145(6) | 138(5) | 156(6) | 20(5) | 71(5) | -30(4) |
| C(1) | 105(9) | 59(7) | 55(6) | | | -1(5) |
| C(2) | 84(8) | 69(6) | 57(6) | | | -5(5) |
| C(3) | 119(9) | 66(7) | 49(6) | | | 10(5) |
| C(4) | 96(8) | 57(6) | 46(5) | | | -6(5) |
| C(5) | 100(9) | 70(7) | 48(6) | | | 7(5) |
| C(6) | 91(9) | 72(8) | 81(8) | | | 4(6) |
| C(7) | 95(9) | 84(8) | 54(7) | | | -10(6) |
| C(8) | 89(8) | 74(8) | 60(6) | | | 5(6) |
| C(9) | 100(9) | 65(7) | 47(5) | | | 5(5) |
| C(10) | 93(8) | 91(8) | 49(6) | | | 10(5) |
| C(11) | 91(8) | 50(6) | 66(6) | | | -21(5) |
| N | 71(5) | 52(4) | 50(4) | | | -5(4) |

Table 6-6

Temperature factors ($\AA^2$) for non-hydrogen atoms ($\times 10^3$) for $(C_{12}H_{16}NO^+)(ClO_4^-)$, 43

| Atom | $U_{11}$ | $U_{22}$ | $U_{33}$ | $U_{12}$ | $U_{13}$ | $U_{23}$ |
|---|---|---|---|---|---|---|
| Cl(1) | 55(1) | 29.7(7) | 32.3(8) | 16.5(7) | 14.1(7) | 6.5(7) |
| O(1) | 53(3) | 50(2) | 81(3) | 25(2) | 34(3) | 0(2) |
| O(2) | 179(6) | 72(3) | 47(3) | 46(3) | 19(3) | 20(5) |
| O(3) | 78(3) | 61(3) | 119(4) | 50(3) | 66(3) | 37(3) |
| O(4) | 96(4) | 41(2) | 39(2) | 1(2) | 20(3) | - 9(2) |
| C(1) | 47(4) | 36(3) | 43(3) | 24(3) | 22(3) | 12(3) |
| C(2) | 38(3) | 32(3) | 29(3) | 18(2) | 15(3) | 7(2) |
| C(3) | 39(3) | 30(3) | 42(3) | 19(3) | 20(3) | 5(3) |
| C(4) | 36(3) | 30(3) | 29(3) | 14(2) | 15(3) | 9(3) |
| C(5) | 38(3) | 39(3) | 32(3) | 14(3) | 14(3) | 8(3) |
| C(6) | 39(3) | 34(3) | 32(3) | 20(3) | 14(3) | 9(3) |
| C(7) | 31(3) | 43(3) | 34(3) | 25(3) | 14(3) | 10(3) |
| C(8) | 41(3) | 34(3) | 30(3) | 13(3) | 12(3) | 5(3) |
| C(9) | 36(3) | 37(3) | 27(3) | 11(3) | 12(3) | 6(3) |
| C(10) | 50(4) | 51(4) | 35(3) | 23(3) | 14(3) | 8(3) |
| C(11) | 81(5) | 58(4) | 61(4) | 49(4) | 37(4) | 32(4) |
| C(12) | 64(4) | 55(4) | 55(4) | 40(3) | 26(3) | 22(3) |
| N | 52(3) | 39(3) | 40(3) | 25(2) | 24(3) | 14(2) |
| O | 57(3) | 47(2) | 34(2) | 25(2) | 17(2) | 16(2) |

Table 6-7

Best planes and torsional angles for trans-N,N-dimethyl-3-(p-methoxyphenyl)-2-propenylideniminium perchlorate, 43

| Plane | Distance of atoms from plane (Å) |
|---|---|
| C(i) i = 4 - 9 | C(4) 0.001(6), C(5) -0.002(7), C(6) 0.004(6)<br>C(7) -0.006(6), C(8) 0.006(7), C(9) -0.003(7)<br>O(1) -0.017(4), C(1) -0.089(7), C(2) -0.069(6)<br>C(3) -0.018(7), N(1) -0.233(6), C(11) -0.274(8)<br>C(12) 0.070(8) |

Torsional angles (deg)

| | | | |
|---|---|---|---|
| C(12)OC(7)C(6) | 4.1(4) | C(12)OC(7)C(8) | -175.3(4) |
| C(10)NC(1)C(2) | 1.9(4) | C(11)NC(1)C(2) | 178.2(4) |
| NC(1)C(2)C(3) | -174.7(4) | C(1)C(2)C(3)C(4) | 179.5(4) |
| C(2)C(3)C(4)C(5) | 1.5(4) | C(2)C(3)C(4)C(9) | -177.2(4) |
| C(3)C(4)C(5)C(6) | -179.4(5) | C(3)C(4)C(9)C(8) | 179.6(5) |

revealed all atoms. At this stage the temperature factors of all non-hydrogen atoms were made anisotropic with appropriate tests for the significance of the use of the increased parameters (183). Except for the temperature factors of the hydrogen atoms, the refinement of all parameters was continued using full-matrix least squares and minimizing $\Sigma\omega(|F_o| - |F_c|)^2$. This was terminated when the maximum shift/error was < 0.1. Throughout, the scattering curves were taken from reference 184 and anomalous dispersion corrections from reference 185 were applied to the curves for C, N, O and Cl. The positional parameters for non-hydrogen atoms are listed in Tables 6-3 and 6-4[+] and the corresponding temperature factors are given in Tables 6-5 and 6-6. Best planes and torsional angles for 43 are summarized in Table 6-7.

F. Fluorescence Measurements

The emission spectrum of 42 was measured using an Aminco-Bowman spectrophotofluorometer (American Instrument Co. Inc.) equipped with an Aminco xenon lamp power supply (Part no. 422-829). The output from this instrument was fed into a Hewlett-Packard model 7047A X-Y recorder. An excitation wavelength of 313 nm was employed and the sample emission was monitored from 320 nm to 600 nm. Samples were prepared such that they

---

[+] All calculations were carried out on a CYBER 170-730 computer. Initial data treatment used the XRAY 76 package (J.M. Stewart, Technical Report TR-446; Computing Science Centre, University of Maryland: College Park, MD, 1976). The structure was solved with SHELX (G.M. Sheldrick, Cambridge University, England, 1976) and finalrefinement and difference calculations used the internally written programs CUDLS (J.S. Stephens) and SYMFOU (J.J. Rutherford). Diagrams were prepared with ORTEP II (C.K. Johnson, Report ORNL-5138; Oak Ridge National Laboratory: Oak Ridge TN, 1976).

had an absorbance of 1.0 at 313 nm.

Spectra at room temperature were obtained in 98% $H_2SO_4$ solution using a standard 10 mm quartz fluorescence cell. Spectra at 77K were measured in a rigid acid glass (3:1 mixture by volume of methane sulphonic and n-propane sulphonic acids) using a thin quartz tube cooled in a partially silvered quartz dewar filled with liquid nitrogen. There was no detectable emission at either of these temperatures.

G. Quantum Yield Measurements

*Aliphatic Iminium Salts*

The light source used in these experiments consisted of 8 low-pressure mercury lamps (Southern New England Ultraviolet Co., RPR-2537A) arranged in a Rayonet Photochemical Reactor (Southern New England Ultraviolet Co., RPR-100) which was fitted with a "merry-go-round". With the lamps on, the inside of the rayonet remained at 25°C. Samples were contained in either 5-mm-i.d. quartz tubes or 5-mm-o.d. quartz nmr tubes. The samples were prepared by weighing the appropriate amount (25 - 80 mg) of imine into the required sample container. Protonations were carried out as described previously (2 mls of acid were used in the larger tubes and 0.5 mls with the smaller ones). To determine the photostationary state concentrations a sample was irradiated until there were no detectable changes in the $^1H$ nmr spectrum of the mixture. The relative concentrations of the isomers were determined from the spectrum by integration.

The quantum yield for the conversion of 39 to 59 in TFA was measured relative to the photodecomposition of potassium ferrioxalate (152). The percent conversion was less than 10% and was corrected for back

reaction (153). The composition of the acid solution was determined by measurement of the relative intensities of the resonances due to the C2 methyl groups for 39 and 59 at δ 2.07 and 2.28, respectively (the peak half-widths for the two signals were the same). To obtain the best value for the percent conversion the appropriate part of the spectrum was recorded 5 or 6 times and the measured relative concentrations were averaged. This was performed for the other cases described below. In this case and those mentioned below, duplicate samples were used in each run.

The yield for the conversion of 39 to 59 in $FSO_3H$ and 96% $H_2SO_4$ was measured relative to the conversion of trans- to cis-pent-3-en-2-one in isopentane (165). The percent conversion of the ketone was determined by analytical GLC and was corrected for back reaction (153). Quantum yields for the conversions of 37 to 54 and 38 to 57 in TFA-d, $FSO_3D$ and 96% $D_2SO_4$ were also measured relative to the conversion of trans- to cis-pent-3-en-2-one in isopentane (165). Assays of the cis iminium salts were achieved by the measurement of the relative intensities for the signals due to the C1 proton at δ 8.14 and 8.55 for 37 and 54, respectively and at δ 8.08 and 8.70 for 38 and 57, respectively. Deuterated acids were used in order to simplify these signals. In both of the latter cases the final isomer was already present in the unirradiated samples (~ 5%). The relative concentrations of the products were measured before and after irradiation and the percent conversion was taken as the difference between these two values. Since the starting concentrations of the cis-isomers were small it was assumed that they did not absorb a significant amount of light. Raw quantum yield data

are given in Table 6-8 and the final values are summarized in Table 4-5.

Most of these quantum yields were remeasured in degassed solution. Degassing was achieved by bubbling dry nitrogen through the samples. Due to the expense of $FSO_3D$ this experiment was not performed in the case of 37 and 38. Problems were encountered in TFA solvent due to its low heat of vaporization. Even at 0°C gas bubbling caused a significant amount of solvent to evaporate. This change in volume lowered the surface area available and as such could result in a low percent conversion. The one degassing experiment (38 → 57) performed in TFA gave a low value for the quantum yield of isomerization and this was probably the reason.

Since the concentrations used in the quantum yield determinations were high (necessary for $^1H$ nmr analysis) there was a possibility of layering. Such an effect would have caused a lowering of the yields from their true values. To check for this effect the quantum yield for the conversion of 39 to 59 in 96% $H_2SO_4$ was remeasured using potassium ferrioxalate actinometry. During the time of irradiation the samples were stirred with a stream of argon. The data for this experiment are given in Table 6-8 and they show that there was no change in the quantum yield. Sulphuric acid was by far the most viscous medium used so that it was the most likely solvent for a layering effect to occur. Since there was no detectable effect in this solvent it was assumed that there was no layering in the other two acid media.

The largest source of error in these measurements was in determining the percent conversion from the $^1H$ nmr spectra. An error of 5% to 10% seems reasonable. To be on the safe side the error in the

Table 6-8

Raw quantum yield data for the aliphatic iminium salts

| Reaction | Solvent | Wgt (gm) $\times 10^3$ | Moles $\times 10^4$ | % Conv. | Moles Conv. $\times 10^5$ | Einsteins of light $\times 10^5$ | $\Phi$ | $\Phi_{corrected}$ |
|---|---|---|---|---|---|---|---|---|
| 37 → 54 | TFA-d | 34.31 | 2.739 | 7.14 | 1.96 | 6.87 | 0.285 | 0.329 |
| " | TFA-d | 35.00 | 2.794 | 4.60 | 1.29 | 5.41 | 0.239 | 0.317 |
| " | TSO D | 36.74 | 2.933 | 6.05 | 1.77 | 7.85 | 0.226 | 0.316 |
| " | $D_2SO_4$ a | 36.90 | 2.946 | 2.68 | 0.789 | 5.89 | 0.134 | 0.173 |
| " | $D_2SO_4$ | 35.10 | 2.802 | 3.10 | 0.869 | 6.48 | 0.134 | 0.179 |
| 38 → 54 | TFA-d | 36.84 | 2.648 | 5.48 | 1.45 | 5.48 | 0.265 | 0.324 |
| " | TFA-d a | 35.92 | 2.580 | 6.76 | 1.74 | 7.31 | 0.238 | 0.299 |
| " | TFA-d | 37.73 | 2.709 | 5.60 | 1.52 | 8.76 | 0.173 | 0.216 |
| " | $FSO_3D$ | 35.49 | 2.549 | 6.96 | 1.77 | 7.08 | 0.250 | 0.322 |
| " | $FSO_3D$ | 36.25 | 2.603 | 6.07 | 1.58 | 6.27 | 0.252 | 0.319 |
| " | $D_2SO_4$ | 36.36 | 2.611 | 6.06 | 1.58 | 10.6 | 0.149 | 0.188 |
| " | $D_2SO_4$ a | 36.49 | 2.620 | 6.16 | 1.61 | 14.4 | 0.112 | 0.143 |
| " | $D_2SO_4$ | 37.16 | 2.669 | 5.82 | 1.55 | 13.8 | 0.112 | 0.149 |
| 39 → 59 | TFA | 81.94 | 6.542 | 4.03 | 2.64 | 24.7 | 0.107 | 0.110 |
| " | TFA | 81.35 | 6.495 | 3.72 | 2.42 | 25.4 | 0.0952 | 0.101 |
| " | $FSO_3H$ | 29.13 | 2.326 | 9.22 | 2.14 | 21.1 | 0.101 | 0.118 |
| " | $FSO_3H$ a | 23.67 | 1.890 | 6.02 | 1.14 | 9.37 | 0.122 | 0.133 |
| " | $FSO_3H$ | 25.90 | 2.068 | 4.79 | 0.990 | 9.09 | 0.109 | 0.117 |
| " | $H_2SO_4$ | 25.28 | 2.018 | 6.76 | 1.36 | 13.9 | 0.0978 | 0.109 |
| " | $H_2SO_4$ a | 28.92 | 2.309 | 7.01 | 1.62 | 14.1 | 0.115 | 0.128 |
| " | $H_2SO_4$ b | 28.05 | 2.240 | 4.51 | 1.01 | 10.3 | 0.0981 | 0.105 |
| " | $H_2SO_4$ b | 47.80 | 3.816 | 8.65 | 3.30 | 33.7 | 0.0979 | 0.113 |
| " | $H_2SO_4$ | 47.58 | 3.799 | 6.15 | 2.34 | 22.2 | 0.105 | 0.116 |

[a] degassed

[b] check for layering

quantum yields was estimated to be ± 10%.

*Aromatic Iminium Salts*

The light source used in these measurements was an Osram HBO 200W high-pressure mercury lamp placed into a Bausch and Lomb SP-200 light source. This was coupled with a Bausch and Lomb monochromator (Catalog No. 33-86-07) with entrance and exit slits set for a 20 nm bandwidth. The collimated beam was passed through a beam splitter inside of a light tight box. Samples were contained in 22-mm-o.d. x 2-mm quartz "lollipops" and 22-mm-o.d. x 10-mm and 22-mm-o.d. x 20-mm quartz actinometer cells were employed. The samples were prepared by weighing the imine or iminium salt (25 - 40 mg) into the sample container and dissolving in TFA (0.5 mls).

The quantum yield for the conversion of 40 to 61 was measured at 313 nm using potassium ferrioxalate actinometry (152). The percent conversion, in all cases, was less than 10% and was corrected for back reaction (153). After irradiation an aliquot was pipetted from the sample holder and placed in a 5-mm-o.d. nmr tube for 400 MHz $^1$H nmr assay. This assay was determined by the measurement of the relative areas (a cut and weigh technique was used) of the signals due to the C1 proton for 40 and 61 at $\delta$ 8.25 and 8.42, respectively. In this case and all those mentioned below at least three separate runs were performed and the ratio for the beam splitter was measured after every other run. Quoted errors are standard deviations calculated from these values. In most cases this error was ± 10% as was estimated for the conversions of 37 to 54, 38 to 57 and 39 to 59.

Quantum yields for the conversions of 42 → 66, 44 → 68, 45 → 69 and 46 → 70 were determined at 313 nm and the yields for the conversions of 42 → 66 and 43 → 67 were measured at 366 nm. These values were determined by an analogous procedure to that described above. Except for the conversion of 46 → 70, the compositions were monitored by the same method as above (resonances at δ 8.20 and 8.26 for 42 and 66 respectively, δ 8.09 and 8.25 of 43 and 67 respectively, δ 8.13 and 8.26 of 44 and 68 respectively and at δ 8.20 and 8.25 of 45 and 69 respectively). In the case of 46 and 70 the composition was monitored by the measurement of the relative areas of the signal due to the C6,8 protons of 70 (δ 7.50) and the resonance for the C2 proton of 46 (δ 7.29). Correction was made for the relative number of protons involved for each resonance. Raw data for all of the above measurements are given in Table 6-9 and the final values are summarized in Table 4-6.

The quantum yields for the conversions of 66 → 42 and 70 → 46 were calculated using equation 21.

$$\Phi_{t\rightarrow c}\, C_t\, \varepsilon_c = \Phi_{c\rightarrow t}\, C_c\, \varepsilon_c \qquad (21)$$

where $\Phi_{t\rightarrow c}$ is the quantum yield for the conversion of the trans- to the cis-isomer (42 → 66 and 46 → 70), $\Phi_{c\rightarrow t}$ is the yield for the reverse reaction (66 → 42 and 70 → 46), $C_t$ and $C_c$ are the concentrations at the photostationary state of the trans- and cis-isomers respectively and $\varepsilon_t$ and $\varepsilon_c$ are the corresponding molar extinction coefficients at the appropriate wavelength.

Table 6-9

Raw quantum yield data for the aliphatic iminium salts

| Reaction | (nm) | Wgt (gm) $\times 10^3$ | Moles $\times 10^4$ | % Conv. | Moles conv. $\times 10^5$ | Einsteins of light $\times 10^5$ | $\Phi$ | $\Phi_{corrected}$ |
|---|---|---|---|---|---|---|---|---|
| 40 → 61 | 313 | 27.64 | 1.476 | 6.96 | 1.03 | 1.93 | 0.534 | 0.576 |
| " | " | 27.82 | 1.485 | 7.10 | 1.05 | 2.18 | 0.484 | 0.524 |
| " | " | 27.33 | 1.459 | 6.23 | 0.909 | 1.52 | 0.598 | 0.641 |
| 42 → 66 | 313 | 35.57 | 1.370 | 8.14 | 1.11 | 2.29 | 0.487 | 0.522 |
| " | " | 46.70 | 1.798 | 6.63 | 1.19 | 2.14 | 0.557 | 0.590 |
| " | " | 37.84 | 1.457 | 9.58 | 1.40 | 2.30 | 0.607 | 0.658 |
| " | " | 43.79 | 1.686 | 7.24 | 1.22 | 2.13 | 0.573 | 0.609 |
| 42 → 66 | 366 | 41.75 | 1.608 | 6.90 | 1.11 | 1.46 | 0.760 | 0.813 |
| " | " | 36.99 | 1.424 | 7.44 | 1.06 | 1.78 | 0.595 | 0.646 |
| " | " | 42.65 | 1.642 | 5.08 | 0.834 | 1.11 | 0.752 | 0.792 |
| " | " | 42.93 | 1.653 | 6.47 | 1.07 | 1.49 | 0.718 | 0.766 |
| 43 → 67 | 366 | 40.94 | 1.413 | 5.67 | 0.801 | 1.48 | 0.541 | 0.574 |
| " | " | 37.35 | 1.289 | 6.21 | 0.801 | 1.32 | 0.606 | 0.649 |
| " | " | 36.47 | 1.259 | 4.39 | 0.553 | 1.02 | 0.542 | 0.565 |
| " | " | 37.92 | 1.309 | 5.69 | 0.745 | 1.41 | 0.528 | 0.560 |
| 44 → 68 | 313 | 27.78 | 1.015 | 7.23 | 0.734 | 1.41 | 0.520 | 0.563 |
| " | " | 35.00 | 1.279 | 7.13 | 0.912 | 1.85 | 0.493 | 0.535 |
| " | " | 35.05 | 1.281 | 4.27 | 0.547 | 1.29 | 0.424 | 0.465 |
| 45 → 69 | 313 | 36.43 | 1.239 | 5.47 | 0.677 | 1.34 | 0.506 | 0.529 |
| " | " | 36.00 | 1.224 | 6.81 | 0.834 | 1.35 | 0.617 | 0.652 |
| " | " | 35.87 | 1.220 | 6.32 | 0.771 | 1.22 | 0.632 | 0.665 |
| " | " | 34.68 | 1.179 | 4.17 | 0.492 | 1.06 | 0.464 | 0.479 |
| 46 → 70 | 313 | 35.72 | 1.172 | 3.33 | 0.390 | 1.52 | 0.257 | 0.267 |
| " | " | 41.45 | 1.360 | 3.27 | 0.445 | 1.71 | 0.260 | 0.272 |
| " | " | 36.56 | 1.200 | 3.35 | 0.402 | 1.70 | 0.236 | 0.247 |
| " | " | 36.71 | 1.205 | 3.54 | 0.427 | 1.58 | 0.270 | 0.283 |

The molar extinction coefficient of 42 at 313 nm ($\varepsilon_t$, 5750 $cm^{-1}M^{-1}$) was determined from its absorption spectrum whereas the value for 66 ($\varepsilon_c$, 6220 $cm^{-1}M^{-1}$) was estimated from the absorption spectrum of the photostationary state mixture. The low energy absorption bands for 42 and 66 were superimposed. It was assumed that the absorbance at 313nm was due to the sum of the absorbances for the two isomers. The relative concentrations of 42 and 66 at the stationary state had been determined by $^1H$ nmr assay so that the extinction coefficient of 66 could be calculated. The only unknown remaining in equation 21 was the quantum yield for the conversion of 66 → 42 ($\phi_{c\rightarrow t}$) and this could be calculated by a simple manipulation of the equation. This procedure was repeated and the two values averaged to give the quantity reported in Table 4-6. It was estimated that the error was ± 10%. A value for the conversion of 70 → 46 was determined by an analogous procedure. The molar extinction coefficients of 46 and 70 determined at 313 nm were 28200 $cm^{-1}M^{-1}$ and 32500 $cm^{-1}M^{-1}$ respectively.

H. Kinetic Measurements

*$H_o$ Measurements*

The Hammett indicator, 2,4-dinitroaniline was recrystallized from $CH_3OH$ to constant melting point (mp = 177.5-8.5°C, literature value 180°C, reference 179). In $CH_2Cl_2$, this material had an absorption maximum at 330 nm ($\varepsilon$ = 1.42x$10^{-4}$ $cm^{-1}M^{-1}$). Absorption spectra of known concentrations were recorded in TFA and 0.015M $H_2SO_4$/TFA solution. The absorbance at 330 nm for each of these spectra was determined and by the use of Beer's law and the previously measured molar extinction coefficient the concentration of the unprotonated aniline was evaluated.

The concentration of the protonated aniline was just the difference between this value and the total concentration of the aniline. The $H_o$ value was then determined using equation 30.

$$H_o = pK_a + Log\frac{[B]}{[BH^+]} \qquad (30)$$

where $pK_a$ = -4.3 for 2,4-dinitroaniline (176) and [B] and $[BH^+]$ are the concentrations of the unprotonated and protonated aniline respectively.

*Isomerization Rate Constants*

The rate constant for the conversion of 66 to 42 at 100°C was determined as follows. An appropriate amount of iminium salt 42 (~ 25 mg) was dissolved in TFA (0.3 mls) and a small amount of $(CH_3)_4N^+BF_4^-$ was added as an internal standard. This mixture was placed into a medium-walled nmr tube which was then sealed. The sample was irradiated in a Rayonet Photochemical Reactor (Southern New England Ultraviolet Co., RPR-100) fitted with 16 RPR-3000 Å lamps until a photostationary state was reached. A $^1H$ nmr spectrum of this mixture was recorded. The peak height of the centre of the triplet at δ 6.26, which was due to the H2 proton of the cis-isomer 66, was ratioed with the peak height of the singlet at δ 3.10 due to the internal standard (peak half-widths were the same). This ratio was used as a dimensionless concentration function.

The sample was heated in a refluxing water bath (T = 100 ± 0.5°C) and about once every 24 hours the sample was cooled quickly to 25°C and its $^1H$ nmr spectrum was obtained. The concentration of 66 was determined from this spectrum by the method described above. This procedure was continued for at least two half-lives and the raw data

thus obtained are given in Table 6-10. A plot of Ln (Ratio) vs time gave a good linear correlation (correlation coefficient = 0.995). The slope of this line ($1.65 \times 10^{-6}$ $s^{-1}$), which was determined by linear regression, was equal to the first-order rate constant. A second run was performed and the two values of the rate constant were averaged (see Table 5-1). These two values did not differ by any more than 10% which was the estimated error. Again the largest source of error was in the $^1H$ nmr analysis which was no greater than 10%.

This procedure was repeated for the conversions 67 to 43, 68 to 44, 69 to 45 and 70 to 46. Naturally the samples were heated for different lengths of time between $^1H$ nmr spectra depending on the rates of the isomerization processes. In all cases the triplet due to the H2 proton of the cis-isomer was used to monitor the kinetics ($\delta$ 6.41 for 67, $\delta$ 6.47 for 68, $\delta$ 6.56 for 69 and $\delta$ 6.79 for 70). The only alteration was that, in the case of 43, the photochemical reactor was fitted with RPR-3500 Å lamps.

The rate constants determined in the 0.015 $H_2SO_4$/TFA solvent were measured by an analogous procedure. Only one run was performed since the measured rate constants in this solvent were statistically different than those determined in TFA (see Table 5-3).

*Rate Constants for Deuterium Exchange at C2*

The above isomerizations were monitored qualitatively in both TFA-d and $D_2SO_4$/TFA-d solvents by a similar method. If exchange had occurred the signals due to H1 and H3 would have collapsed to singlets and the signal due to H2 would have diminished. In all cases there was no detectable exchange at any site during the time of the isomerizations.

Table 6-10

Raw rate constant data for the isomerization of the unsubstituted aromatic iminium salt, 66 → 42

| Time min | Ratio[a] | Ln(Ratio) |
|---|---|---|
| 0 | 3.84 | 1.34 |
| 1710 | 4.32 | 1.46 |
| 2880 | 5.29 | 1.67 |
| 4320 | 6.07 | 1.80 |
| 5895 | 6.78 | 1.91 |
| 7230 | 7.67 | 2.04 |
| 8550 | 8.80 | 2.17 |
| 9720 | 10.38 | 2.34 |
| 10440 | 10.64 | 2.36 |
| 11160 | 10.71 | 2.37 |
| 12720 | 14.71 | 2.65 |

[a] $\text{Ratio} = \frac{\text{Peak height of resonance at } \delta\ 3.10}{\text{Peak height of resonance at } \delta\ 6.26}$

The rate constants for the exchange of the C2 proton of the trans-isomers 42 to 46 were determined at 100 ± 0.5°C in both TFA-d and $D_2SO_4$/TFA-d solvents. Except for 43, this was accomplished by a procedure analogous to that described for the rate constants of isomerization. The height of a convenient peak of the doublet of doublets due to the H2 proton (δ 7.08 for 42, δ 7.01 for 44, δ 7.05 for 45 and δ 7.29 for 46) was ratioed with the singlet at δ 3.10 due to the internal standard. In the case of 43 the signal due to H2 (δ 6.92) was overlapped by the doublet for H6 and H8 (δ 6.92). This latter resonance also exchanged so that the simultaneous disappearance of these signals was monitored by integration. Since the exchange of the ring protons was faster than that of the C2 proton, the rate constants, which were determined, were upper limits for the exchange of H2.

As before the samples were cooled periodically to 25°C and their $^1H$ nmr spectra were recorded. The decrease in the resonance for H2 was determined by one of the two methods described above. In the case of 44 and 46 there was no detectable exchange in either solvent after heating at 100°C for 2 days whereas 42 and 45 showed no detectable exchange after 6 days. The constants for these processes are summarized in Table 5-4.

## References


1. G. Wald, Science, 162, 230 (1968).
2. D. Bownds, Nature, 216, 1178 (1967).
3. M. Akhtar, P.T. Blosse and P.B. Dewhurst, Biochem. J., 110, 694 (1968).
4. B. Honig, Ann Rev. Phys. Chem., 29, 31 (1978).
5. R.R. Birge, Ann Rev. Biophys. Bioeng., 10, 315 (1981).
6. D. Oesterhelt and W. Stoekenius, Nature New Biol., 233, 149 (1971).
7. B. Honig and T.G. Ebrey, Ann. Rev. Biophys. Bioeng., 3, 151 (1974).
8. T.G. Ebrey and B. Honig, Quart. Rev. Biophys., 8, 129 (1975).
9. R. Uhl and E.W. Abrahamson, Chem. Rev., 81, 291 (1981).
10. R.H. Callender and B. Honig, Ann. Rev. Biophys. Bioeng., 6, 33 (1977).
11. D. Narva and R.H. Callender, Photochem. Photobiol., 32, 273 (1980).
12. A. Lewis, J. Spoonhower, R.A. Bogomolni, R.H. Lozier and W. Stoekenius, Proc. Natl. Acad. Sci. U.S.A., 71, 4462 (1974).
13. B. Anton, A.G. Doukas, R.H. Callender, B. Becher and T.G. Ebrey, Biochemistry, 16, 2995 (1977).
14. J. Favrot, J.M. Leclercq, R. Roberge, C. Sandorfy and D. Vocelle, Photochem. Photobiol., 29, 99 (1979).
15. J. Favrot, D. Vocelle and C. Sandorfy, Photochem. Photobiol., 30, 417 (1979).
16. F.I. Harosi, J. Favrot, J.M. Leclercq, D. Vocelle and C. Sandorfy, Rev. Can. Biol., 37, 257 (1978).

17. A. Lewis, M.A. Marcus, B. Ehrenberg and H. Crespi, Proc. Natl. Acad. Sci. U.S.A., 75, 4642 (1978).

18. B. Ehrenberg, A. Lewis, T.K. Porta, J.F. Nagle and W. Stoekenius, Proc. Natl. Acad. Sci. U.S.A., 77, 6571 (1980).

19. G.M. Sharma and O.A. Roels, J. Org. Chem., 38, 3648 (1973).

20. J.W. Shriver, E.W. Abrahamson and G.D. Mateescu, J. Am. Chem. Soc., 98, 2407 (1976).

21. Y. Inoue, A. Takahashi, Y. Tokito, R. Chujo and Y. Miyoshi, Org. Mag. Res., 6, 487 (1974).

22. Y. Tokito, Y. Inoue, R. Chujo and Y. Miyoshi, Org. Mag. Res., 7, 485 (1975).

23. A.M. Schaffer, T. Yamaoka and R.S. Becker, Photochem. Photobiol., 21, 297 (1975).

24. J. Favrot, C. Sandorfy and D. Vocelle, Photochem. Photobiol., 28, 211 (1978).

25. A.R. Oseroff and R.H. Callender, Biochemistry, 13, 4243 (1974).

26. A.M. Schaffer, W.H. Waddell and R.S. Becker, J. Am. Chem. Soc., 96, 2063 (1974).

27. W.H. Waddell, A.M. Schaffer and R.S. Becker, J. Am. Chem. Soc., 99, 8456 (1977).

28. D.S. Kliger, S.J. Milder and E.A. Dratz, Photochem. Photobiol., 25, 277 (1977).

29. Y. Inoue, Y. Tokito, R. Chujo and Y. Miyoshi, J. Am. Chem. Soc., 99, 5592 (1977).

30. Y. Inoue, Y. Tokito, S. Tomonoh and R. Chujo, Bull. Chem. Soc. Jpn., 52, 265 (1979).

31. R.S. Becker, G. Hug, P.K. Das, A.M. Schaffer, T. Takemura, N. Yamamoto and W.H. Waddell, J. Phys. Chem., 80, 2265 (1976).

32. W.H. Waddell, A.M. Schaffer and R.S. Becker, J. Am. Chem. Soc., 95, 8223 (1973).

33. T. Rosenfeld, A. Alchalel and M. Ottolenghi, Photochem. Photobiol., 20, 121 (1974).

34. R.R. Birge and L.M. Hubbard, J. Am. Chem. Soc., 102, 2195 (1980).

35. T. Rosenfeld, B. Honig, M. Ottolenghi, J. Hurley and T.G. Ebrey, Pur. Appl. Chem., 49, 341 (1977).

36. A. Alchalel, B. Honig, M. Ottolenghi and T. Rosenfeld, J. Am. Chem. Soc., 97, 2161 (1975).

37. T.G. Ebrey, R. Govindjee, B. Honig, E. Pollack, W. Chan, R. Crouch, A. Yudd and K. Nakanishi, Biochemistry, 14, 3933 (1975).

38. R.H. Callender, A. Doukas, R. Crouch and K. Nakanishi, Biochemistry, 15, 1621 (1976).

39. F.D. Collins, Nature, 171, 469 (1953).

40. R.A. Morton and G.A.J. Pitt, Biochem. J. 59, 128 (1955).

41. H. Suzuki, K. Nakachi and T. Komatsu, J. Phys. Soc. Jpn., 37, 751 (1974).

42. B. Honig, U. Dinur, K. Nakanishi, V. Balogh-Nair, M.A. Gawinowicz, M. Arnaboldi and M.G. Motto, J. Am. Chem. Soc., 101, 7084 (1979).

43. V. Balogh-Nair, J.D. Carriker, B. Honig, V. Kamat, M.G. Motto, K. Nakanishi, R. Sen, M. Sheves, M. Arnaboldi Tanis and K. Tsujimoto, Photochem. Photobiol., 33, 483 (1981).

44. T. Kakitani and H. Kakitani, J. Phys. Soc. Jpn., 38, 1455 (1975).

45. C.S. Irving, G.W. Byers and P.A. Leermakers, Biochemistry, 9, 858 (1970).

46. H. Suzuki, T. Komatsu and H. Kitajima, J. Phys. Soc. Jpn., 37, 177 (1974).

47. B. Honig, A.D. Greenberg, U. Dinur and T.G. Ebrey, Biochemistry, 15, 4593 (1976).

48. A.D. Greenberg, B. Honig and T.G. Ebrey, Nature, 257, 823 (1975).

49. J.P. Corsetti and B.E. Kohler, J. Chem. Phys., 67, 5237 (1977).

50. R. Mathies and L. Stryer, Proc. Natl. Acad. Sci. U.S.A., 73, 2169 (1976).

51. A. Kropf and R. Hubbard, Ann. N.Y. Acad. Sci., 74, 266 (1958).

52. M. Arnaboldi, M.G. Motto, K. Tsujimoto, V. Balogh-Nair and K. Nakanishi, J. Am. Chem. Soc., 101, 7082 (1979).

53. M. Sheves, K. Nakanishi and B. Honig, J. Am. Chem. Soc., 101, 7086 (1979).

54. A. Lewis, R.S. Fager and E.W. Abrahamson, J. Raman Spectrosc., 1, 465 (1973).

55. B. Anton, A.G. Doukas, D. Narva, R.H. Callender, U. Dinur and B. Honig, Biophys. J., 29, 79 (1980).

56. J. Shriver, G. Mateescu, R. Fager, D. Torchina and E.W. Abrahamson, Nature, 270, 271 (1977).

57. A. Yamaguchi, T. Unemoto and A. Ikegami, Photochem. Photobiol., 33, 511 (1981).

58. R. Korenstein, K.A. Muszkat and S. Sharafy-Ozeri, J. Am. Chem. Soc., 95, 6177 (1973).

59. T. Yoshizawa and G. Wald, Nature, 197, 1279 (1963).

60. G.E. Busch, M.L. Applebury, A.A. Lamola and P.M. Rentzepis, Proc. Natl. Acad. Sci. U.S.A., 69, 2802 (1972).

61. K. Peters, M.L. Applebury and P.M. Rentzepis, Proc. Natl. Acad. Sci. U.S.A., 74, 3119 (1977).

62. M.L. Applebury, K.S. Peters and P.M. Rentzepis, Biophys. J., 23, 375 (1978).

63. J. Favrot, J.M. Leclercq, R. Roberge, C. Sandorfy and D. Vocelle, Chem. Phys. Lett., 53, 433 (1978).

64. P. Dupuis, F.I. Harosi, C. Sandorfy, J.M. Leclercq and D. Vocelle, Rev. Can. Biol., 39, 247 (1980).

65. A. Lewis, Proc. Natl. Acad. Sci. U.S.A., 75, 549 (1978).

66. K. van der Meer, J.J.C. Mulder and J. Lugtenburg, Photochem. Photobiol., 24, 363 (1976).

67. B. Mao, T.G. Ebrey and R. Crouch, Biophys. J., 29, 247 (1980).

68. A. Warshel, Nature, 260, 679 (1976).

69. G. Eyring, B. Curry, R. Mathies, A. Broek and J. Lugtenburg, J. Am. Chem. Soc., 102, 5390 (1980).

70. G. Eyring, B. Curry, R. Mathies, R. Fransen, I. Palings and J. Lugtenburg, Biochemistry, 19, 2410 (1980).

71. G. Eyring, B. Curry, A. Broek, J. Lugtenburg and R. Mathies, Biochemistry, 21, 384 (1982).

72. G. Hayward, W. Carlsen, A. Siegman and L. Stryer, Science, 211, 942 (1981).

73. K. Nakanishi, Pur. Appl. Chem., 49, 333 (1977).

74. H. Akita, S.P. Tanis, M. Adams, V. Balogh-Nair and K. Nakanishi, J. Am. Chem. Soc., 102, 6370 (1980).

75. B. Honig, T.G. Ebrey, R.H. Callender, U. Dinur and M. Ottolenghi, Proc. Natl. Acad. Sci. U.S.A., 76, 2503 (1979).

76. A. Warshel and N. Barboy, J. Am. Chem. Soc., 104, 1469 (1982).

77. T. Suzuki and R.H. Callender, Biophys. J., 34, 261 (1981).

78. E.E. Broda and C.F. Goodeve, Proc. Roy. Soc. London, A179, 151 (1942).

79. R.G. Matthews, R. Hubbard, P.K. Brown and G. Wald, J. Gen. Physiol., 47, 215 (1963).

80. S.E. Ostroy, F. Erhardt and E.W. Abrahamson, Biochim. Biophys. Acta, 112, 265 (1966).

81. R.J. Lythgoe and J.P. Quilliam, J. Physiol., 93, 24 (1938).

82. V. Sundström, P.M. Rentzepis, K. Peters and M.L. Applebury, Nature, 267, 645 (1977).

83. T. Kobayashi, FEBS Lett., 106, 313 (1979).

84. E.W. Abrahamson and J.R. Weisenfeld in "Handbook of Sensory Physiology", 7/1, H.J.A. Dartnall, Ed., Springer-Verlag, Berlin, Germany, 1972, p. 69.

85. C. Baumann and Reinheimer in "Biochemistry and Physiology of Visual Pigments", H. Langer, Ed., Springer-Verlag, Berlin, Germany, 1972, p. 89.

86. S.E. Ostroy, Biochim. Biophys. Acta, 463, 91 (1977).

87. L. Salem and P. Bruckmann, Nature, 258, 526 (1975).

88. L. Salem, Acc. Chem. Res., 12, 87 (1979).

89. S. Yoshikami and W.A. Hagins, Ann. N.Y. Acad. Sci., 307, 545 (1978).

90. S.A. Lipton, S.E. Ostroy and J.E. Dowling, J. Gen. Physio., 70, 747 (1977).

91. M.M. Fisher and K. Weiss, Photochem. Photobiol., 20, 423 (1974).

92. A. Warshel, Proc. Natl. Acad. Sci. U.S.A., 75, 2558 (1978).

93. H. Boehme and H.G. Viehe, "Iminium Salts in Organic Chemistry", J. Wiley and Sons, New York, New York, 1976.

94. P.S. Mariano, J.L. Stavinoha and R. Swanson, J. Am. Chem. Soc., 99, 6781 (1977).

95. P.S. Mariano, J.L. Stavinoha, G. Pèpe and E.F. Meyer, Jr., Ibid., 100, 7114 (1978).

96. P.S. Mariano and A. Leone-Bay, Tetrahedron Lett., 4581 (1980).

97. P.S. Mariano, J. Stavinoha and E. Bay, Tetrahedron, 37, 3385 (1981).

98. J.L. Stavinoha and P.S. Mariano, J. Am. Chem. Soc., 103, 3136 (1981).

99. J.L. Stavinoha, P.S. Mariano, A. Leone-Bay, R. Swanson and C. Bracken, Ibid., 103, 3148 (1981).

100. G.M. Badger, C.P. Joshua and G.E. Lewis, Tetrahedron Lett., 3711 (1964).

101. A.V. El'tsov, O.P. Studzinskii and N.V. Ogol'tsova, Zh. Org. Khim., 6, 405 (1970).

102. H.-H. Perkampus and B. Behjati, J. Heterocyclic Chem., 11, 511 (1974).

103. G. Scheibe, J. Heiss and K. Feldmann, Ber. Bunsenges. Physik. Chem., 70, 52 (1966).

104. G. Scheibe, J. Heiss and K. Feldmann, Angew. Chem. Int. Ed. Engl., 4, 525 (1965).

105. H. Guesten and D. Schulte-Frohlinde, Chem. Ber., 104, 402 (1971).

106. H. Guesten and D. Schulte-Frohlinde, Tetrahedron Lett., 3567 (1970).

107. H. Guesten and D. Schulte-Frohlinde, Z. Naturforsch., 34B, 1556 (1979).

108. M.L. Filleux-Blanchard, D. LeBotlan, A. Reliquet and F. Reliquet-Clesse, Org. Mag. Res., 6, 471 (1974).

109. G. Scheibe, C. Jutz, W. Seiffert and D. Grosse, Angew. Chem. Int. Ed. Engl., 3, 306 (1964).

110. D. Le Botlan, M.-L. Filleux-Blanchard, G. Le Coustumer and Y. Mollier, Org. Mag. Res., 6, 454 (1974).

111. M.P. Sammes, J. Chem. Soc., PT2, 1501 (1981).

112. A. Krebs and J. Breckwoldt, Tetrahedron Lett., 3797 (1969).

113. A. Krebs, Ibid., 1901 (1971).

114. G.J. Martin and S. Poignant, J. Chem. Soc. PT2, 1964 (1972); 642 (1974).

115. D. Schulte-Frohlinde and H. Guesten, Liebigs Ann. Chem., 749, 49 (1971).

116. A. Padwa, Chem. Rev. 77, 37 (1977).

117. C.G. McCarty in "The Chemistry of the Carbon Nitrogen Double Bond", S. Patai, Ed., Interscience, New York, New York, 1970, p. 363.

118. J.M. Lehn, B. Munsch and P. Millie, Theoret. Chim. Acta, 16, 351 (1970).

119. G. Wettermark, J. Weinstein, J. Sousa and L. Dogliotti, J. Phys. Chem., 69, 1584 (1965).

120. D.Y. Curtin and J.W. Hausser, J. Am. Chem. Soc., 83, 3474 (1961).

121. H. Kessler, Tetrahedron, 30, 1861 (1974).

122. H.O. Kalinowski and H. Kessler, Topics in Stereochem., 7, 295 (1972).

123. J.M. Lehn, Top. Curr. Chem., 15, 311 (1970).

124. R.F. Childs, E.F. Lund, A.G. Marchall, W.J. Morrisey and C.V. Rogerson, J. Am. Chem. Soc., 98, 5924 (1976).

125. R.A. Sack and S. Seltzer, Vision Res., 18, 423 (1978).

126. P.C. Mowery and W. Stoeckenius, J. Am. Chem. Soc., 101, 414 (1979).

127. P.C. Mowery and W. Stoeckenius, Biochemistry, 20, 2302 (1981).

128. T. Kakitani and H. Kakitani, J. Phys. Soc. Jpn., 38, 1455 (1975).

129. R.F. Childs, B.D. Dickie, R. Faggiani, C.A. Fyfe, C.J.L. Lock and R.E. Wasylishen, submitted to J. Org. Chem.

130. R.F. Childs, A. Varadarajan, C.J.L. Lock, R. Faggiani, C.A. Fyfe and R.E. Wasylishen, J. Am. Chem. Soc., 104, 2452 (1982).

131. C.S. Yannoni, Acc. Chem. Res., 15, 201 (1982).

132. S.J. Opella and M.H. Frey, J. Am. Chem. Soc., 101, 5854 (1979).

133. G.A. Olah and P. Kreienbuehl, J. Am. Chem. Soc., 89, 4756 (1967); G.A. Olah and D.J. Donovan, J. Org. Chem., 43, 860( 1978).

134. R.F. Childs and B.D. Dickie, J. Chem. Soc. Chem. Comm., 1268 (1981).

135. V.M. Parikh, "Absorption Spectroscopy of Organic Molecules", Addison-Wesley Pub. Co., London, England, 1974, p. 117.

136. M. Suzuki and K. Kozima, Bull. Chem. Soc. Jpn., 42, 2183 (1969); M. Suzuki and K. Kozima, J. Mol. Spec., 38, 314 (1971); A.J. Bowles, W.O. George and W.F. Maddams, J. Chem. Soc., B, 810 (1969).

137. P.A. Kollman in reference 93, p. 1.

138. R.C. Bingham, M.J.S. Dewar and D.H. Lo, J. Am. Chem. Soc., 97, 1294 (1975).

139. R.F. Childs, D.L. Mulholland and A. Nixon, Can. J. Chem., 60, 801 (1982).

140. K.S. Dhami and J.B. Stothers, Can. J. Chem., 43, 510 (1965).

141. L.M. Trefonas, R.L. Flurry, Jr., R. Majeste, E.A. Meyers and and R.F. Copeland, J. Am. Chem. Soc., 88, 2145 (1966).

142. F. Chentli-Benchikha, J.-P. Declercq, G. Germain and M. Van Meerssche, Acta Cryst., B33, 3428 (1977).

143. H.G. Norment and I.L. Karle, Acta Cryst., 15, 873 (1962).

144. E.D. Becker, "High Resolution NMR", Academic Press, New York, New York, 1969, p. 68.

145. L.C. Cross and W. Klyne (Collators), Pure Appl. Chem., 45, 11 (1976).

146. G.C. Levy and G.L. Nelson, "Carbon-13 Nuclear Magnetic Resonance for Organic Chemists", Wiley-Interscience, New York, New York, 1972, p. 81.; B.G. Sayer, Private Communication.

147. D.G. Farnum, Adv. Phys. Org. Chem., 11, 123 (1975).

148. G.R. Kieczykowski, R.H. Schlessinger and R.B. Sulsky, Tetrahedron Lett., 597 (1976).

149. M. Scholtz and A. Wiedemann, Chem. Ber., 36, 845 (1903); C.F. Goehring, Ibid., 18, 871 (1885).

150. N.J. Leonard and J.V. Paukstelis, J. Org. Chem., 28, 3021 (1963).

151. T.H. Lowry and K.S. Richardson, "Mechanism and Theory in Organic Chemistry" 2nd Ed., Harper and Row, New York, New York, 1981, p. 129.

152. C.G. Hatchard and C.A. Parker, Proc. Roy. Soc. London, A235, 518 (1956).

153. A.A. Lamola and G.S. Hammond, J. Chem. Phys., 43, 2129 (1965).

154. R.F. Childs and M. Pankratz, unpublished results.

155. N.J. Turro, "Modern Molecular Photochemistry", Benjamin/Cummings Publishing Co. Inc., Menlo Park, California, 1978, p. 589.

156. P.G. Tarasoff, Ph.D. Thesis, The George Washington University, Washington, D.C. 1974.

157. J. Saltiel, J. D'Agostino, E.D. Megarity, L. Metts, K.R. Neuberger, M. Wrighton and O.C. Zafiriou in "Organic Photochemistry", Volume 3, O.L. Chapman, Ed., Marcel Dekker, Inc., New York, New York, 1973, p. 1.

158. R.F. Childs and M.E. Hagar, J. Am. Chem. Soc., 101, 1052 (1979).

159. R.F. Childs and M.E. Hagar, Can. J. Chem., 58, 1788 (1980).

160. R.F. Childs and A.W. Cochrane, J. Org. Chem., 46, 1086 (1981).

161. K. Inuzuka and R.S. Becker, Bull. Chem. Soc. Jpn., 44, 3328 (1971).

162. O.T. Fasullo, "Sulphuric Acid: Use and Handling", McGraw-Hill, New York, New York, 1965, p. 304.

163. J. Barr, R.J. Gillespie and R.C. Thompson, Inorg. Chem., 3, 1149 (1964).

164. J.B. Milne, in "The Chemistry of Nonaqueous Solvents", Volume VB, J.J. Lagowski, Ed., Academic Press, New York, New York, 1978, p. 1.

165. J.F. Graf and C.P. Lillya, Mol. Photochem., 9, 227 (1979).

166. E.M. Kosower, "An Introduction to Physical Organic Chemistry", J. Wiley and Sons Inc., New York, New York, 1968, p. 49.

167. from reference 151, pp. 130-136.

168. M. Liler, Adv. Phys. Org. Chem., 11, 267 (1975).

169. G.S. Hammond, J. Am. Chem. Soc., 77, 334 (1955).

170. M.J.S. Dewar and S. Kirschner, J. Am. Chem. Soc., 96, 6809 (1974).

171. C.F. Wilcox and B.K. Carpenter, J. Am. Chem. Soc., 101, 3897 (1979); J.I. Brauman and W.C. Archie, Jr., Tetrahedron, 27, 1275 (1971).

172. H.C. Brown and Y. Okamoto, J. Am. Chem.Soc., 80, 4979 (1958).

173. R. Wolfenden and W.P. Jencks, J. Am. Chem. Soc., 83, 2763 (1961).

174. H.H. Hyman and R.A. Garber, J. Am. Chem. Soc., 81, 1847 (1959).

175. C. Eaborn, P.M. Jackson and R. Taylor, J. Chem. Soc., B, 613 (1966).

176. C.D. Johnson, A.R. Katritzky and S.A. Shapiro, J. Am. Chem. Soc., 91, 6654 (1969).

177. L.P. Hammett, "Physical Organic Chemistry", 2nd Ed., McGraw-Hill Book Co., New York, New York, 1970, p. 323.

178. P.R. Schleyer, T.M. Su, M. Saunders, J.C. Rosenfeld, J. Am. Chem. Soc., 91, 5174 (1969).

179. R.C. Weast, Ed., "CRC Handboo of Chemistry and Physics", 59th Ed., CRC Press Inc., Boca Raton, Florida, p. C-115.

180. G.S. Hammond and R.C. Newman, Jr., J. Phys. Chem., 67, 1655, 1659 (1963).

181. B. Lippert, C.J.L. Lock, B. Rosenberg and M. Zvagulis, Inorg. Chem., 16, 1525 (1977).

182. R.P. Hughes, N. Krishnamachari, C.J.L. Lock, J. Powell and G. Turner, Inorg. Chem., 16, 314 (1977).

183. W.C. Hamilton, Acta Cryst., 18, 502 (1965).

184. D.T. Cromer and J.T. Waber, "International Tables for X-ray Crystallography", J.A. Ibers and W.C. Hamilton, Eds., Kynoch Press, Birmingham, 1974, Vol. IV, Table 2.2A, p. 72ff.

185. D.T. Cromer in reference 184, Table 2.3.1, pp. 149-150.